COMPUTATIONAL MODELING OF BIOLOGICAL CELLS AND SOFT TISSUES

A Dissertation

by

GINU UNNITHAN UNNIKRISHNAN

Submitted to the Office of Graduate Studies of
Texas A&M University
in partial fulfillment of the requirements for the degree of

DOCTOR OF PHILOSOPHY

May 2008

Major Subject: Mechanical Engineering

COMPUTATIONAL MODELING OF BIOLOGICAL CELLS

AND SOFT TISSUES

A Dissertation

by

GINU UNNITHAN UNNIKRISHNAN

Submitted to the Office of Graduate Studies of
Texas A&M University
in partial fulfillment of the requirements for the degree of

DOCTOR OF PHILOSOPHY

Approved by:

Chair of Committee,	J.N. Reddy
Committee Members,	Ramesh Talreja
	Harry Hogan
	Xin-Lin Gao
Head of Department,	Dennis L. O'Neal

May 2008

Major Subject: Mechanical Engineering

ABSTRACT

Computational Modeling of Biological Cells and Soft Tissues. (May 2008)

Ginu Unnithan Unnikrishnan,

B.Tech., Kerala University, India;

M.S., Indian Institute of Technology Madras, Chennai, India

Chair of Advisory Committee: Dr. J.N. Reddy

Biological materials are complex hierarchical systems subjected to external stimuli like mechanical forces, chemical potentials and electrical signals. A deeper understanding of the behavior of these materials is required for the response characterization of healthy and diseased conditions. The primary aim of this dissertation is to study the mechanics of biological materials like cells and tissues from a computational perspective and relate its behavior with experimental works, so as to provide a framework for the identification and treatment of pathological conditions like cancer and vascular diseases.

The first step towards understanding the behavior of a biological cell is to comprehend its response to external mechanical stimuli. Experimentally derived material properties of cells have found to vary by orders of magnitude even for the same cell type. The primary cause of such disparity is attributed to the stimulation process, and the theoretical models used to interpret the experimental data. The variations in mechanical properties obtained from the experimental and theoretical

studies can be overcome only through the development of a sound mathematical framework correlating the derived mechanical property with the cellular structure. Such a formulation accounting for the inhomogeneity of the cytoplasm due to stress fibers and actin cortex is developed in this work using Mori-Tanaka method of homogenization. Mechanical modeling of single cells would be extremely useful in understanding its behavior in an experimental setup.

Characterization of *in-vivo* response of cells requires mathematical modeling of the embedding environment like fibers and fluids, which forms the extra cellular matrix. Studies on fluid-tissue interactions in biomechanics have primarily relied on either an iterative solution of the individual solid or tissue phases or a sequential solution of the entire domain using a coupled algorithm. In this dissertation, a new computational methodology for the analysis of fluid-tissue interaction problem is presented. The modeling procedure is based on a biphasic representation of fluid and tissue domain, consisting of fluid and solid phases. The biphasic-fluid interaction model is also implemented to study the transfer of low-density lipoprotein from the blood to the arterial wall, and also the nutrient transfer in the tissue scaffolds of a bioreactor.

DEDICATION

TO MY PARENTS

ACKNOWLEDGEMENTS

I express my sincere gratitude to Professor J.N. Reddy, my dissertation advisor, for his constant support and guidance during the course of this work and also for his confidence in allowing me to pursue a research topic of my interest.

I am also grateful to my doctoral committee members, Prof. Ramesh Talreja, Prof. Harry Hogan and Dr. Xin-Lin Gao, for their insightful knowledge and keenness in my research work.

I am indebted to all my teachers for their encouragement and support, especially to Prof. A. Meher Prasad, Prof. R. Krishna Kumar and Dr. P. N. Dileep and the late Prof. C. S. Krishnamoorthy.

My parents have been a constant source of inspiration throughout my life. I am extremely grateful to them for providing me with opportunities to pursue my studies at the highest level possible.

I would also like to thank my brothers, Dr. Vinu Unnithan Unnikrishnan and Mr. Vipin Unnithan, for their love and understanding. The immense help and affection of Dr. Vinu Unnikrishnan, my colleague and fellow researcher, during my stay at TAMU is deeply appreciated. I would also like to thank my sister-in-law, Mrs. Deepa Sobha, for her help and support. Finally, I would like to thank my wife, Mrs. Ragi Unnithan, for her love and understanding towards the completion of this research work.

TABLE OF CONTENTS

CHAPTER Page

CHAPTER Page

LIST OF FIGURES

Page

Page

Page

LIST OF TABLES

CHAPTER I

INTRODUCTION

A. Background

Biochemical and biomechanical stimuli affects the physiological response of biological materials critical for the functioning of organs. For example, hearing is aided by the conversion of mechanical vibration into electrical signals that travel to the brain; compression and dilation of arterial walls in response to blood flow patterns; growth and remodeling of tissues to external stress as in bones following fracture. The biochemical response of the cells and tissues to external mechanical stimuli is called *mechanotransduction,* and it involves interactions at the tissue, cellular and molecular level. The basic mechanism of transduction is still not clearly understood, and is an active area of research involving experimental and theoretical works. Experimental methods are required to stimulate the biological system and identify its physiological response while the correlation between the stimulation and response is achieved through mathematical models. Mathematical modeling of the distribution and magnitude of mechanical forces corresponding to different stimulation procedures forms the first step towards understanding the mechanotransduction in biological systems. For the correlation of experimental results, an accurate representation of the external stimulation and material model is required. One of the potential applications of such a mathematical model is in stem cell research. Stem cells are non-specific cells that

---

This dissertation follows the style of Journal of Biomechanical Engineering.

can develop into specialized cells through external stimuli like mechanical forces. Studies on the force distribution on stem cells and its corresponding physiological response would immensely help in designing cells for specific purposes. Thus, the primary focus of this research work is the development of mathematical models for cells and tissues to analyze its response to external mechanical loading.

The response of a normal and pathological biological structure is drastically different. The alteration in the sensing and material property is the primary reason behind the change in the physiological response. Of late, the variation in the response of the cells and tissues are used to determine the pathological nature of these materials. Detection of malaria affected cells through cell extension and compression of tissues for tumor detection are some of the examples. So, along with the determination of stress distribution in the biomaterials, it is aimed to implement the mathematical models to predict the behavior of pathological cells for diagnostic purposes and also in tissue engineering.

B. Motivation

A *generalized cell*, which consists of features from all cell types, is shown in Figure 1.1. The major parts of the generalized cell are cytoplasm, nucleus and cell membrane. The cytoplasm consists of biopolymer filaments called cytoskeleton. Actin, microtubule, and intermediate filaments are the three main cytoskeletal filaments providing stiffness to the cell structure. Scanned images and experimental procedures have shown that there exist regions in cytoplasm having distinct physical properties.

Through suitable experimental and theoretical formulations, the mechanical properties of cells have been derived by a number of researchers [1-3]. These derived material properties have found to vary by orders of magnitude even for the same cell type. The primary cause of such a disparity is attributed to the stimulation process and the theoretical model used in interpreting the experimental data [4]. This drawback can only be overcome by developing a sound mathematical framework correlating the material of the cell with the evaluation of the experimental data.

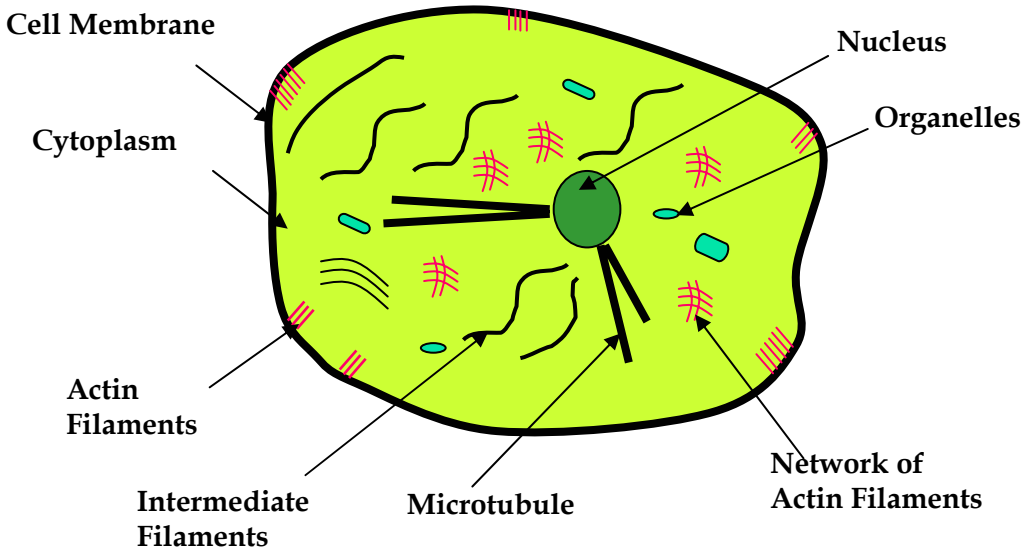

Figure 1.1. Schematic representation of a generalized cell.

The contribution of the cytoskeletal filaments, especially the actin stress fibers, in influencing the mechanical properties of cells is well established in literature [5, 6]. Rotsch and Radmacher [5] reported a considerable reduction in the elastic modulus of cells when treated with actin disruptive chemicals. Similar findings were also published

by other authors [7, 8], and it is reported that the stiffness of the cell reduces in certain pathological conditions like cancer [9, 10]. A precise representation of the anisotropic, nonlinear behavior of the cytoskeletal architecture is required for any computational analysis of a living cell. The homogenous material property definition of the cell is far from being accurate, especially for an adherent cell in which stress fiber introduces significant inhomogeneity.

Discrete cell models like the cellular tensegrity models [11], which represent the cell using a finite number of cytoskeletal filaments, have limitations in studying cell behavior. These limitations have led to a number of researchers turning towards continuum based models through the use of simplifying assumptions. Most of the earlier works, based on continuum hypothesis, homogenize the entire cell and do not explicitly consider the effect of inhomogeneity of the cell, with some exceptions being the works of [2, 3, 6]. These have lead to nonphysical correlation of the experimentally observed parameters to the mechanical characteristics of the cell. To overcome such a limitation, a constitutive model capable of accounting for the inhomogeneity of the cytoplasm is proposed in this dissertation.

Mechanical modeling of single cells would be extremely useful in understanding the behavior of cells in an experimental setup. *In-vivo* response of cells requires mathematical modeling of the embedding environment like fibers and fluid making the extra cellular matrix. As the transmission of mechanical stimuli in cells occurs either through the extra cellular matrix surrounding the cells the determination

of mechanical properties of the surrounding matrix of the cells is necessary for the development of a comprehensive mathematical model for cell.

Physiological importance of cell response when subjected to shear stress due to fluid flow as in blood-arterial wall interface, cartilage-synovial fluid interface also cannot be neglected. Mechanical stress on the tissue lining of the arterial walls causes diseases like atherosclerosis. Therefore, mathematical modeling of fluid interfaces is critical in the study of normal and pathological tissue behavior. The main difficulty in the analysis of fluid-tissue interfaces is the modeling of matching conditions at the interfaces. In this work, along with the mathematical modeling of cells, macroscopic behavior of soft tissues as well as fluid-tissue interface is also carried out.

Soft tissues like tendon ligament articular cartilages are multiphasic materials composed of a mixture of collagen/elastin fibrils, water, glycoaminoglycans and cells. The presence of large amounts of fluid in a solid matrix of collagen, cells and other proteins greatly influences the behavior of soft tissues. The effect of this interstitial fluid is more pronounced in the deformation characteristics of soft tissues like cartilage and skin. Articular cartilage, the widely investigated soft tissue, is often termed as a multiphasic, nonlinearly permeable viscoelastic material consisting of solid organic matrix (collagen fibrils in a gel of proteoglycans, cells) and a liquid phase predominantly water [12]. Biphasic theories have been extensively used in the modeling of similar tissues, where it assumes a coexistence of solid and fluid medium [13-16]. The interaction between the different phases drives the physical characteristics of these media Single phase solid materials, using linear elastic, viscoelastic properties have also

been used extensively in the modeling of tissues like arterial wall [17]. The single phase models can be considered as a special case of the multiphase models. In this scenario, we propose to study the mechanics of soft tissues through the multiphasic material models which could be converted to a single phase model depending on the type of problems.

Fluid-structure interaction problems, as applied to biomechanical systems, have been solved using a wide range of methods [18-20]. A sequential solving of the individual solid and fluid phases to coupled algorithm with a biphasic representation of tissue have been developed to study the interactions [21-24]. A new fluid-tissue interface finite element model to study blood tissue interactions is developed in this dissertation.

C. Objective

The different stages in the application of computational model to a complex system like biological cells/tissues are: a) development of a mathematical model, b) numerical solution of the mathematical model, and c) verification and implementation of the model to study cell/tissue behavior.

The main objective of this dissertation is to develop a computational framework for the mechanical behavior of eukaryotic cells (cells with nucleus). The primary steps undertaken in the modeling of cells are as follows:

a. identify primary microcellular components responsible for the biomechanical behavior of cells.

b. develop constitutive models of biological cells based on microcellular components.

c. implement the proposed constitutive models in the finite element analysis of cells.

d. study the behavior of pathological cells (cancer).

To understand the behavior of cells when embedded in a tissue structure and to study the physiological environment for cells subjected to fluid shear stress, a biphasic model of soft tissue is developed. The major objectives in modeling in soft tissue modeling are

a. develop constitutive models of soft tissues and study fluid-tissue interactions, and

b. study behavior of artery walls subjected to blood flow.

The cell-soft tissue model is implemented to study the response of pathological cells so as to aid in the development of a diagnostic tool. The flow behavior through an artery and compression testing on cancer cells are the main issues that are undertaken, and they involve the following features:

a. development of the biphasic representation for arterial walls.

b. implementation of the proposed constitutive framework to study flow behavior of blood through healthy and stenosed artery wall.

c. computational model development of cancer cell and AFM testing.

Physiological behavior of cells and tissues are dependent on the transfer of nutrients and proteins in the tissues. So, a model to study transfer of nutrients and proteins from fluid into tissues by

a. incorporating mass transfer of macromolecule into the fluid-tissue finite element model,
b. studying the influence on flow characteristics on LDL deposition in the artery wall, and
c. distribution of nutrients in a controlled environment for tissue engineering application.

This dissertation is organized as follows. The development of a mechanical formulation of cell accounting for the inhomogeneity of the cytoplasm is given in Chapter II. The validation of the constitutive model using finite element analysis by atomic force microscopy (AFM) and magnetic twisting cytometry (MTC) is presented in the chapter. A good correlation between simulated results and experimental values are observed from the analysis. In this chapter, the probable cause of difference in the derived mechanical property of cell is also identified.

In Chapter III, the material properties of the extra cellular matrix surrounding the cells in a soft tissue is analyzed using a biphasic model. The biphasic material model is extended to study fluid-tissue interface to model blood flow through a healthy and diseased artery. The variations in the fluid flow and behavior of artery wall is also analyzed in this chapter.

Chapter IV studies the effects of cancer on the material property of the cell. Using the constitutive model developed in Chapter II, and with the identification of cytoskeletal filament density the material properties are derived in this chapter. AFM simulation for a normal and cancerous cell is carried out and the results are found to be in good correlation with experimentally derived values.

Analysis of mass transfer occurring in blood-arterial wall interface and also in a bioreactor for tissue engineering is presented in Chapter V. The fluid-biphasic interface model is extended to incorporate mass transfer phenomenon in this chapter. The finite element modeling of low density lipoprotein transfer in arterial wall and glucose distribution in a hollow fiber membrane bioreactor is presented in this chapter.

Finally, the dissertation concludes with a summary and future works in Chapter VI.

CHAPTER II

COMPUTATIONAL MODELING OF BIOLOGICAL CELL

A. Introduction

Cell is the fundamental unit of any living organism and has long been observed to respond physiologically to external mechanical stimuli. The first step towards understanding the physiological behavior is to comprehend its response to external mechanical stimuli. Through suitable experimental and theoretical formulations the mechanical properties of cells have been derived by a number of researchers [1-3, 8]. These derived material properties have found to vary by orders of magnitude even for the same cell type. The primary cause of such a disparity is attributed to the stimulation process, and the theoretical model used in interpreting the experimental data [4]. This drawback is to be overcome by the developing a sound mathematical framework correlating the material of the cell with the evaluation of the experimental data.

B. Cell Physiology

Cytoplasm, cell membrane, and nucleus are the main structural components of the cell. Cytoplasm consists of fluid like cytosol containing organelles (mitochondria, nucleus, etc), the cytoskeleton, and a variety of other molecules. Cytoskeleton, which forms the biomechanical framework, is responsible for maintaining the structural integrity and also the distribution of forces in a cell. The organelles present in cytosol, except for the nucleus, do not contribute significantly to the structural integrity of a cell

and are generally neglected in mechanical modeling of cell. The major components of cells are explained below.

1. Cytoskeleton

Cytoskeleton is a complex network of protein filaments consisting of: actin, microtubule and intermediate filaments distributed throughout the cytoplasm. The filaments help the cell to adopt a variety of shapes during cellular motion and also act as pathways for transfer of organelles inside the cell. Cytoskeleton consists of three filaments: actin, intermediate filaments and microtubule. Figure 2.1 shows the distribution of actin filaments (marked as green), microtubules (as red) in an adherent bovine cell. The cytoskeletal filaments have dissimilar characteristics and thus their contribution to overall cell response is dissimilar. It has been found experimentally that the actin has higher stiffness than the microtubule, but fails at lower extensions (Figure 2.2). The intermediate filaments have characteristics between the two. The interactions of the cytoskeleton with one another and with accessory proteins are responsible for the biological response of the cell.

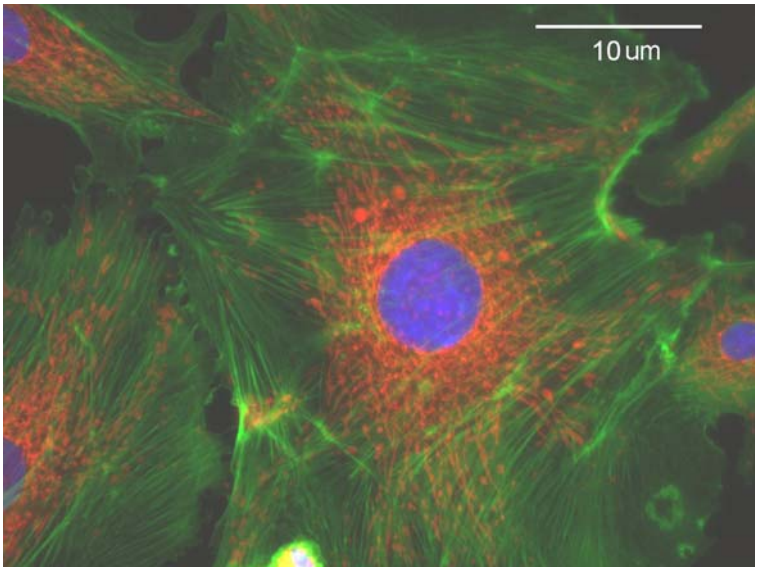

Figure 2.1. Stained image of bovine cell, green and red indicates cytoskeletal filaments and blue is the nucleus.

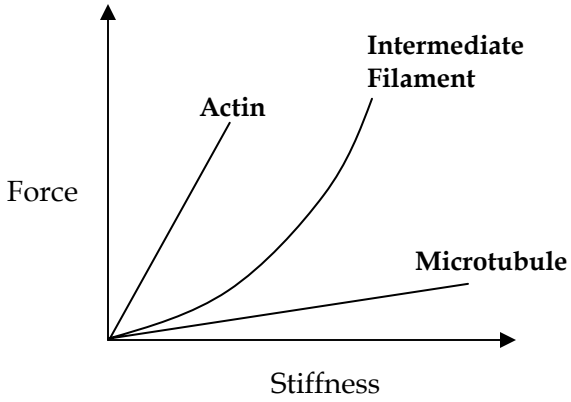

Figure 2.2. Behavior of cytoskeletal filaments.

Actin Filament: Actin filaments are formed by the polymerization of actin protein monomers and have a diameter of approximately 8nm. Actin is the abundant protein in many eukaryotic cells and constitutes about 5-10% of the total protein content

in a cell. They are distributed throughout the cell with typical concentrations of 1-5mg/ml. Actin filaments in the presence of the Actin Binding Proteins (ABPs), like filamin and fimbrin, forms a series of networks or bundles. Two prominent structures formed by actin filaments are the actin cortex, and stress fibers. Actin cortex is a three-dimensional networks formed as a thick band below the plasma membrane providing additional strength to the membrane. Actin stress fibers are formed by the bundling of actin filaments through rigid connections in an adherent cell. The stress fibers originate from the cortical layer where it connects to the plasma membrane through focal points and either connects with another focal point or would end in a network of other cytoskeletal filaments. They act as structural regulators within the cells influencing cell behavior like adhesion and cell contraction.

Intermediate Filaments (IF): Intermediate filaments are woven rope like structures, slightly thicker than F-actin, with a diameter of 8-10 nm. Unlike actin filaments, the fundamental units of intermediate filaments are fibrous proteins of 2-3 nm wide. Keratin, vimentin, neurofilament, desmin are some of the intermediate filaments which comes under the broad classification of Type I, Type II and Type III intermediate filaments. The intermediate filament network envelopes the nucleus and is closely interconnected with the microtubule filaments extending throughout the cytoplasm. The interrelation between intermediate filaments and microtubule is largely unknown though it is believed that MT pulls the intermediate filaments towards the membrane [25]. The primary function of intermediate filament is to provide mechanical stability to the cytoplasm and the nucleus.

Microtubules (MT): Microtubules are the thickest of the cytoskeletal filaments with a diameter of 23-25 nm made of alpha and beta tubulin subunits. They are formed through the polymerization of tubulin units and are found to radiate from the centrosome. Unlike the intermediate filaments and the actin filaments, microtubule is distributed across the cytoplasm as individual filaments. Microtubule acts as contractile members in the cytoskeleton, a view deduced from the fact that cells become stiffer when treated with microtubule disruptive chemicals [5]. Apart from providing structural stability, microtubules also act as pathways for the transfer of organelles inside the cytoplasm. They also help in the cellular division by forming a polarized region due to difference in the arrangement of alpha and beta tubulin units. Similar to the ABPs, the Microtubule Binding Proteins, (MBPs) stabilize the organization of the microtubule and also acts as mediators in their interactions with other cell components.

Experimental and theoretical works have shown that the mechanical properties of the cells, like adhesion and viscoelastic nature, are depended on these cytoskeletal framework [26, 27]. The changes caused by pathological conditions like malaria; aging and cancer on the cellular behavior have also been correlated to the structural and morphological changes in the cytoskeleton [10]. Apart from the deformations, cell filaments are also constantly in the process of polymerization and depolymerization inducing additional changes in these load bearing components.

2. Cytosol and organelles

The cytosol is a fluid medium in the cytoplasm consisting of the organelles and the cytoskeleton. Cytosol aids in the biological response of the cell and preserves the incompressible nature of cell. The organelles present in cytosol, except for the nucleus, do not contribute significantly to the structural integrity of a cell. So these effects are not considered for computational analysis in most of the cases. Nucleus occupies a volume of nearly 20% of cytosol has a significant bearing on the behavior of the cell (see Figure 2.1). Structurally it can be considered as a single entity and experimentally it is found to have a shear modulus higher than the cytoplasm [28]. The cytosol is responsible for the viscoelastic nature of the cell.

3. Cell membrane

The cell membrane is composed of a semi permeable bilipid layer. The effect of the cell membrane on the structural property varies according to the type of the cell. For example, in erythrocyte the cell membrane contributes significantly to the structural behavior of the cell. In constant, the influence of plasma membrane for an adherent cell is negligible. Cell membrane is responsible for adherence and the motion of cell over a substrate. Adhesion is achieved through a series of transmembrane proteins which connects the extra cellular matrix with the cytoskeleton. Movement of cell is achieved through the lamellipods and through a series of polymerization and depolymerization of cell skeleton. Focal points are created in the membrane which connects with the cytoskeleton and that helps in the movement of cell.

C. Formulation of Constitutive Model

1. Mechanical models of cell

Cells have long been observed to respond physiologically to mechanical forces. They are highly integrated systems capable of "sensing" external forces. The external forces like shear due to blood flow changes the sub-cellular organization thereby triggering regulatory physiological information vital to the cell. The need to comprehend and predict the effect of forces on a cell instigated the development of mathematical cell models. The limited knowledge in the behavior of the cell has prevented the development of a universal constitutive cell model. A wide range of models applicable to distinct types and functions of cell are available in the literature [6, 29]. These cell models can be broadly classified into discrete and continuum based models.

In discrete cell model a finite number of load bearing members are employed to explain the cell behavior. In these models, analysis is concentrated on the behavior of the individual members as well as a network of members formed through a series of interconnections called the nodal points. Cellular tensegrity models, percolation based models are examples of discrete mechanical models of cell. The widely accepted cellular tensegrity model developed by Ingber and colleagues [11] considers the whole cell to be a prestressed tensegrity structure. Continuum based models assumes the cell satisfies the continuum hypotheses. It treats the cell to be composed of material that is continuous in space, called the "continuum". The continuum assumption allows the definition of quantities like stress, strain, energy at every point in the material.

Governing equations are developed using these quantities to predict the mechanical behavior of the cell when subjected to relevant boundary conditions. The continuum mechanical models available in the literature range from simple directly solvable models to complex models that require numerical solution tools like finite element method.

Most of the mechanical cell models consider the entire cytoplasm as a single unit, a fact which is far from being physiologically accurate. These models, even though reduces the mechanical parameters, fails to capture the properties caused by the structural inhomogeneity of cytoplasm, like actin network layer, stress fibers etc. This becomes a crucial factor in the study of mechanical behavior of cells *in-vivo* as well as in the determination of mechanical parameters using experimental techniques like atomic force microscopy and micropipette suction.

In this work, a mechanical model of an adherent cell based on continuum micromechanics considering the structural inhomogeneity of the cytoplasm is developed. The homogenized cytoplasm is considered to be a matrix reinforced with stress fibers; the periplasm or the actin cortex as a layer of semi-flexible polymer networks and the nucleus are the various constituents whose properties considered individually. The degree of influence of individual layers on the mechanical response of a cell using atomic force microscopy is also studied in this work. This work also deals with the effect of actin filaments (stress-fibers) on the mechanical properties of the cell and its variations in the presence of actin disrupting chemicals like cytochalasin D so as to provide a foundation towards building a tissue model to predict cancer growth.

2. Theoretical formulation

Numerous scanned images of cells have established the genuineness of a text book image of a compartmentalized cell structure [5, 25, 30, 31]. The cell can be divided into three distinct layers: an outer cortical layer formed by the actin filament networks (outer cytoplasm - cortex); inner cytoplasmic region, and the nucleus. Most of the previous works on continuum based constitutive modeling of cell use a homogenous isotropic model of the cytoplasm so as to reduce the number of unknown material parameters. However, such simplifications limit the applicability of the model in connecting the physiological phenomenon with the mechanical properties of the cell. For example, when a cell is attached to a substrate, the mechanical properties are altered due to the formation of stress fibers, a fact that cannot be explained with the available continuum cell models. To overcome such a limitation, a constitutive model capable of accounting the inhomogeneous cytoplasm is carried out in this work. The inhomogeneity is due to the presence of stress fibers that originate from the focal points and end either in another focal point or in the filament network and it is also due to the actin cortex which forms a layer beneath the cell membrane. Using the micromechanics approach, and treating the cell as a fiber-reinforced composite medium satisfying the continuum hypothesis, the material modeling is carried out. The Mori-Tanaka method of homogenization that considers the amount of fiber formed as well as its orientation is employed to develop the material model of a cell. Modeling of the actin cortex and the cytoplasm with the nucleus as an inclusion is outlined next.

Modeling of Cortical Cytoplasm: The actin cortex region is modeled as a hyperelastic material by assuming the cortical region to be of an isotropic distribution of the actin network filaments. The general form of strain energy is given as [32]

$$W(I_1, I_2, I_3) = \sum_{p,q,r=0}^{\infty} c_{pqr} \left(I_1 - 3\right)^p \left(I_2 - 3\right)^q \left(I_3 - 3\right)^r \tag{2.1}$$

where c_{pqr} are the material properties, (I_1, I_2, I_3) are the strain invariants that can be expressed in terms of the principal stretches $(\lambda_1, \lambda_2, \lambda_3)$ as

$$\begin{aligned} I_1 &= \lambda_1^2 + \lambda_2^2 + \lambda_3^2 \\ I_2 &= \lambda_1^2\lambda_3^2 + \lambda_2^2\lambda_1^2 + \lambda_3^2\lambda_2^2 \\ I_3 &= \lambda_1^2\lambda_2^2\lambda_3^2 \end{aligned} \tag{2.2}$$

Modeling of Inner Cytoplasm: Cytoplasm is composed of an organized network of cytoskeletal filaments of actin, intermediate filaments and microtubules. The distribution of the cytoskeletal filaments differs according to the type and environment of the cell, thus changing their material properties. The stress fibers are contractile bundles of actin filaments [25] having diameters in the range of one-tenths of microns. Experimental and theoretical works have shown that the cell behaviors like adhesion and motion are dependent on these stress fibers [26, 27]. The constitutive model developed in this work considers the stress fibers as being distributed in the cytoplasm, satisfying the continuum hypothesis. With an idealization of the cytoplasm to be a "fiber-reinforced composite", the effective property is obtained by borrowing ideas from the widely accepted homogenization theories in composite materials. The

homogenization is achieved by replacing the heterogeneous composite material by an equivalent homogeneous continuum using a suitable homogenization technique.

The property of a homogeneous continuum is based on a statistically homogeneous volume element, called the representative volume element (RVE). The RVE is a representation of the material at the microscale: small in comparison to the macrostructure (i.e., whole cell) to have negligible influence on macroscopic property, but large in comparison to the microstructure (i.e., stress fibers) to have a meaningful sampling. In order to have a good sampling of the entire domain, the selected RVE should ideally have a couple of stress fibers. As an example, RVE with dimensions of unit microns, encompassing three stress fibers having a mean diameter of 0.1 microns, would have fiber volume fraction of 9.428%. Based on the stress fiber volume fraction the effective modulus of an equivalent homogenized structure could be calculated.

A brief explanation of the micromechanics approach is presented next for completeness; detailed descriptions can be found in [33]. In any region of an inhomogeneous material, the microscopic strain and stress fields are given by relations of the form

$$\begin{aligned} \varepsilon(\mathbf{x}) &= \mathbf{A}(\mathbf{x})\langle\varepsilon\rangle \\ \sigma(\mathbf{x}) &= \mathbf{B}(\mathbf{x})\langle\sigma\rangle \end{aligned} \tag{2.3}$$

where A and B are the stress and strain concentration tensors, ε and σ are the strain and stress tensors, respectively, and

$$\langle \varepsilon \rangle = \frac{1}{\Omega} \int_{\Omega} \varepsilon(\mathbf{x})\, d\Omega$$
$$\langle \sigma \rangle = \frac{1}{\Omega} \int_{\Omega} \sigma(\mathbf{x})\, d\Omega \tag{2.4}$$

denotes the volume-averaged stress and strain tensors, respectively, over the RVE volume Ω.

Various approximations techniques, like variational bounds or mean field method, are invoked to obtain the concentration tensors due to the complexity of real micro-structures. The mean field methods are generally based on Eshelby equivalent inclusion formulation [34]. When an elastic homogeneous ellipsoidal inclusion in infinite matrix is subjected to a uniform strain field ε_t, called the eigenstrain, uniform stress and uniform strain is induced in the constrained inclusion. As an improvement over the Eshelby type formulation, Mori-Tanaka method considers the average strain as being caused by the inclusion as well as the perturbed matrix stress due to other reinforcements.

The relation for the effective strain in the Mori-Tanaka method is given as

$$\langle \varepsilon \rangle^1 = \mathbf{A}\mathbf{A}_M \langle \varepsilon \rangle^0 \tag{2.5}$$

where $\mathbf{A}_M$ is the influence of the inclusion, and it is represented as

$$\mathbf{A}_M = \mathbf{A}\left[\left(1 - v_f\right)\mathbf{I} + v_f \mathbf{A}\right]^{-1} \tag{2.6}$$

and A is represented as

$$\mathbf{A} = \left[\mathbf{I} + \mathbf{S}\mathbf{C}^0 \left(\mathbf{E}^1 - \mathbf{E}^0 \right) \right]^{-1} \tag{2.7}$$

where, S is the Eshelby tensor, E is the elastic tensor, C is the compliance tensor , v_f is the volume fraction of fiber and 0 and 1 superscript indicates the matrix and fiber respectively. Thus from the strain concentration tensors the effective elastic property of the inhomogeneous matrix is calculated.

The effective material properties (E_{eff}) through the correlation between the averaged stress and average strains over the composite is given as

$$\langle \sigma \rangle = \mathbf{E}_{\mathbf{eff}} \langle \varepsilon \rangle \tag{2.8}$$

where, E_{eff} is the elastic tensor of an equivalent homogeneous material, which is a function of concentration tensors obtained from equations (2.6) and (2.7).

To develop a suitable material model of the cell capable of capturing the large deformations, a nonlinear material model of the cytoplasm is required. A standardized incremental linearization of the matrix-fiber composite is carried out to obtain the nonlinear stress strain behavior of the homogenized cytoplasm. Based on the above formulation, specific example on the modeling of an adherent cell having a random distribution of actin stress fibers in the cytoplasm and bounded by actin cortical layer is carried out.

D. Results

1. Constitutive modeling example

Actin cortex is considered as a semi-dilute polymer solution of actin filaments, cross-linked with actin binding proteins. Assuming a persistence length of 17 μm, with a mesh size 0.19 μm, the linear elastic shear modulus is calculated as 275 Pa for small strains [35]. The nonlinear stress strain behavior of the actin network is captured by introducing a neo-Hookean material model (Eqn (2.9)), using the calculated shear modulus with cortex treated as an incompressible material

$$W(I_1) = \frac{\mu_0}{2}\left(I_1 - 3\right) \tag{2.9}$$

where μ_0 is the small strain shear modulus.

The cytoplasm is considered as having randomly distributed stress fibers in a matrix of microtubules and intermediate filaments, as observed in various experiments. The cross-section of a typical adherent cell with a random distribution of actin stress fibers is shown in Figure 2.3. In this work, reinforcements in the form of stress fibers alone are considered in deriving the material properties of the cell. The matrix is assumed as a hyperelastic material, nearly incompressible with a small strain shear modulus of 100 Pa. The material properties of the stress fiber is taken from stretching tests carried out by Deguchi et al. [36], and Poisson's ratio of 0.33 is assumed. The linear effective modulus of the composite having a random distribution of the fiber in a uniform matrix is given as [37]

$$K_{eff} = K_1 + \frac{v_0}{\left\{\frac{1}{K_0 - K_1} + \frac{3v_1}{3K_1 + 3\mu_0 + \mu_1}\right\}}$$
$$\mu_{eff} = \mu_1 + \frac{v_0}{\left\{\frac{1}{\mu_0 - \mu_1} + \frac{2v_1}{5}\left[\frac{1}{\mu_0 + \mu_1} + \frac{1}{\mu_1 + \mu_0/(3-4\upsilon_0)} + \frac{1}{2(3K_1 + 3\mu_0 + \mu_1)}\right]\right\}} \quad (2.10)$$

where, μ is the shear modulus, K is the bulk modulus, υ Poisson's ratio, v the volume fraction of the materials defined by the subscripts: 0=matrix, 1=fiber, eff=effective matrix.

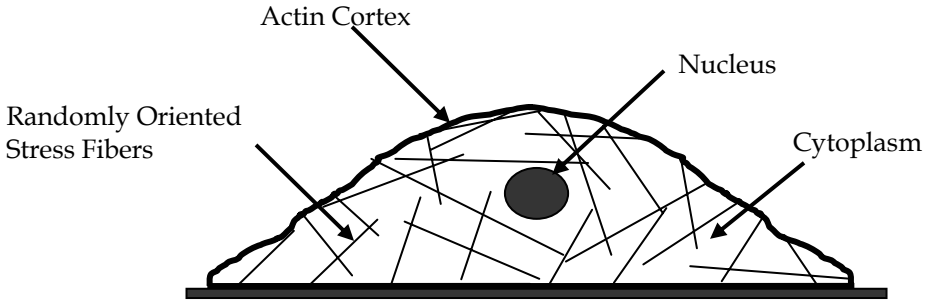

Figure 2.3. The cross section of a typical adherent cell showing the random distribution of actin stress fibers.

In literature, various methods are available to model the homogenized nonlinear behavior of the composite [33]. In this work, the nonlinear behavior is captured using an incremental approach. The stress-strain curve for the material after homogenization for different volume fractions of the fiber is shown in Figure 2.4. As the volume fraction of the fiber decreases the property of matrix becomes less influenced by the fiber, thus decreasing the composite stiffness. The same effect is observed in many experimental

studies, and they have reported a decrease in the measured elastic modulus of cell when treated with actin disrupting chemicals [7]. For sufficiently large values of stress fiber volume fraction, Poisson's ratio decreases, reaching the fiber Poisson's ratio as shown in Figure 2.5 (0.35 for a stress fiber volume fraction of 2.5%). This is a significant observation as it partly explains the wide differences reported in Poisson's ratio values ranging from a nearly incompressible value to the range of 0.25±0.05. The nucleus is assumed to be linear elastic with Young's modulus of 400 Pa and Poisson's ratio of 0.35, as reported in [28].

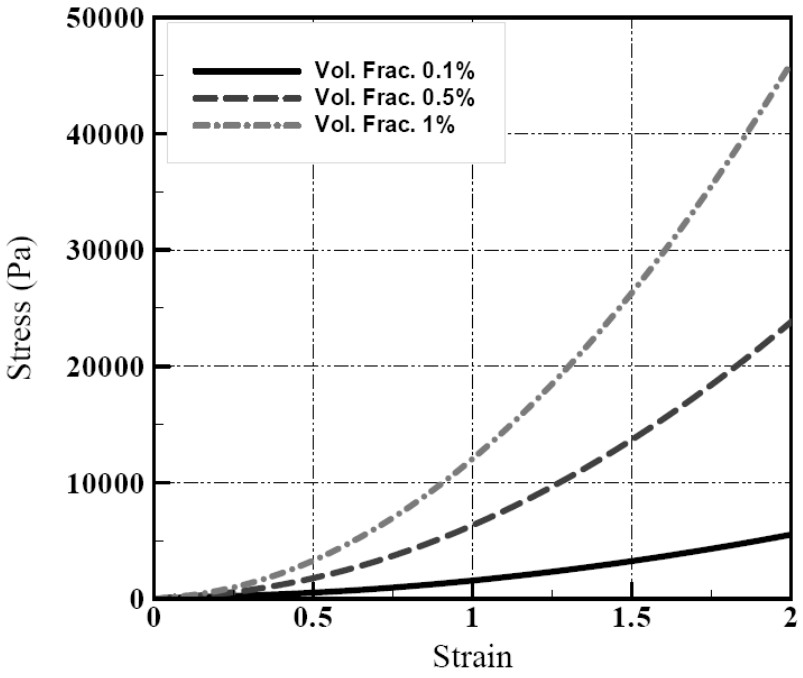

Figure 2.4. The stress-strain curve for the material after homogenization for different volume fractions of the fiber.

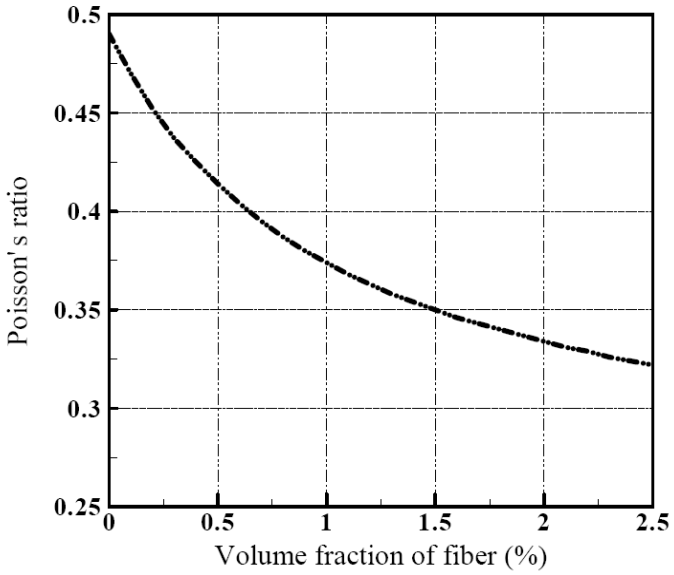

Figure 2.5. The effect of stress fiber volume fraction on Poisson's ratio of the composite.

2. Numerical verification-finite element analysis

The effectiveness of the developed model in accurately interpreting the experimental results is illustrated through the numerical simulation of two experimental procedures in cell mechanics: Atomic Force Microscopy (AFM) and Magnetic Twisting Cytometry (MTC). Following assumptions are considered in this investigation:

a) The material is elastic.

b) The presence of the local inhomogeneity in the probing area is neglected.

c) The stress fibers are randomly distributed in the cytoplasm creating an isotropic material, whose effective properties are calculated using micromechanics.

Atomic Force Microscopy (AFM): AFM experiment is widely accepted in the area of cell mechanics due to its high quality of derivable structural and functional information. In general, the properties derived from the interpretation of data from the AFM experiments are based on certain assumptions. These assumptions become invalid in the case of biological cell due to: large deformation compared to the cell size; inherent inhomogeneity of the cytoplasm, and so on. Thus, in the interpretation of the results obtained from the atomic force microscopy, a more detailed numerical approach like the finite element method is required [38]. The implementation of the developed constitutive model of the cytoplasm in the numerical study of AFM is described below.

Loading and boundary condition: Finite element analysis [39, 40] of an AFM indentation using spherical indenter of 0.4 microns diameter acting on the cell surface above the nucleus is carried out. The material properties are obtained through the procedure outlined in the previous section. The cell geometry considered is of 3.5 microns in half width, 3.0 microns in height, with a nucleus of 0.9 microns diameter at a height of 0.75 microns from the base. The cortical region is assumed to be 0.2 microns thick and the cross section of the cell is as shown in Figure 2.3. The cell is assumed to be axisymmetric with a rigid spherical indenter acting on the cell surface above the nucleus. Displacement boundary conditions are applied on the indenter and also at the base of the cell, while symmetric boundary conditions are taken along the axis of symmetry. The indenter is given a vertical displacement and the cell base is constrained in all directions to assume a perfect contact with the substrate. The symmetric half cell model is discretized using an axisymmetric finite element with a finer mesh towards

the top of the cell (Figure 2.6). Finite element analysis is performed using commercial software, ABAQUS [41]. The finite element model consists of 2,637 nodes with a total of 2,746 linear axisymmetric elements. The material property of the cell is assumed to remain constant throughout the analysis and no active force generation is considered.

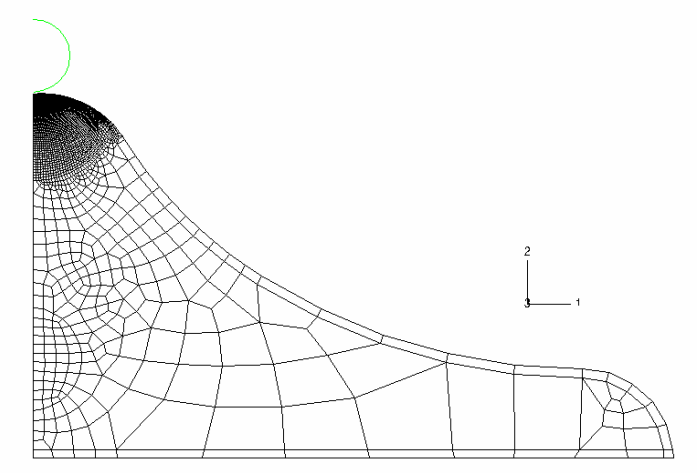

Figure 2.6. Half cell axisymmetric finite element model of the cell having a graded finer mesh towards the region of indentation.

Results: Numerical simulation of an AFM on a cell with a spherical indenter is carried out using ABAQUS [41]. The strain distribution of the cell with stress fiber volume fraction of 0.1% subjected to an indentation of 0.5 microns is shown in Figure 2.7. The actin cortical layer, which is in direct contact with the indenter, sustains the maximum deformation. The inner cytoplasm near the region of indentation also experiences very high strains and the intensity decreases away from the center. The total reaction force acting on the indenter is calculated by considering the horizontal

and vertical reaction forces at the reference point of the rigid indenter. To ascertain the effect of stress fibers on the reaction force, numerical simulations are carried out for cytoplasm having stress fibers volume fractions of 0.1% and 1%. The corresponding force deflection curve obtained from the analysis is shown in Figure 2.8. As expected, with an increase in the fiber volume fraction, the cytoplasm becomes stiffer and a higher reaction force is predicted for the same geometry and boundary conditions. A larger reaction force is needed to make the same indentation on a stiffer material compared to a softer material. The simulated force-deflection curve is compared with experimental force-deflection curves of cells L929 [7], and HCV29 & Hu609 [9]. It is evident from Figure 2.8 that a qualitative prediction of the force-deflection graph using the model developed herein matches well with the experimental results. This comparison is shown to highlight the trend of the force-deflection curve obtained from the analysis rather than a one-to-one numerical correlation with the experimental values. The variation between the numerical predictions and experimentally observed results could be due to the difference in the experimental parameters, like the indenter type and stress fiber volume fraction. The mapping of actin stress fiber influence to AFM indentation study is one of the advantages of the developed computational model over prevailing models, and it is immensely useful in understanding the behavior of a cell.

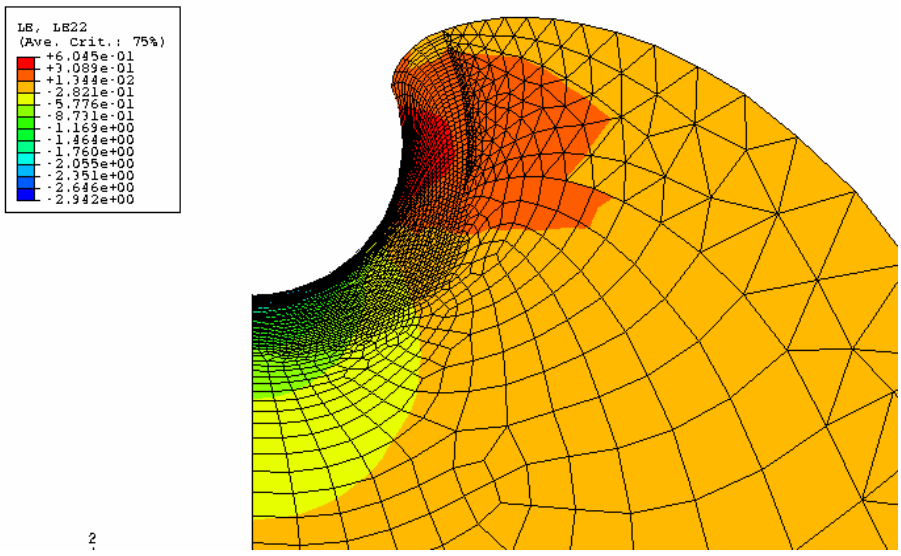

Figure 2.7. Strain distribution obtained from the finite element analysis of axisymmetric cell model due to an indentation of 0.5 microns on the cell.

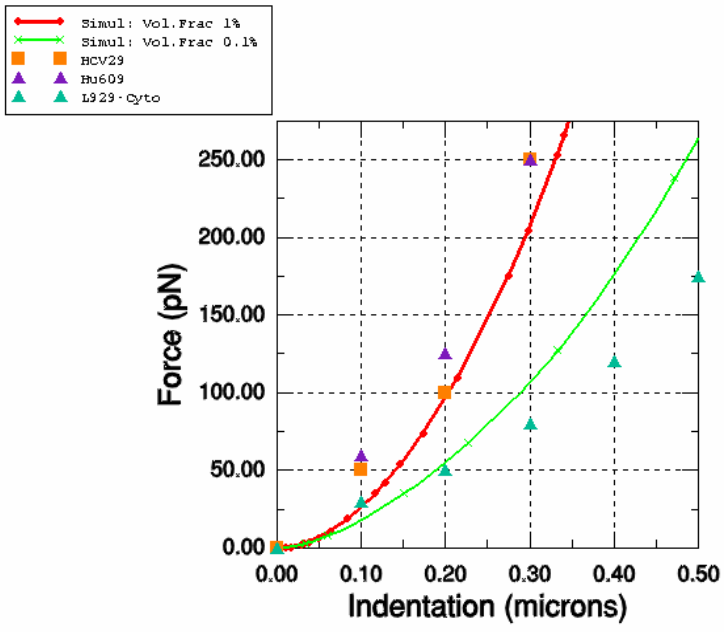

Figure 2.8. Force deflection curve for the cytoplasm having stress fiber volume fraction of 0.1 % and 1%.

Magnetic Twisting Cytometry: Magnetic Twisting Cytometry (MTC) is another experiment widely used to determine the mechanical property of the cell. Through a correlation between the magnetic force acting on the bead and the lateral bead displacement or through magnetic moment and angular rotation, the material properties of the cell are calculated. Most of the previous works on the simulation of MTC considers the entire cell to be a homogenous entity [3, 42]. Apart from the actin cortex, focal adhesion point generation, and thereby the stress fibers, also affects the determination of the material property from experimental methods [8]. With this background, we investigated the effectiveness of the developed computational model in the numerical simulation of MTC. The material properties are obtained using similar methods to that described for the atomic force microscopy in the previous section. To establish the influence of the stress fibers, their volume fraction is changed and corresponding force-displacement values are determined through the finite element analysis. The bead radius, indentation angle and cell geometry is kept constant for all the simulations.

Loading and Boundary Conditions: The cell geometry is modeled as a 3D rectangular block 20 microns long, 10 microns wide and 5 microns thick, with the spherical bead of 4 microns diameter making an indentation angle of 90 degrees at the centre of the block. The cortical thickness is assumed to be of 0.2 microns with the inner region being the cytoplasm (Figure 2.9). A symmetric loading and boundary condition is assumed, and only half of the indenter and material body is modeled. The finite element model consists of 3742 nodes with 3102 hexahedral hybrid (C3D8H) elements

with a finer mesh towards the bead region. The base of the block was constrained in all directions to create a cell fully adhered to the substrate and symmetric boundary conditions were applied to the half section. The bead centre was given a lateral force of 500 pN and the lateral displacement of the bead centre is determined from the analysis. The magnetic force was chosen based on the work by Karcher et al [2]. The bead and cell surface have a tied contact as no slippage between bead and surface is considered for the analysis.

Results: The displacement of the bead centre is obtained from the finite element analysis of a cell block having a cytoplasm with a random distribution of stress fiber and an isotropic actin cortex, subjected to an axial force of 500 pN. The strain induced in the cell block with a volume fraction of 0.1% stress fiber under the load is shown in Figure 2.10 (A &B). The Figure shows that large strains are induced at the actin cortex. The region directly below the bead shows less deformation in comparison to the deformation at either end of the bead-cell contact region. Figure 2.11 shows the vertical displacement distribution of the cell block due to the load at the centre of the bead.

The effect of stress fiber in the MTC simulation is shown in Figure 2.12, which indicates that as the volume fraction of the stress fiber increases a significant drop in the bead displacement occurs. This decrease in the displacement is an indication of the stiffening of the underlying material due to higher stress fiber volume fraction. To compare the simulated results with works by Ohayon et al. [43], the boundary condition in the finite element analysis was modified to model a torque instead of the lateral load at the bead center. Figure 2.13 compares the results from the literature and

the simulated bead rotations for different volume fractions of stress fibers subjected to torque at the bead center, and shows a good comparison with the published results. Also, as observed in the bead displacement behavior the bead rotation also decreases on increasing the volume fraction of stress fiber. Only a qualitative correlation is attempted since Ohayon et al. [43] used a linear elastic modulus of the cell compared to the nonlinear elastic model used in the present work.

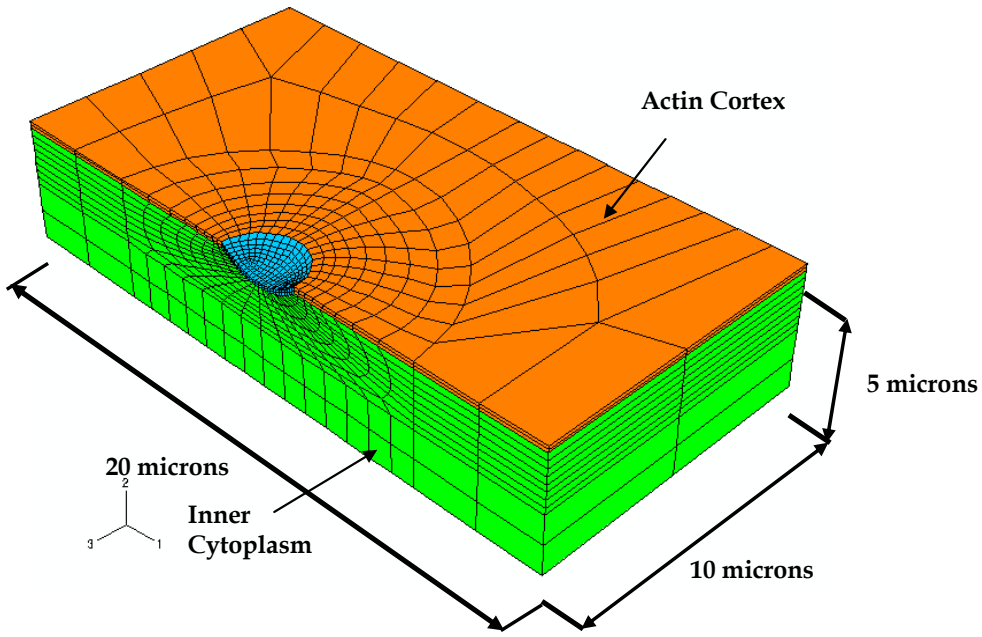

Figure 2.9. Finite element mesh of the cell block selected for MTC simulation.

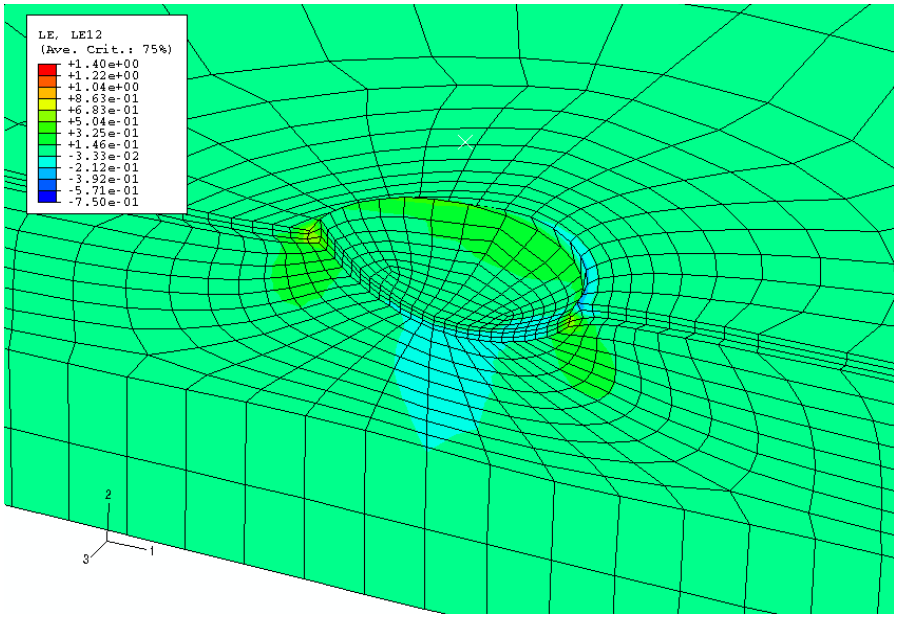

(a)

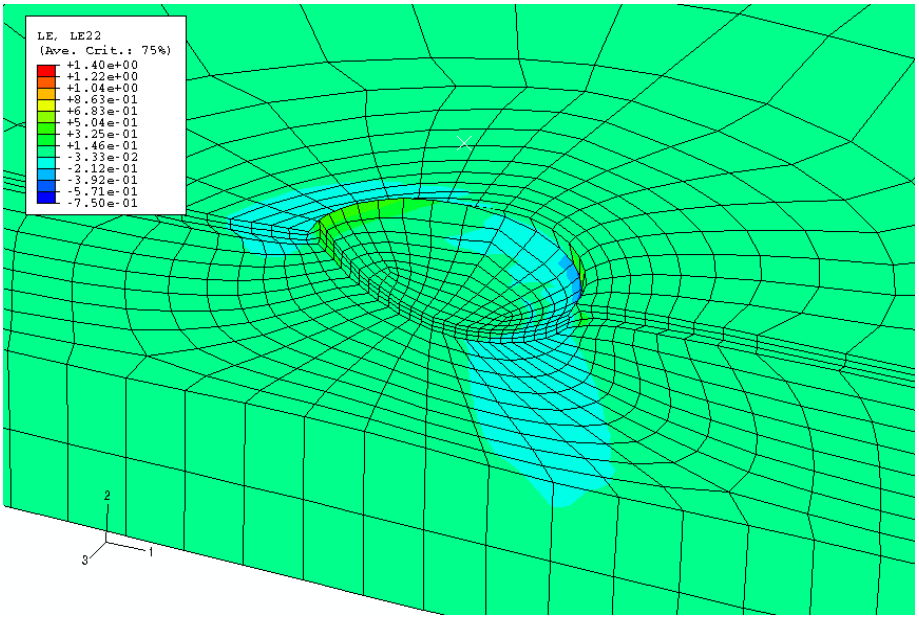

(b)

Figure 2.10. Strain distribution induced by bead displacement along 1-2 (a), and 2-2 (b) directions due to a lateral load of 500 pN.

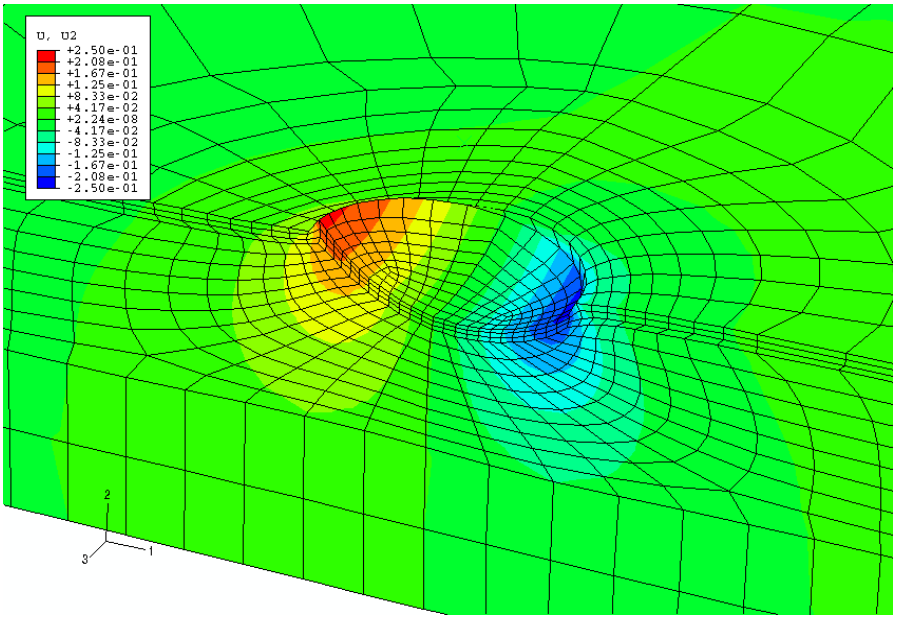

Figure 2.11. The vertical displacement distribution due the action of the load at the centre of the bead.

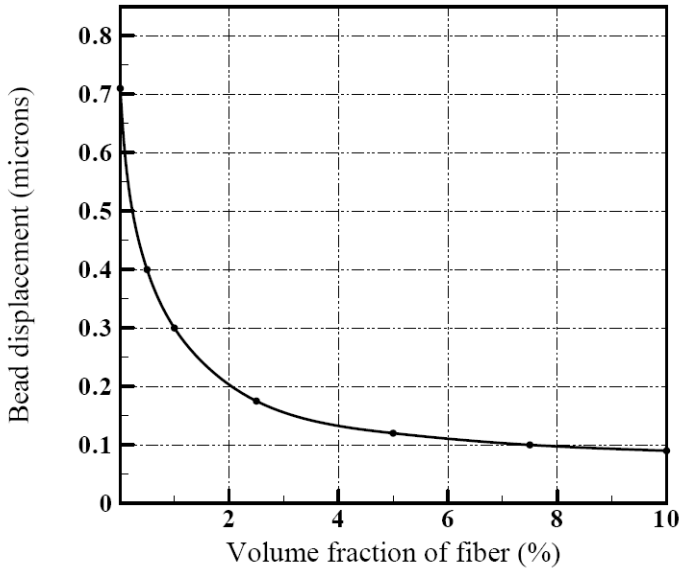

Figure 2.12. The variation of the displacement of the bead centre with the change in stress fiber volume fraction.

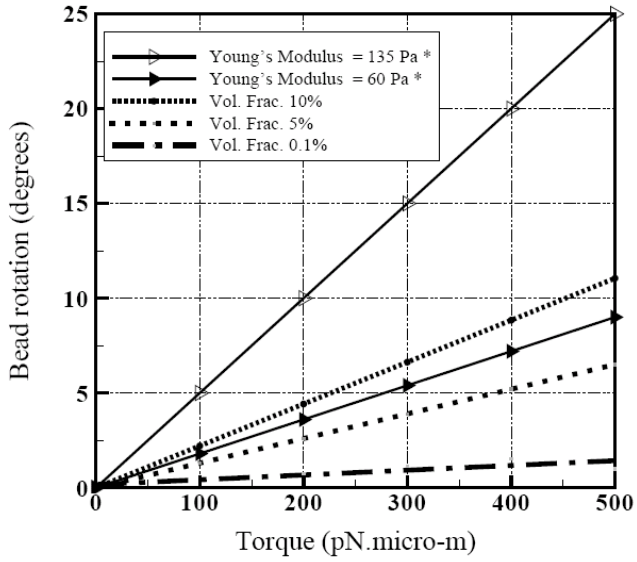

Figure 2.13. The comparison of bead rotation obtained from simulation with the results published in [43] (indicated by *) for a torque applied at the centre of the bead.

E. Discussion

Scanned images and experimental procedures have shown that there exist regions in cytoplasm having distinct mechanical properties. The homogenous material property definition of the cell is far from being accurate especially for an adherent cell in which stress fiber introduces significant inhomogeneity. Discrete cell models like the cellular tensegrity models, which model the cell using a finite number of cytoskeletal filaments, have limitations in studying cell behavior. These limitations have led to a number of researchers turning towards continuum based models through the use of simplifying assumptions. One of the major limitations of simplified continuum based models, as pointed by Ingber et al. [11], is their inability to provide specific predictions related to the functional contribution of cytoskeletal filaments as effectively as the

discrete model. In this work this limitation is overcome by modeling the cytoplasm as being reinforced with the stress fibers using a micromechanics approach. The work carried out here differs from earlier works in cell behavior modeling, as those works have either been from the discrete perspective or a homogenized continuum framework without explicitly modeling the stress fibers. Also, the method outlined in this chapter is capable of correlating experimentally determined parameters of a cell as a function of the amount of the stress fibers in the cytoplasm.

The correspondence of the volume fraction of stress fibers on the indentation for AFM and rotation/displacement of the MTC brings out the effect of the stress fibers on the mechanical properties of the cell, as illustrated in Figure 2.8 and Figure 2.10. The results from AFM simulation show that greater nonlinearity and small reaction force are observed at low volume fractions of stress fiber. The simulated results for low and high stress fiber volume fractions match qualitatively with the reported results [9, 43] on force indentation on the cell for a healthy and as well as diseased and actin disrupted cell. With an increase in the stress fiber volume fraction, the stiffness of the cell increases and the displacement/indentation reduces exponentially. This dependency of the cell stiffness on the stress fibers provides an understanding of the cause of wide discrepancies of stiffness obtained from experiments. It is also observed that actin cortical region suffers the maximum deformation during AFM and MTC experiments. Thus for an accurate computational model of the cell the actin cortex should be modeled separately from the inner cytoplasm.

For simplicity, the formulation adopted in this work considers only an elastic response, which is acceptable since the loading time is assumed to be very small. Also an isotropic behavior is assumed for the homogenized cytoplasm due to the random distribution of stress fibers. Experimental studies using 3-D MTC by Hu et al. [8] have shown that the orientation of stress fibers is also important in determining the cellular material properties. Even though the current study does not consider the anisotropic nature of the cell due to the stress fiber orientation, its implementation along the lines of continuum micromechanics is possible. This factor would be captured by the RVE which would have oriented fibers leading to anisotropic behavior of the homogenized continuum. Thus, a natural extension of the present work is to consider the viscoelastic components of the composite as well as to model the anisotropic properties of the cell due to aligned stress fibers.

F. Summary

A homogenized constitutive model of the cell incorporating the distribution and amount of stress fibers has been developed in this study. The validation of the constitutive model using the finite element analysis on two most conventional experimental techniques of atomic force microscopy and magnetic twisting cytometry has been carried out. A satisfactory correlation between the simulated results and previously published results corroborate the accuracy of the micromechanics model. Through this model, we have been able to state the stress fiber as a likely cause of the wide disparity in the above mentioned experimental results. Thus, through this model a

correlation of the mechanical behavior of the cell, its composition, and experimental results is developed, which would be extremely important in the field of cell mechanics.

CHAPTER III

ANALYSIS OF SOFT TISSUE ENVIRONMENT USING BIPHASIC MATERIAL MODEL

A. Introduction

The stimulus acting on cells *in-vivo* is altered by the properties of the surrounding environment. For example, cells response in soft tissues is influenced by the mechanical properties of the extra cellular matrix. So, to predict the behavior of cells *in-vivo*, the material properties of the environment should be included in the mathematical model. In this chapter, the behavior of soft tissues is analyzed using a biphasic material representation. A biphasic finite element model is developed and is also extended to model the tissue-fluid interfaces occurring in human body.

Common examples of the tissue-fluid interactions are a) blood flowing through the artery wall, and b) synovial fluid and cartilage interactions [20, 44]. The computational models to study fluid-structure interactions in biomechanics have primarily relied on either an iterative solution of the solid and fluid domains or a sequential solution of the entire domain using a coupled algorithm [18-20]. Iterative solutions methodologies are computationally very expensive and hence cannot be used for large applications. Proper identification of boundary conditions at the interface posed significant difficulties in numerical solution of sequential algorithm.

Complexity of the fluid-structure interactions in biomechanical systems due to the geometry and the material properties requires numerical techniques like finite

element methods. Representation of soft tissues as biphasic materials have led to the development of biphasic-fluid interaction models to study the fluid-structure interactions in biomechanics [45]. Physical phenomenon of a biphasic material is based on the characteristics of the coexisting solid and fluid phases and their interactions. Even though various studies on the application of biphasic theories with the finite element methods have been carried out [14, 46, 47], serious limitations in modeling the fluid-biphasic interfaces exists. Selection of accurate boundary conditions and its proper implementation in the finite element code is one of the major difficulties in the simulation of fluid-biphasic interfaces. A review of the various boundary conditions for study of fluid-structure interactions analysis using finite element method is provided by Alazmi et al. [48]. Lee et al. [21] analyzed the blood flow and arterial wall motion separately and then combined their effects using an iteratively coupled algorithm. A sequential treatment of tissue-fluid interface was considered by Chan et al. [22] using a biphasic representation of the tissue.

A new methodology to incorporate the fluid-biphasic interface is described in this chapter. A biphasic representation of the tissue is utilized in the development of the new algorithm. Suitable mathematical representation of the fluid and solid phases in the biphasic model of the tissue and through proper finite element implementation of the mathematical model the tissue-fluid interaction model is developed. The formulation is computationally less intensive, when compared to iterative solution and robust when compared to the transformation matrix algorithms. The proposed model is verified with standard fluid flow problems over a porous region and is applied in the

normal and diseased artery wall. This chapter is organized in the following manner: The biphasic approach adopted in solving the solid fluid interface is outlined in Section B. In Section C the finite element verification of the adopted method is detailed and the application of the developed methods in solving blood arterial wall behavior is shown in Section D. Finally, summary and conclusion are drawn in Section E.

B. Materials and Methods

A study of blood flow through the artery, or synovial fluid interaction with the cartilage requires an efficient computational methodology, capable of modeling a) the complicated geometry, b) representing the interface boundary conditions. The primary obstacle in a fluid-biphasic finite element model is the identification and implementation of matching interface boundary condition. Matching interface conditions for velocity, pressure and temperature in FE biphasic model is still not well established in literature [22, 48-52]. A detailed review of various descriptions of the FE boundary conditions is provided by Alazmi et al [48]. Satisfaction of continuity of mass, momentum and energy, lead to the implementation of additional boundary conditions and of transformation functions in the FE formulation, which increased computational complexity of the formulation and also made the formulation problem specific. In this work, a new formulation avoiding the above drawbacks is presented.

The computational domain selected for the finite element analysis, consists of a fluid domain Ω_F and a tissue domain Ω_T separated by the interfacial boundary Γ_I as shown in Figure 3.1. The entire domain is represented as a biphasic material having

different fluid phase volume fractions in the fluid and tissue domain. A review of constitutive modeling of the biphasic material, and its finite element implementation is outlined next.

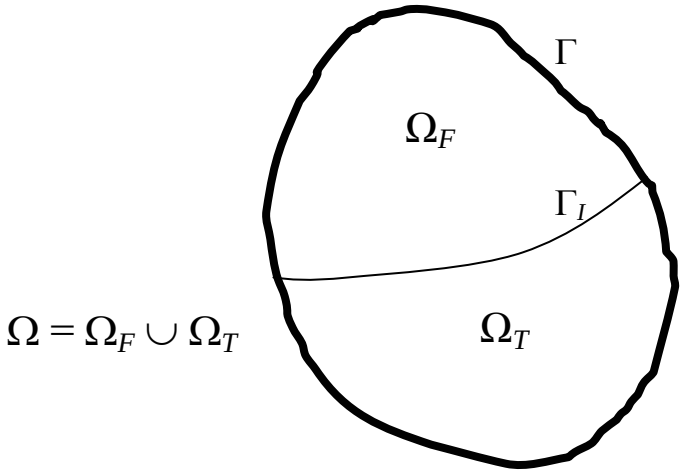

Figure 3.1. A schematic representation of the domain showing interface between the fluid and biphasic medium bounded by a smooth boundary Γ separated by the boundary layer Γ_I.

1. Biphasic constitutive equations

Soft tissues like artery, cartilage is essentially a biphasic material consisting of solid organic matrix (collagen fibrils, in a gel of proteoglycans, cells) and a liquid phase predominantly water (see Figure 3.2). The behavior of these materials is influenced by the deformation characteristics of the solid and the flow of fluid through the solid skeleton. The properties and the volume fraction of solid and fluid phase and their interactions with one another determine the overall behavior of these biphasic tissues.

Assuming the biphasic material is composed of intrinsically incompressible components which are chemically inert, the governing equations are derived in the following manner for a domain Ω having a boundary Γ with total volume V which is the sum of fluid volume V^f and solid volume V^s. The fluid is assumed to be viscous and incompressible, while the solid is assumed to be linearly elastic and isotropic. The volume fractions of the fluid and solid phases are represented as ϕ^f and ϕ^s respectively, where $\phi^\alpha = V^\alpha / V$, $\alpha = s, f$ refers to the solid and fluid phases respectively. It is to be noted that $\phi^s + \phi^f = 1$.

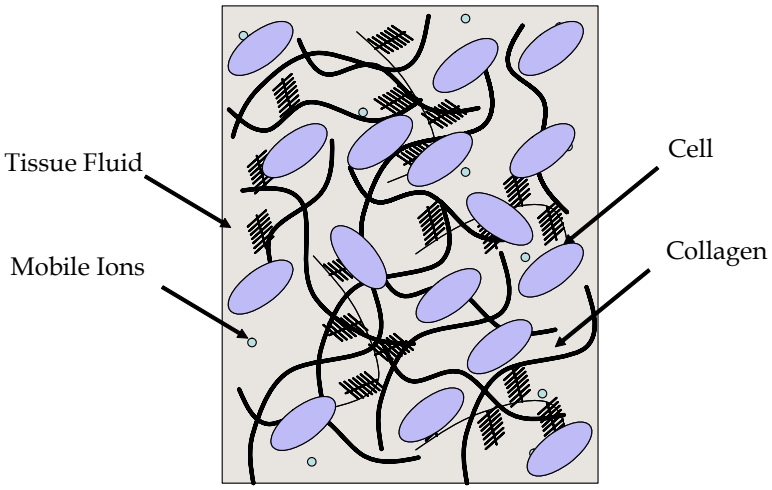

Figure 3.2. Schematic representation of soft tissue showing the distribution of water and solid phase in a cartilage.

The continuity equation for the biphasic material is given as

$$\nabla . \left(\phi^f \mathbf{v}^f + \phi^s \mathbf{v}^s \right) = 0 \tag{3.1}$$

Neglecting inertia and body forces, conservation of linear momentum yields the following equations [53]:

$$\begin{aligned} &\nabla.\boldsymbol{\sigma}^s + \Pi^s = 0 \\ &\nabla.\boldsymbol{\sigma}^f + \Pi^f = 0 \\ &\Pi^s = -\Pi^f = -p\nabla\phi^f - K\left(\mathbf{v}^s - \mathbf{v}^f\right) \end{aligned} \tag{3.2}$$

where $\boldsymbol{\sigma}^\alpha$ is the Cauchy stress tensor of α phase, Π^α is the diffusive momentum exchange between the two phases, p the apparent pressure, $\mathbf{v}^\alpha$ is the velocity field vector, and K is the diffusive drag coefficient [14] given as

$$K = \frac{\left(\phi^f\right)^2}{\kappa_0} \tag{3.3}$$

where κ_0 is the tissue permeability constant

Cauchy stress for an incompressible linear elastic solid and a viscous incompressible fluid is given as [53]

$$\begin{aligned} &\boldsymbol{\sigma}^s = -\phi^s p\mathbf{I} + \lambda_s tr(\mathbf{e})I + 2\mu_s\mathbf{e} \\ &\boldsymbol{\sigma}^f = -\phi^f p\mathbf{I} + \mu_f\left[\nabla\mathbf{v}^f + \nabla\left(\mathbf{v}^f\right)^T\right] \end{aligned} \tag{3.4}$$

where λ_s, μ_s are the Lamé constants of the solid material and μ_f the viscosity of fluid, and e is the solid phase strain tensor and I is the identify tensor. One of the advantages of a biphasic representation of a medium is that by setting the volume fraction of any one phase to zero, the medium could be characterized by the governing equation of the other phase alone. For example, a fluid domain can be characterized from the

governing equation of biphasic medium by setting the volume fraction of solid phase to zero.

2. Finite element formulation

Mixed finite element formulation, penalty finite element formulations, and a combination of mixed and penalty based formulations are some of the formulations implemented to consider the pressure term in modeling the biphasic model of tissue [47, 54, 55]. A penalty based finite element formulation is considered in this work [39, 40]. The penalty finite element formulation is based on the interpretation that the continuity equation can be considered as a constraint on the velocity components, and is represented as [39, 40]

$$\nabla.\left(\phi^f \mathbf{v}^f + \phi^s \mathbf{v}^s\right) + \frac{p}{\beta} = 0 \tag{3.5}$$

where, β is the user-specified penalty parameter.

Using the above equation the modified governing differential equation is given as

$$\begin{aligned} \nabla.\left(-\phi^s p\mathbf{I} + \lambda_s tr(\mathbf{e})I + 2\mu_s \mathbf{e}\right) &+ \beta\left[\nabla.\left(\phi^s \mathbf{v}^s + \phi^f \mathbf{v}^f\right)\right]\nabla\phi^f - K\left(\mathbf{v}^s - \mathbf{v}^f\right) = 0 \\ \nabla.\left(-\phi^f p\mathbf{I} + \mu_f\left[\nabla\mathbf{v}^f + \nabla\left(\mathbf{v}^f\right)^T\right]\right) &- \beta\left[\nabla.\left(\phi^s \mathbf{v}^s + \phi^f \mathbf{v}^f\right)\right]\nabla\phi^f + K\left(\mathbf{v}^s - \mathbf{v}^f\right) = 0 \end{aligned} \tag{3.6}$$

The weak form of the equation is given as

$$\int_\Omega \delta u.\left\{\nabla.\boldsymbol{\sigma}_E^s - \phi^s \nabla p - K\left(\mathbf{v}^s - \mathbf{v}^f\right)\right\} d\Omega = 0 \tag{3.7}$$

$$\int_{\Omega}\left\{\left(\nabla\delta u\right)^{T}:\boldsymbol{\sigma}_{E}^{s}+\beta\,\nabla.\left(\phi^{s}\delta u\right)\nabla.\left(\phi^{s}\mathbf{v}^{s}+\phi^{f}\mathbf{v}^{f}\right)+\delta u.K\left(\mathbf{v}^{s}-\mathbf{v}^{f}\right)\right\}d\Omega=\mathbf{f}^{s} \tag{3.8}$$

$$\int_{\Omega}\delta w.\left\{\nabla.\boldsymbol{\sigma}_{v}^{F}-\phi^{f}\nabla p+K\left(\mathbf{v}^{s}-\mathbf{v}^{f}\right)\right\}d\Omega=0 \tag{3.9}$$

$$\int_{\Omega}\left\{\left(\nabla\delta w\right)^{T}:\boldsymbol{\sigma}_{v}^{F}+\beta\,\nabla.\left(\phi^{f}\delta w\right)\nabla.\left(\phi^{s}\mathbf{v}^{s}+\phi^{f}\mathbf{v}^{f}\right)-\delta w.K\left(\mathbf{v}^{s}-\mathbf{v}^{f}\right)\right\}d\Omega=\mathbf{f}^{f} \tag{3.10}$$

The primary variables are identified from the weak form as $\mathbf{d}^{s},\mathbf{v}^{s},\mathbf{v}^{f}$, which are the displacement of the solid phase, velocity of solid and fluid phases respectively. By discretization of the above equation, the primary variables are represented in terms of the nodal values using interpolation functions ψ^{1} & ψ^{2} as

$$\mathbf{u}^{s}=\psi^{1}\mathbf{d}_{e}^{s},\ \ \mathbf{v}^{s}=\psi^{1}\mathbf{v}_{e}^{s},\ \ \mathbf{v}^{f}=\psi^{2}\mathbf{v}_{e}^{f} \tag{3.11}$$

where, $\mathbf{d}_{e}^{s},\mathbf{v}_{e}^{s},\mathbf{v}_{e}^{f}$ are the elemental solid displacement, solid velocity and fluid velocity respectively. The elemental matrix representation of equations (3.8) and (3.10) is

$$\begin{bmatrix}K_{s}^{11} & K_{s}^{12} & 0 & 0\\ K_{s}^{21} & K_{s}^{22} & 0 & 0\\ 0 & 0 & 0 & 0\\ 0 & 0 & 0 & 0\end{bmatrix}\begin{Bmatrix}d_{x}^{s}\\ d_{y}^{s}\\ 0\\ 0\end{Bmatrix}+\begin{bmatrix}C^{11} & C^{12} & C^{13} & C^{14}\\ C^{21} & C^{22} & C^{23} & C^{24}\\ C^{31} & C^{32} & C^{33} & C^{34}\\ C^{41} & C^{42} & C^{43} & C^{44}\end{bmatrix}\begin{Bmatrix}v_{x}^{s}\\ v_{y}^{s}\\ v_{x}^{f}\\ v_{y}^{f}\end{Bmatrix}=\begin{Bmatrix}F_{x}^{s}\\ F_{y}^{s}\\ F_{x}^{f}\\ F_{y}^{f}\end{Bmatrix} \tag{3.12}$$

or

$$\mathbf{Kd}\ +\ \mathbf{Cv}=\mathbf{F} \tag{3.13}$$

Implementing the space and time decoupled formulation, the following definition of the nodal variables are used

$$\begin{aligned}\mathbf{v}^s(\mathbf{x},t) &= \sum_{j=1}^{n} \psi_j^1(\mathbf{x})\left(\mathbf{v}_e^s(t)\right)_j, \\ \mathbf{v}^f(\mathbf{x},t) &= \sum_{j=1}^{n} \psi_j^2(\mathbf{x})\left(\mathbf{v}_e^f(t)\right)_j\end{aligned} \tag{3.14}$$

Assuming a time difference of Δt, separating time at t_{n+1} and t_n, $\Delta t = t_{n+1} - t_n$ the displacement and velocity for time t_{n+1} is given as

$$\begin{aligned}\mathrm{d}_{n+1} &= \mathrm{d}_n + \Delta t\ \mathrm{v}_{n+\alpha} \\ \mathrm{v}_{n+\alpha} &= (1-\alpha)\,\mathrm{v}_n + \alpha \mathrm{v}_{n+1}, \quad \alpha \in [0,1]\end{aligned} \tag{3.15}$$

Substituting equation (3.15) into the equivalent relation (3.13), gives the following matrix equation [14]

$$(\mathbf{C} + \alpha \Delta t \mathbf{K})\,\mathbf{v}_{n+1} = \mathbf{F}_{n+1} - \mathbf{K}[\mathbf{d}_n + \Delta t\,(1-\alpha)\mathbf{v}_n] \tag{3.16}$$

with $\alpha > 0.75$. Solution of equation (3.16) with an appropriate choice of the penalty parameter [14], gives the velocity components of the solid and fluid phase in the biphasic medium.

3. Tissue-fluid interface modeling

The volume fraction of fluid phase in the tissue-fluid domain is discontinuous along the interface surface. To develop a well-posed mathematical problem it is required to satisfy conservation of mass, energy and momentum in the domain and also additional kinematical boundary condition at the interface surface [20].

For an incompressible solid and incompressible fluid phase for the conservation of mass on interfacial surface is represented by the following jump condition

$$\left[\!\left[\phi^f\left(\mathbf{v}^f-\mathbf{v}^s\right)\right]\!\right].\mathbf{n}=0 \tag{3.17}$$

where, n is the unit outward normal of the interface surface. Using the relation $\phi^f=1-\phi^s$, equation (3.17) can be represented as

$$\left[\!\left[\phi^f\mathbf{v}^f+\phi^s\mathbf{v}^s\right]\!\right].\mathbf{n}=0 \tag{3.18}$$

which is defined as the weighted velocity of the mixture at the interface.

Using the "pseudo-no slip" boundary condition, which allows different velocities for the solid and fluid phase at the interface surface, and equation (3.18) the following relation for the mass conservation on the surface is obtained [20].

$$\left[\!\left[\phi^f\mathbf{v}^f+\phi^s\mathbf{v}^s\right]\!\right]=0 \tag{3.19}$$

or can be explicitly represented as

$$\left(\phi_F^f\mathbf{v}_F^f+\phi_F^s\mathbf{v}_F^s\right)-\left(\phi_T^f\mathbf{v}_T^f+\phi_T^s\mathbf{v}_T^s\right)=0 \tag{3.20}$$

where subscripts *F* and *T* denote the fluid and tissue domains, respectively.

For a tissue-fluid interface ($\phi_F^f=1,\phi_F^s=0$), equation (3.20) would give the following interface boundary condition.

$$\mathbf{v}_F^f=\left(\phi_T^f\mathbf{v}_T^f+\phi_T^s\mathbf{v}_T^s\right)\ \text{at}\ \Gamma_I \tag{3.21}$$

This means that the velocity of the fluid in the fluid domain would induce a velocity in the solid and fluid phase in the tissue domain proportional to its volume fraction at the tissue domain.

In previous works, the above boundary condition was incorporated in the finite element formulation using a set of interface elements connecting fluid and tissue domains [22]. Interface elements satisfied the interface boundary condition over an elemental area, thus introducing artificial thickness to the interface. This lead to the prescription of duplicate nodes at a point on the interface surface, connected through multipoint constraints or through transformation matrixes. The formulation of finite element along these lines increased its computational overheads.

A new approach to satisfy equation (3.21) without an interelement layer is presented below. A continuous function of solid phase volume fraction, which tends to zero ($\phi_T^s \to 0$) near the interface boundary in the tissue domain, is assumed in this work. Thus, in the limit as we approach the interface surface from the tissue domain Γ_I^T the above assumption leads to the following continuity equation over the boundary surface.

$$\lim_{\phi_T^s \to 0|_{\Gamma_I^T}} \left(\phi_T^f \mathbf{v}_T^f + \phi_T^s \mathbf{v}_T^s \right) = \mathbf{v}_T^f \tag{3.22}$$

The following boundary condition for fluid velocity is obtained at the interface

$$\mathbf{v}_T^f = \mathbf{v}_F^f \text{ at } \Gamma_I \tag{3.23}$$

and on comparison with equation (3.21) and (3.22), satisfies the compatibility equation.

Thus it is assumed that the fluid velocity in the fluid domain and the tissue domain across the interface surface is satisfied one-on-one basis and not in the weighted sense as described in other works. The change in ϕ_T^s occurs at elements in the interface boundary in the tissue domain and at every point inside the element the

function is continuous, leading to an well posed finite element problem. The entire domain is meshed such that the interface surface lies on an interelement boundary for continuity of ϕ^s in an element.

This methodology avoids the use of additional constraints and interface elements in the finite element implementation of tissue-fluid interface modeling. When compared to a sequential algorithm the proposed formulation is robust as iterative satisfaction of equilibrium and specification of additional boundary conditions is not required. A formulation capable of simultaneously solving the fluid and biphasic domains and avoiding any explicit interface modeling in the finite element formulation forms the major contributions of this work.

4. Verification of finite element formulation

A standard Taylor-Couette flow over a rigid and deformable porous medium is simulated to verify the proposed algorithm. The standard Taylor-Couette problem consists of a steady viscous fluid at a uniform speed v, flowing over a biphasic material (see Figure 3.3). The continuity of field variables in individual domains and at the transition from the fluid and biphasic domain is checked for its accuracy. Fluid flow over a rigid and deformable biphasic material is simulated and the results are compared with solution presented by Chan et al [22].

To capture wide range of material properties the following set of parameters is defined and varied in the simulation,

$$\delta = \sqrt{\frac{\mu_T^f}{h_2^2 K}} \tag{3.24}$$

$$\xi = \frac{h_1}{h_2} \tag{3.25}$$

$$\eta = \frac{\left(\phi^f\right)^2 \mu_F^f}{\mu_T^f} \tag{3.26}$$

where, δ relates the viscous effect of fluid channel to the drag of fluid flow in the porous layer, μ_T^f is the viscosity of fluid in the porous medium, and η is the weighted viscosity ratio, and h_1 and h_2 are the heights of fluid and biphasic medium, respectively, and are set to 1.0 μm and 0.25 μm, respectively. The computational domain and material parameters are selected from Chan et al [22]. The solid volume fraction of the porous medium is assumed to approach zero towards the interface region.

In a rigid porous medium the displacement and velocity of the solid phase are set to zero for the entire domain. The viscosity of the fluid in Ω_F is taken as 1.0 Ns/m^2 and a unit velocity is prescribed at the top layer of fluid domain. The simulation is carried out for different values of δ and η and compared with results presented in [22]. The normalized fluid flux $\left(\phi^f \, \mathrm{v}_x^f / \mathrm{v}_0\right)$ in the fluid layer and their comparison for a rigid biphasic-fluid medium for different test cases is shown in Figure 3.4. The variation of the fluid flux across the interface is found to be smooth in the present analysis. From these figures it is evident that the new formulation is capable of predicting the fluid flux in the rigid biphasic region and the fluid region accurately.

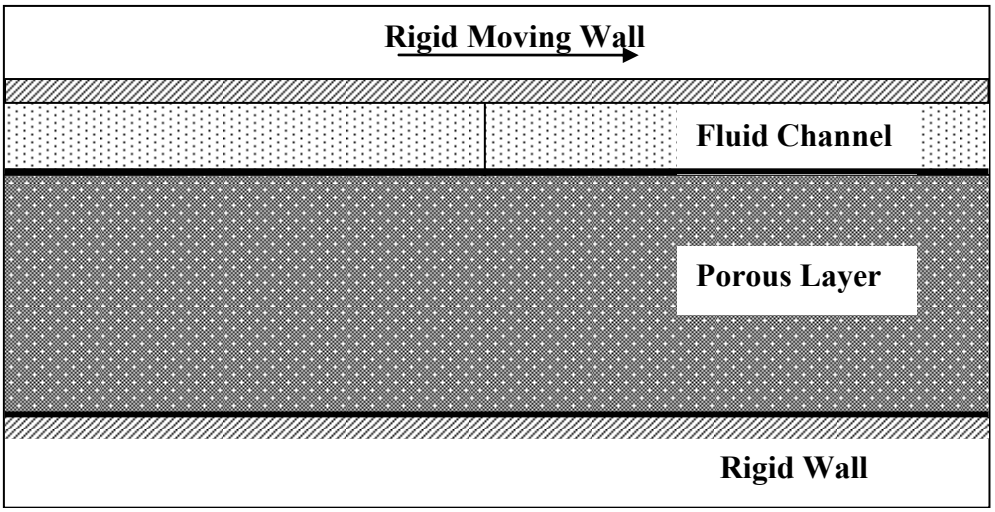

Figure 3.3. Viscous flow over a porous medium represented as a biphasic material.

To study the applicability of the model in the analysis of soft tissues, similar tests are carried out for a deformable-biphasic fluid domain. The boundary conditions and material properties of the Ω_F domain are kept the same. In the Ω_T domain, solid phase displacement and velocity is constrained at the base of the domain. The corresponding variation of fluid flux is shown in Figure 3.5. The normalized solid phase deformation in the deformable biphasic region is shown in Figure 3.6. The results are compared with analytical solutions from Chan et al. [22] and shows a good correlation. Thus, based on the simulation of the Couette flow over a rigid and a deformable biphasic region, the algorithm developed in this chapter can be considered as being capable of treating fluid-biphasic interfaces with sudden variations in the volume fraction of the biphasic material. As the variation of the material properties in this test problem is similar to that in a soft tissue having fluid and biphasic domains, the FE

formulation is implemented in the study of blood flow through an artery, which forms the rest of the chapter.

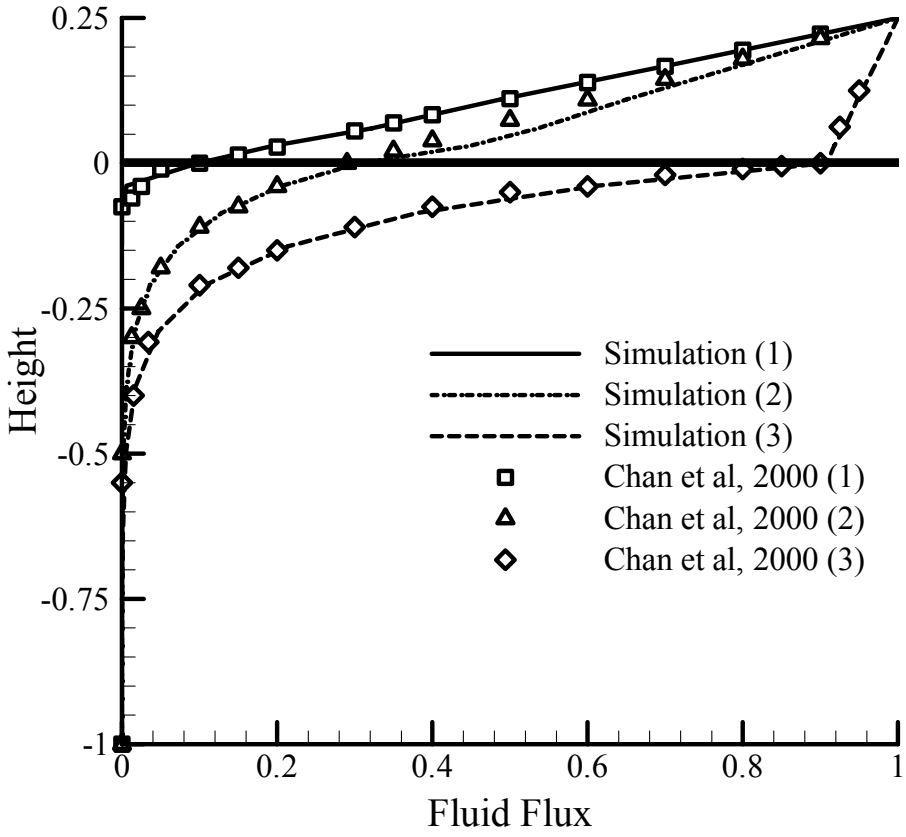

Figure 3.4. Comparison of simulated normalized fluid flux distribution across a rigid biphasic and fluid layer and analytical solutions for different flow conditions.

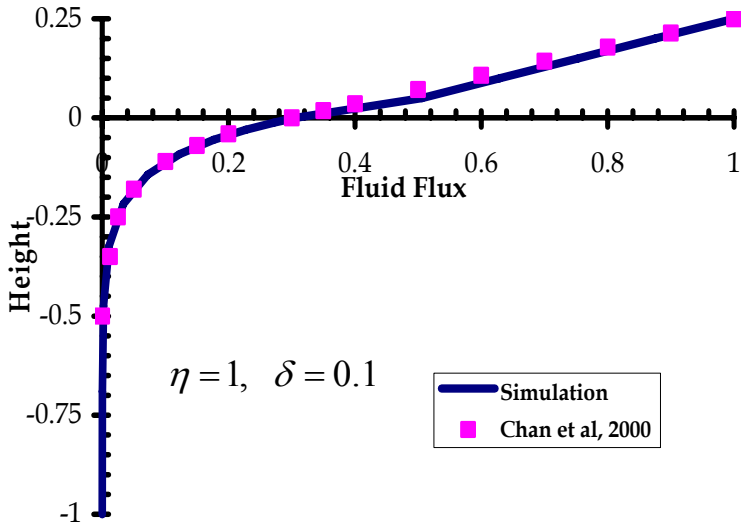

Figure 3.5. Normalized fluid flux distribution across a biphasic deformable biphasic and fluid layer. Similar to the flow over a rigid biphasic layer, a smooth transition between the fluid flux in the fluid and biphasic region is observed.

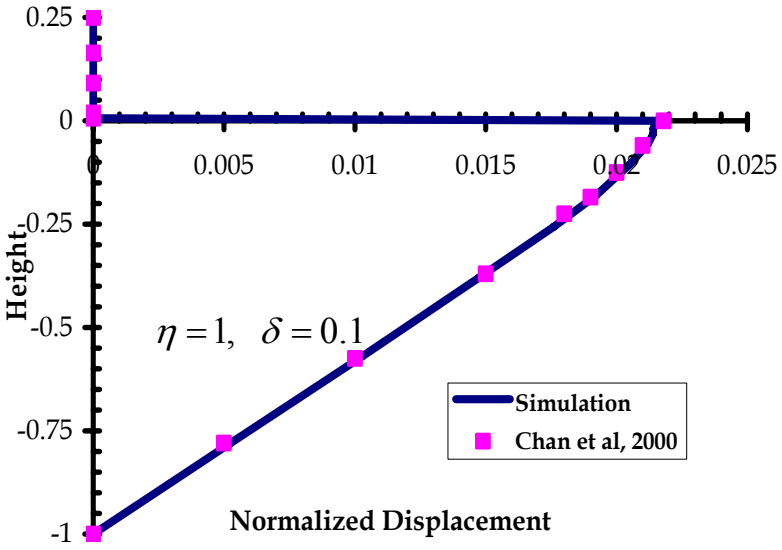

Figure 3.6. Normalized solid displacement of the deformable biphasic layer obtained from simulation compared with that from the literature.

C. Biphasic Artery-Blood Interface Simulation

Arterial walls are incompressible materials having a nonlinear stress-strain response with a stiffening effect at high pressures. Analysis of arterial wall using linear/nonlinear elastic/viscoelastic approaches for different physiological conditions has been carried out by many authors. A review on the various constitutive models used for artery wall is provided by [56]. Artery wall-blood flow interactions have been treated extensively with a detailed review provided by Quarteroni et al. [57]. In almost all of the models, artery wall was treated as a solid material and fluid-solid interactions were considered using additional boundary conditions. Biphasic models of artery walls have been previously implemented to study the transfer of macromolecules in the arterial walls from the blood [58-60].

A schematic representation of the cross-section of symmetric artery wall is shown in Figure 3.7. Blood flows through the inner region called the lumen, which is bounded by a thin layer of endothelial cells, called the endothelium. A glycocalyx of macromolecules, having an average thickness of 60 nm coats the luminal surface of the endothelium. The solid volume fraction of glycocalyx region is very small in the limit tending to zero [61, 62]. Compared to the lumen diameter and endothelial layer the thickness of glycocalyx is very small and is neglected in most of the analysis. Outer to the endothelial layer is the intima, consisting of connective tissues. In normal healthy artery intima layer is very thin and makes an insignificant contribution to the material properties of the arterial wall. Thickening of intima is associated with pathological condition called arteriosclerosis [63]. The intima is bounded on the outer region by the

internal elastic lamina (IEL). Media and adventitia, which provides the tensile strength and prevent disruption of artery wall, forms the outer regions of artery wall.

The arterial wall-blood interface is analyzed using the biphasic-fluid FE formulation described in the previous section. In the biphasic material representation of artery wall, the fluid phase represents the tissue fluid in the wall and the solid phase represents matrix phase consisting of collagen fibrils, proteoglycans, cells etc. [64]. The fluid in the tissue is assumed to be viscous and the solid a linearly elastic material. The values for arterial wall thickness and the lumen diameter are taken from literature. Blood flow through a healthy artery and a diseased artery due to atherosclerosis is analyzed using fluid-biphasic finite element model for time period of 1.0 s.

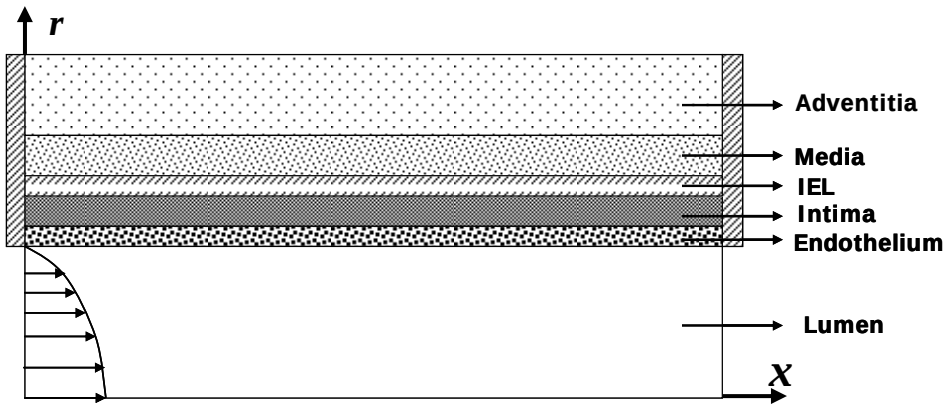

Figure 3.7. Loading and boundary conditions of a symmetric lumen and arterial wall.

1. Blood flow through healthy artery

A multilayered model of a symmetric artery with a lumen radius of 3.10×10^{-3} m and having distinct endothelial, intima, media and adventitia layers is selected (see

Figure 3.7). The viscosity of blood is 3.5×10^{-3} Pa.s and the viscosity of fluid in the arterial wall is taken as 0.72×10^{-3} Pa.s. The geometric and material parameters selected for the analysis is shown in Table 3.1. As the thickness of glycocalyx layer is in the order of nanometers, the region is not explicitly modeled in the finite element model. Also, it is assumed that the solid phase volume fraction of the arterial wall tends to zero at the glycocalyx region near the blood-wall interface. At the inlet a fully developed blood flow velocity is prescribed with a central line velocity of 0.17 m/s and at the outlet of the lumen free boundary conditions are prescribed. The solid displacement of the lateral ends of the arterial wall is fixed in both directions and kept free at the top outer adventitia layer. Symmetric boundary conditions are taken at the center of the lumen. The rectangular artery tube is meshed using 100 quadrilateral elements. A finer mesh is provided near the interface surface to capture the sudden variation in the field variables.

Table 3.1. Material parameters of artery wall.

	Endothelial Layer	Intima	IEL	Media	Adventitia
Porosity	0.005	0.083	0.002	0.258	0.001
Permeability ($m^4/(N.s)$)	6.25×10^{-6}	2.0×10^{-12}	4.32×10^{-11}	2.0×10^{-14}	4.32×10^{-19}
Thickness (microns)	5	10	5	160	300
Elastic Modulus	67.5 Pa	6.75 kPa	0.0675 Pa	6.75 Pa	67.5 kPa

Finite element analysis of the artery tube domain with a symmetric center line is carried out. The variation of fluid velocity in the arterial wall and the lumen at the longitudinal center of the domain is shown in Figure 3.8. Similar to the inlet profile, a

parabolic profile is observed in the flow through the lumen, while in the arterial wall the fluid velocity is negligible. Similar axial velocity for the fluid near the arterial wall-blood interface was reported by [61]. Figure 3.9 shows the variation of the radial fluid velocity in the lumen and the arterial wall. The radial velocity in the lumen increases to a maximum value of 2.81×10^{-6} m/s before reducing to 2.77×10^{-6} m/s in the artery wall. The radial fluid velocity in the arterial wall is called the filtration velocity, and it drives the solutes and other nutrients from the blood into the arterial wall through convection. The filtration velocity is affected by the permeability and the stiffness of the arterial wall layers and is also a good indicator of the probable uptake of lipids by the arterial wall which is critical in diseases like arthrosclerosis.

In a rigid artery wall, studies have reported a radial fluid velocities of 3.0×10^{-8} m/s [65], 2.31×10^{-8} m/s [66], and 1.76×10^{-8} m/s [67]. For a rigid artery wall simulation yielded a filtration velocity of 2.51×10^{-8} m/s at the interface surface, which is comparable to the reported values. Figure 3.10 and Figure 3.11 shows the variation of the radial and axial displacement of the biphasic artery wall. The radial solid displacement increases, reaching a peak value of 2.75×10^{-6} m, and then decreases to the prescribed boundary condition at either ends of the artery wall. The axial displacement profile shows a sinusoidal variation along the length of the wall.

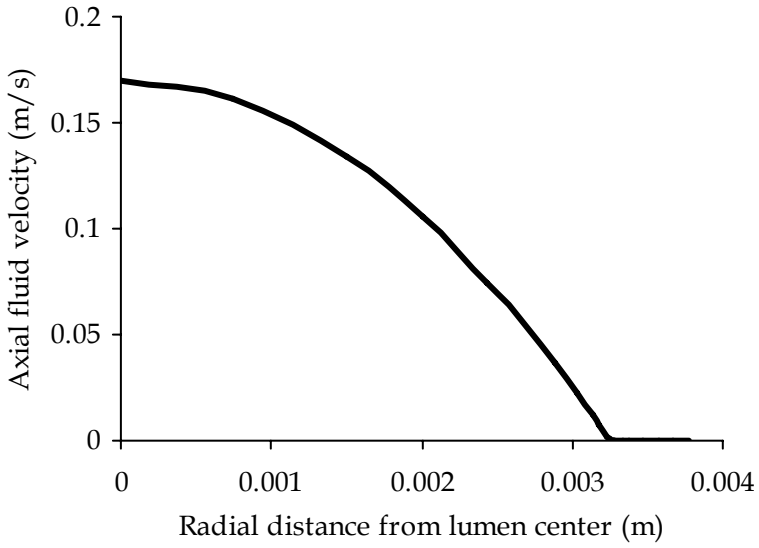

Figure 3.8. Axial fluid velocity in the lumen and arterial wall showing a parabolic velocity profile in the lumen while in the arterial wall a negligible axial fluid flow is observed.

To model the physiological event of a failure of the lining (e.g. cell death), the permeability of the epithelial layer is now varied. Figure 3.12 shows the variation of the filtration velocity with change in the ratio of permeability of the epithelial tissue keeping a standard value of $3.2\times10^{-16}\,\mathrm{m}^2$. The values are chosen to provide a wide range of permeability differences to effectively capture the influence of the endothelial layer to blood flow. It is evident from the figure that as the permeability is increased the filtration velocity also increases. In actuality, these conditions translate as a forerunner to atherosclerosis where the arterial wall becomes porous to lipids, due to an injury to the cell lining.

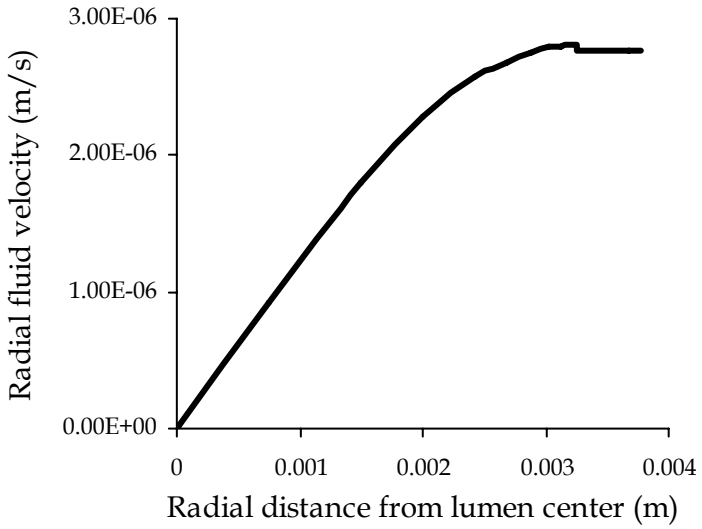

Figure 3.9. Radial fluid velocity in the lumen and arterial wall taken at axial center of domain. The radial fluid velocity increases in the lumen and then reaches a constant value in the arterial wall.

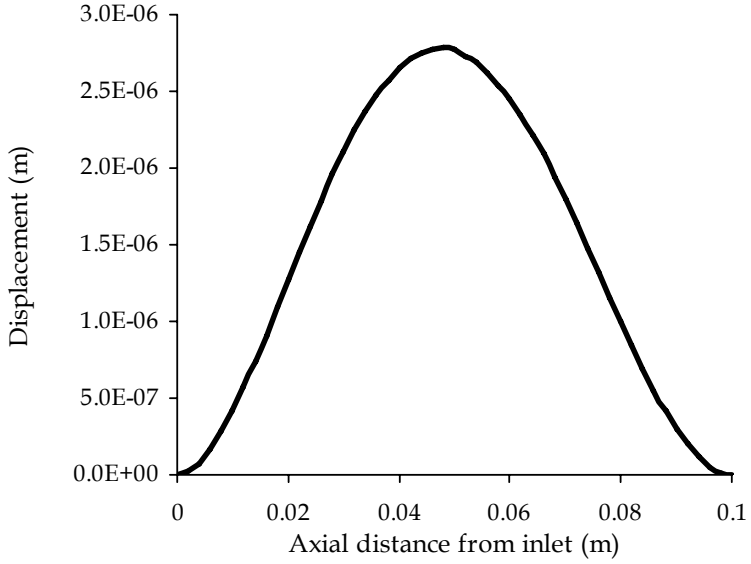

Figure 3.10. Radial solid displacement of top arterial layer shows a maximum value of 2.75 X 10^{-6} m at the center of the wall.

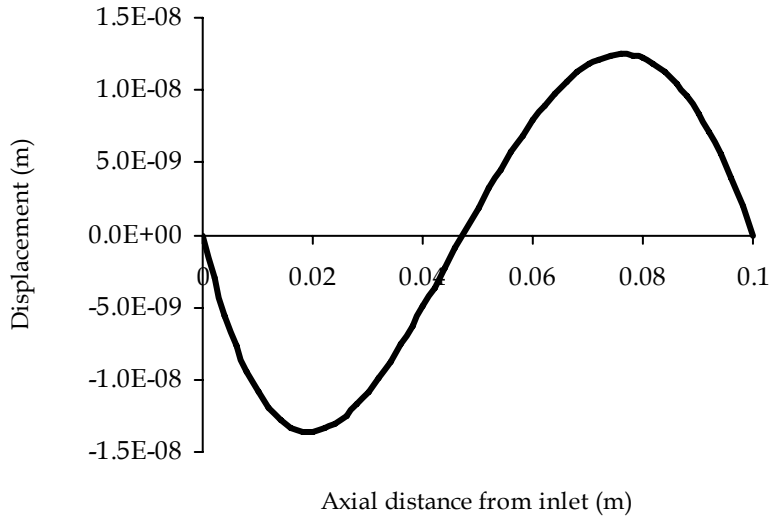

Figure 3.11.Axial solid displacement profile of the top arterial wall layer, a sinusoidal displacement profile is observed from the analysis.

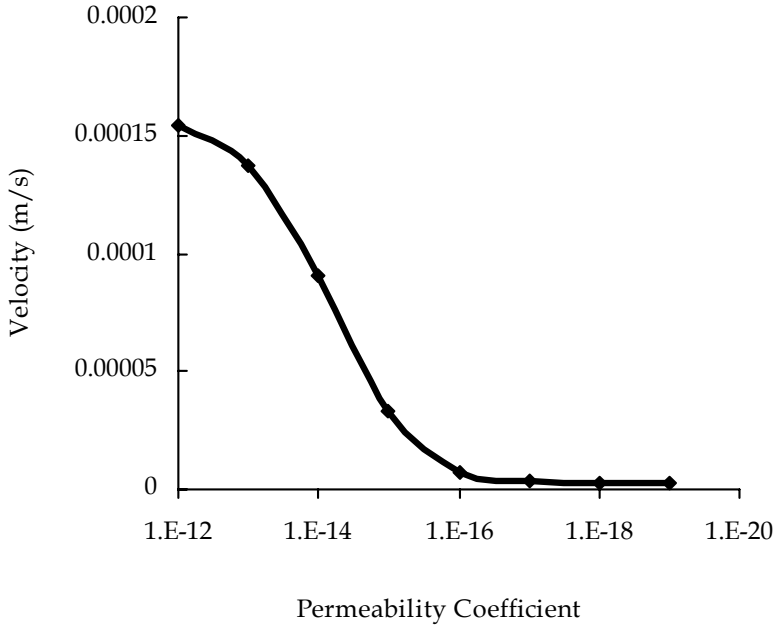

Figure 3.12.Variation of filtration velocity with permeability coefficient of epithelial layer, as the permeability decreases the filtration velocity also decreases.

2. Blood flow through stenosed artery

Atherosclerosis is a common form of disease affecting large and medium sized arteries. The formation of atherosclerosis is primarily caused by the blood flow conditions and arterial wall properties, which induce uptake of atherogenic substances into the artery wall. The formation of atherosclerotic plaque leads to changes in the blood flow patterns, which in turn may increase the artery block. When flowing through a narrowed artery the blood velocity increases leading to a negative pressure in the constricted region. This could lead to flow separation after the stenosis and can also lead to the collapse of arterial wall. The study of blood flow through stenotic artery thus requires a coupling of the fluid and arterial wall mechanics [68, 69]. Various researchers have studied the blood flow through a stenosed artery, considering artery wall as linear/nonlinear elastic, biphasic material with fluid structure interaction [18, 21, 70-72]. In most of the works, the walls are considered to be rigid and impervious. In actuality, computational analysis of diseased arteries requires the material to be non-rigid and permeable to water and other molecules, like LDL. Through the fluid-biphasic interface formulation we study the blood flow characteristics in a stenosed artery for different blocks in this section. In this study, we consider

(a) interaction of fluid and artery wall to study the influence of the material property, and

(b) influence of the constrictions on the blood flow.

To reduce the computational intensity of the analysis, the complex mechanical property of the artery wall is simplified and modeled as an isotropic bilayer having the inner media, and outer adventitia layers only, similar to the analysis carried out in [65].

The axial length of the domain is taken as 0.085 m, with the stenotic region modeled at a distance of 0.035 m from the inlet. The thickness of the wall assumed to be of 4×10^{-4} m, with equal thickness for media and adventitia. The porosity of inner layer is assumed to be 0.25 while for the outer layer it is taken as 0.05. An elastic modulus of 67.5 kPa and 6.75 GPa is assumed for the inner and outer layer respectively. Viscosity of fluid in the arterial wall is taken as 0.72×10^{-3} Pa.s. The blood is assumed to be viscous and incompressible. To analyze the influence of stenosis in the blood flow, simulation is carried out for stenotic blocks of 25 %, 40%, 50% and 60%. A block is defined as "Block %= (R_0-R_{new})/ R_0 X 100)," where R_{new} is the radius of the constricted tube. The variation of fluid velocity and solid displacement and the pressure drop due to the blocks are studied and compared.

A 4-noded quadrilateral element having 4 degrees of freedom per node is used to mesh the entire domain. The tissue-fluid interface lies along an interelement boundary region and a finer mesh is provided at the entrance and at the stenotic region of the artery. A tolerance limit of 0.001 was provided for convergence in the analysis. At the lumen inlet a fully developed velocity profile is prescribed with a central velocity of 0.024 m/s and at the outlet of the lumen, free boundary conditions are given. The arterial wall was constrained in both directions at the two ends. The axial velocity profile of the blood for the various cases of blocks is shown in Figure 3.13.

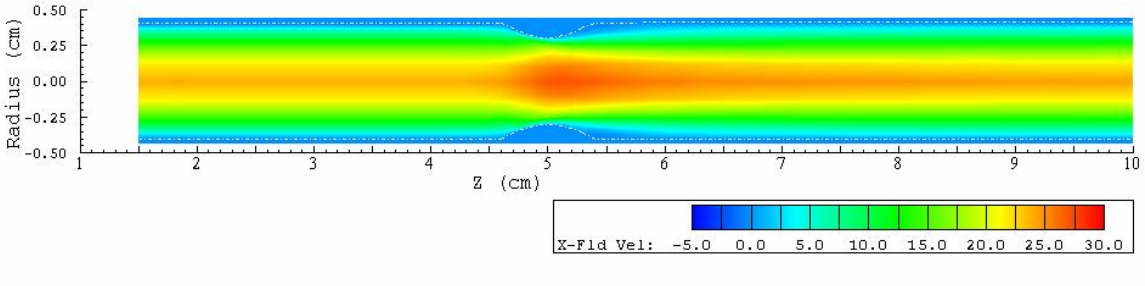

(a) 25 % block

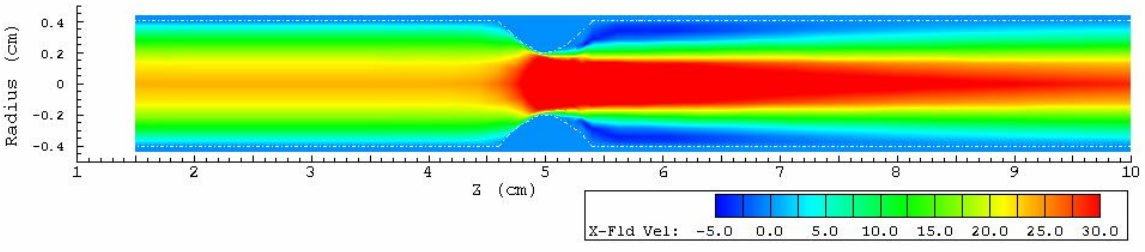

(b) 50 % block

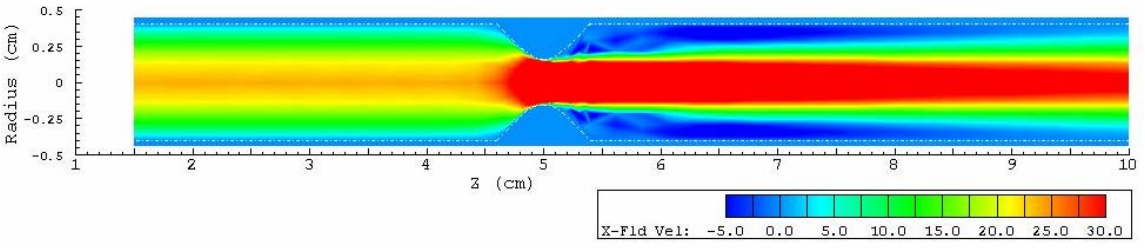

(c) 60 % block

Figure 3.13. Velocity profile for an artery with various degrees of constrictions.

In the figure, the white dotted line shows the interface region between the fluid and arterial wall. With a change in the stenosis the velocity profile is significantly altered in the lumen. The maximum velocity increases with an increase in the degree of block as shown in Figure 3.14. Also, it is observed that the fluid velocity for 60% block has negative velocities in the post-stenosis region showing fluid re-circulation. The

recirculation effects of blood flow alter the blood flow and increase the intensity of atherosclerosis through other physiological events.

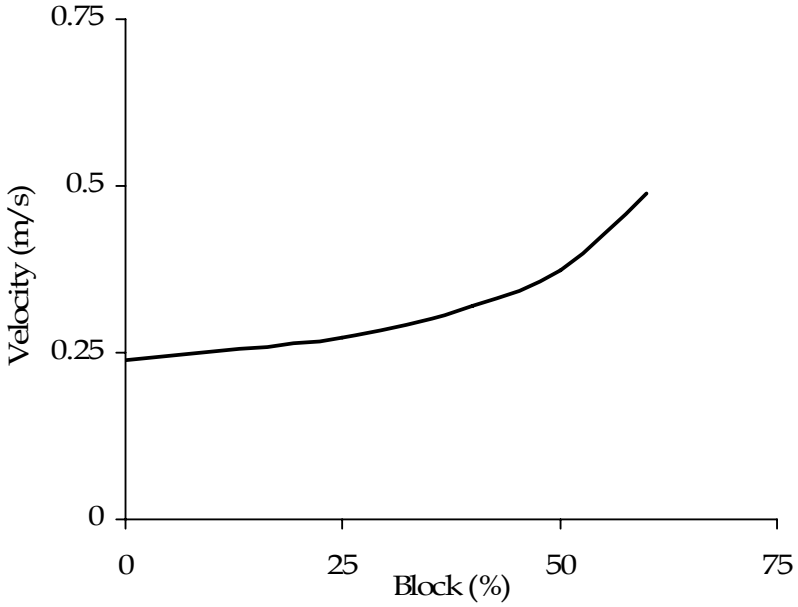

Figure 3.14. Variation of maximum fluid velocity with block %.

The variation of the fluid pressure drop along the axial direction for different blockages of lumen is shown in Figure 3.15. Pressure drop in an artery is very critical as it may lead to total blockage of the artery causing *stroke*. The difference between the inlet and outlet pressure is considered for ease of plotting. It can be observed from the figure that the pressure remains positive before stenosis, with the value increasing for increasing blocks at regions nearer to the block. At the region of stenosis, a sharp decrease in the pressure is observed, even going to the range of negative values followed by a recovery at the post stenotic region. Also, the negative pressure is

observed to increase with stenosis severity. Similar findings for changes in the negative pressure for different blocks were published by Bathe and Kamm [18].

The variation of the solid vertical displacement of the top layer of wall for different degrees of block of the tube is shown in Figure 3.16. An inward (negative) displacement of the top layer near to the fluid inlet is seen which then recovers and have an outward displacement in the pre-steonsois region. The maximum displacement attained at the pre-stenosis region is less for constricted tube when compared to a normal tube. The maximum value of the displacement decreases with increasing block upto 50% block and a reduction in the solid displacement of 60% block positive displacement is observed. The likely reason for this change is the influence of the negative pressure on the arterial wall behavior as evident from the maximum negative displacement profile seen at post stenosis region for 60% block artery. In the post-stenosis region inward (negative) displacement is maximum for 60% block, and decreases for 50% block and no inward displacement is observed for other blocks.

The alteration of the fluid flow pattern and wall behavior has been reported to be responsible for the further deterioration of the artery wall causing vascular diseases. For a complete analysis of the progression of disease more cases needs to be studied.

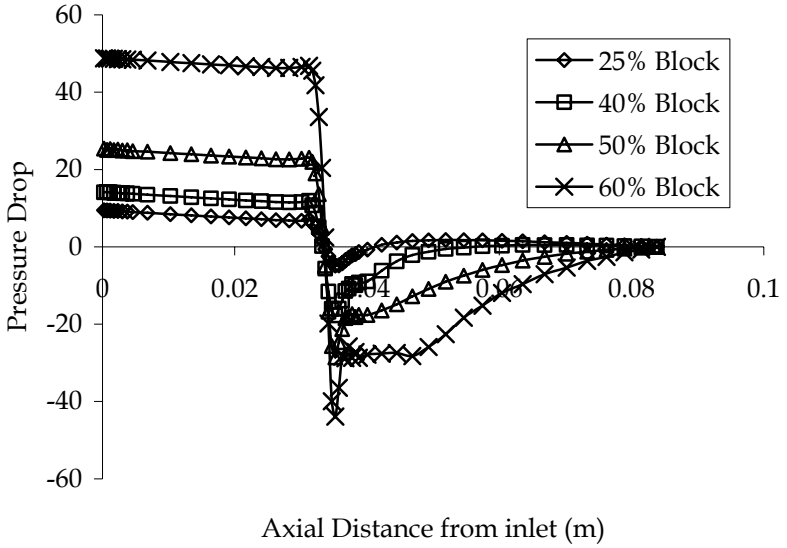

Figure 3.15. Pressure variation (N/m^2) due to stenosis. The maximum drop in pressure is observed for the 60% block.

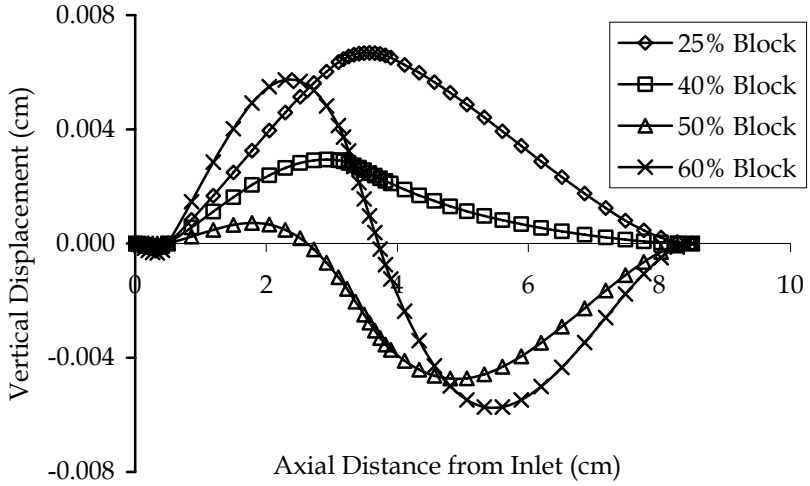

Figure 3.16. Displacement of artery wall for the computational domain selected. 60 % block of artery causes considerable undulations in the artery wall.

D. Summary

The close interaction of fluid flow and soft tissues in the biological systems makes the study of solid-fluid interaction a critical component in understanding the behavior of soft tissues. Studies of the fluid-structure interaction in biomechanics have mostly relied on the use of iterative solutions of the solid and fluid phases. These methods require multiple iterations due to the coupling of the fluid and solid phases. A new tissue-fluid interface model using biphasic representation of the fluid and tissue is developed in this chapter. The computational methodology does not require the prescription of additional boundary conditions or interface elements. Conservation requirements of mass, momentum, and energy are satisfied across the interelement boundary. The finite element implementation of the model is carried out and verified with standard problem of fluid flow over a porous medium and is used in the study of blood flow through an artery.

Mathematical modeling of blood flow-arterial wall systems is difficult as it involves large wall deformations, pulsative flow behavior and fluid structure interaction. To simplify the analysis in this work, the flow is assumed to be of steady state and the heterogeneity of the blood was also neglected. The material properties of the wall were considered as linearly elastic even though the vessel wall should be multilayered, orthotropic and non-uniform in nature. The effect of the permeability of arterial wall on the filtration velocity, which is a forerunner to atherosclerosis, is also studied in this work.

The tissue-fluid model is also implemented to study the blood flow through a constricted artery. From the analysis it is seen that considerable negative pressure, negative displacement and flow separation occurs at downstream region of the stenosis. These observed characteristics have a direct relation to the behavior of the plaque, and ultimately causes the plaque cap to rupture leading to arterial blockage. The study on the stenosis effect of the arterial wall was carried out on a simplified model of the wall, which did not consider the nonlinear material properties of the solid, and also the anatomically critical components of endothelial layer and IEL. But these approximations nevertheless does not reduce the impact of this research work in obtaining a computationally inexpensive and accurate model, capable of obtaining the flow patterns, pressure on the wall and wall deformations so critical in vascular angiogenesis. It is clearly evident from the analysis that the algorithm developed in this work would greatly enhance the study of blood flow through the blood vessels and helps in a better understanding of artery diseases. The developed finite element computational approach could also be extended in understanding fluid and solid tissue interactions, like vascular tumor interactions as well as in fields other than mechanobiology.

CHAPTER IV

COMPUTATIONAL MODELING OF CANCER CELLS AND TUMOR TISSUES

A. Introduction

Cancer, which can develop from cells of virtually all types of tissue, is one of the leading causes of premature death in the western world. A recent release from the World Health Organization (WHO) shows that malignant tumors were responsible for 12% of nearly 56 million deaths from all causes worldwide in the year 2000. It also predicts that the cancer rates will increase by 50% and will emerge as a major public health problem. The alarming rate of contracting cancer has caused a great deal of research activities in the identification and treatment of cancer. Although research on cancer in the medical field is predominantly experimental, theoretical and computational modeling research into the biomechanics and biophysics of cancer can contribute significantly towards the understanding of cancer. Through an effective correlation between the modeling and experimental studies, various interactions occurring in a cancer tissue can be used for the development of a comprehensive model. Also, any mathematical/mechanistic model of tumor will increase the pace of the research by cutting down on the experimental requirements.

Cancer is a multistep phenomenon in which "normal" healthy cells are converted to abnormal cells that can multiply uncontrollably. Cancer develops due to the damage of genetic material in a cell and further its accumulation over a period of time either due to biological factors or environmental factors. Genetically three factors

are responsible for the formation of tumors: a) Presence of cancer genes – responsible for cell multiplication (oncogenes), b) Absence of tumor suppressor genes, c) Inability to repair damaged genes. Along with these genetic factors a series of other chemical and biological events, leads to the formation of cancerous cell in a healthy tissue (Figure 4. 1).

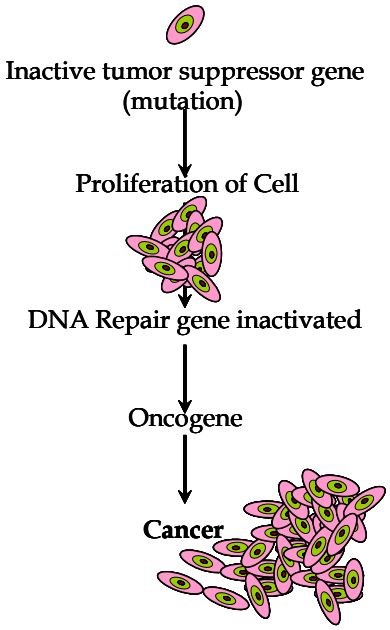

Figure 4.1. Flow chart of oncogenesis.

The uncontrollable growth of cancerous cells leads to an abnormal mass of new tissue defined as tumor. In the early stages of tumor (avascular tumor), nourishment to the cells is obtained from surrounding healthy tissues primarily through diffusion. As the nutrients diffuse through the tumor they get absorbed by the tumor cells causing a deficiency at the center of tumor tissue. As the tumor grows, inner cells get increasingly deprived of nutrients and oxygen ultimately leading to cell death. At this stage, there

are two distinct regions in the tumor tissue, an inner necrotic core consisting of dead cells, and an outer rim of proliferating tumor cells. As tumor grows, it induces stress on surrounding healthy tissues. At this stage, tumor is normally benign and has a low probability of recurrence after treatment.

The enzymatic dissolution of dead tumor cells releases angiogenic growth factors in the tumor tissue. The growth factors diffuse from the center of the tumor to the edges, finally reaching surrounding blood vessels. Through a series of physiological processes new blood vessels, which supply nutrients to tumor tissue, are developed. This process is called tumor angiogenesis. With no limitation on the supply of nutrients, tumor tissues grow profusely leading to the metastases stage. In the primary metastases stage, as shown in Figure 4.2, the tumor invades the surrounding tissues by breaking the tissue membrane. The tumor tissue at this stage consists of an increased number of dividing cells, with variation in nuclear size and shape, variation in cell size and shape, loss of specialized cell features, and loss of normal tissue organization. At an advanced stage of metastases, cancer cells enter the vascular and lymphatic system and reach different regions of the body. This leads to the formation of secondary tumor at sites far from the initial formation region. These tumors are malignant and have a higher probability of recurrence even after removal of the tumor. Malignant tissue also has distinctive appearance under the microscope that influences the mechanical behavior of tumor tissue. Experiments on benign and malignant breast tissues have found that cancerous tissues are 10 times stiffer than a normal tissue at 1% strain and more than 70 times as stiff at 15 %strain [73].

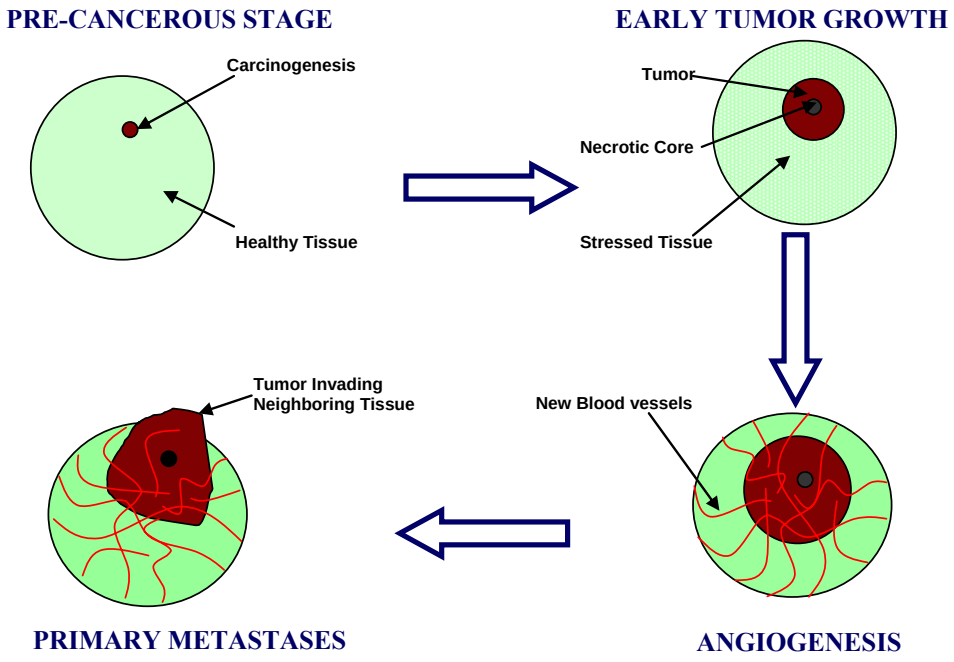

Figure 4.2. Development of tumor.

B. Cancer Cell Mechanical Properties

Cytoskeleton apart from providing structural rigidity to a cell, maintain and regulate various metabolic activities in a cell and are closely related to its physiological response. Pathological condition like cancer, aging and malaria induces considerable changes in the structural characteristics of cell and thereby affects its mechanical behavior. By measuring the mechanical property of the cell, and by noting the difference between a normal cell, a marker for diagnostic purposes could be developed [7, 9, 10]. Material properties of cells are derived from experimental data using theoretical models, like Hertz model is used for analysis of data from atomic force microscopy indentation study. Other widely used experimental techniques in cell

mechanics to derive the material properties are optical tweezers, and micropipette aspirations [1, 3, 8, 74]

Experimental studies have shown that the actin structures changes drastically from a normal cell to a malignant cancer cell. Two forms of actin filament structures are found in a cell: a) actin cortex: which is a network formed beneath the plasma membrane and b) stress fibers which are formed at focal adhesion regions, that ends either in a different adhesion region or in a network of filaments in the cytoplasm. The influence of these structures on the mechanical rigidity of the cell has been extensively studied using experimental and simulation procedures. Unfortunately, there is a lack of accurate computational model capable of quantifying the change in material property obtained from the AFM experiments on cancer cells to its structural makeup.

Numerous images of cells has revealed the compartmentalized nature of cells [8, 25, 30], and therefore a multilayered computational model of the cell with properties for each region derived through a bottom to top approach, is carried out in this work. The model exclusively considers the actin cortex, the cytoplasm and the nucleus. The material models for actin cortex and the cytoplasm are developed and the property of the nucleus is assumed from literature.

1. Materials and methods

Analysis of experimental data from atomic force microscopy should be based on a computational model which accurately considers the known cellular material properties. Previous works on continuum based constitutive modeling of cell for

analysis of AFM data uses a homogenous isotropic model of the cytoplasm so as to reduce the number of unknown material parameters [30]. Such simplifications of material properties limit the applicability of these models in understanding the effects of pathological conditions like cancer. The effect of cancer is localized and its effect is primarily felt on the disruption of actin structures [75]. Experimental evidence also suggests that corresponding material stiffness of cell changes with cancer.

Previous computational models of cells are incapable of connecting the physiological changes in a cell due to cancer with its mechanical property [30]. Thus a new mathematical model, based on structural micro-constituents of cell is developed in this work. The material model is developed so as to be capable of incorporating large deformations suffered during AFM and also capable of considering the alteration in mechanical properties of cell with pathological conditions.

This work is based on the assumption that actin cytoskeleton suffers the maximum alteration, compared to other cytoskeletal filaments, in the event of cancer attack [76]. Actin filament forms two primary structures of actin cortex and stress fibers in the cytoplasm. These changes in these structures due to cancer affect the mechanical property of the cell. Thus, the material model is developed based on the compartmentalized structure of outer actin cortex, inner cytoplasm and nucleus as presented in Chapter II.

Numerical Simulation: The material constitutive model of the cytoplasm is implemented in a finite element analysis of AFM, as shown below. In this work, an elastic analysis is considered and it is assumed that only basal stress fibers are formed

for benign cells and no stress fibers are considered for malignant cells. The geometric and structural makeup of cancer cells is obtained from experiments conducted by Mr. Qingsen and Dr. C.T. Lim at National University of Singapore.

Benign and malignant tumor cell shows distinct morphologies. The benign cells having an extended profile, similar to a normal cell which indicates the likelihood of formation of stress fibers with good contact with the substrate. Malignant tumor cells shows a spherical structure indicating the near absence of stress fibers. The corresponding finite element model of the benign and malignant tumor cell, with a spherical indenter of 4 microns acting directly above the nucleus is shown in Figure 4.3.

The nucleus is considered to be of 0.5 microns in diameter for the benign tumor and 0.75 microns in diameter for the malignant tumor. Actin cortex is of 0.2 microns thickness for a benign tumor and 0.1 microns for the malignant tumor cell. The model is discretized using an axisymmetric finite element with the mesh gradually made finer towards the area of indentation. A benign tumor-cell finite element model consists of 2,549 elements and 2,123 nodes while the malignant tumor-cell model is meshed with 1,278 elements having 956 nodes. The rigid indenter is given a downward displacement and the base of cell is constrained in all directions, with symmetry boundary conditions along the axis of symmetry. The nucleus is assumed as linear elastic with a Young's modulus of 400 Pa and a Poisson ratio of 0.35 (McGarry et al. [28]).

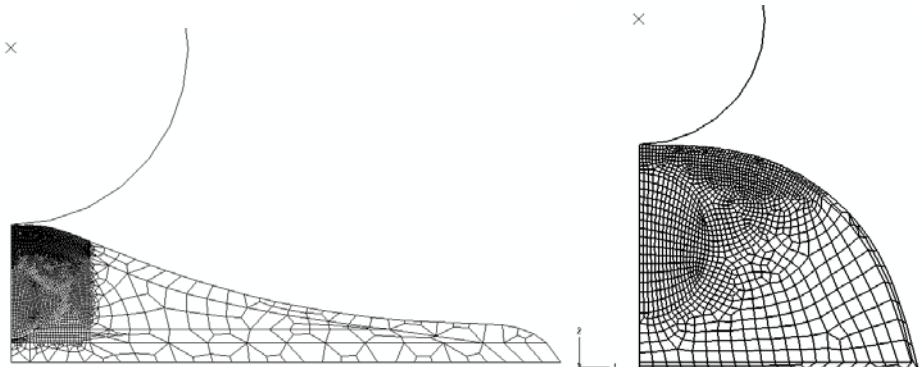

(a) (b)

Figure 4.3. Finite element model for the analysis of a) benign and b) malignant tumor cell obtained with an indentation using a spherical indenter of 4 microns actin directly above the nucleus.

2. Results and discussion

Numerical simulation of an AFM on a benign and malignant tumor cell with a spherical indenter of 4 microns, with the boundary conditions as outlined in the previous section is carried out using ABAQUS [41]. The actin cortex and cytoplasm is considered as a hyperelastic material and for the ease of modeling a neo-Hookean material model is applied. Assuming the filament length and persistence length of actin in benign and tumor cells to be a constant, the entire network is assumed to be made of crosslinked actin filaments only. Small strain shear modulus is calculated for benign tumor cell using polymer physics theories [35]. The decrease in the elastic modulus of actin cortex for malignant tumor is then attributed to the actin filament concentration alone. Theoretical and experimental studies have shown that decrease in actin filament concentration decreases the network elasticity (see Figure 4.4).

The material property of nucleus for benign and malignant tumor cell is assumed to be same due to the lack of data. Only the geometric effects of nucleus as observable in the confocal images of the cell are considered in this work. The material properties of actin cortex cytoplasm and nucleus for benign tumor cells are now varied to correlate with the force deflection curves obtained from simulation with experimentally determined values. The shear modulus of actin cortex, cytoplasm and nucleus are determined using a parametric study and the values obtained are 250 Pa and 125 Pa, respectively. The volume fraction of stress fibers at the base of cytoplasm is assumed to be 0.05%. Along similar lines the material property of the malignant tumor cells are also determined but the property of the nucleus is kept the same as that derived from the benign tumor. The small strain shear modulus for the actin cortex and cytoplasm for the malignant tumor cell is 50 Pa and 50 Pa, respectively. Comparison of the material property between malignant and benign tumor cell shows that the malignant tumor cell is less stiff at the cortex and the cytoplasm. As we decrease the concentration of actin filaments the material property drastically decreases. The same behavior is seen in confocal images of cells where the actin filament concentration is considerably low for malignant tumor cells. As there is little experimental evidence to suggest changes in intermediate filament and microtubule distributions in the malignant and benign tumor cell the reduction in material stiffness could wholly be attributed to actin filament concentrations [35].

Finite element analysis of AFM simulation over benign and malignant tumor cell is carried out to obtain the force deflection curve. Force deflection curves are

obtained by noting the total reaction force acting at the reference point of the rigid indenter for an increase in displacement of the indenter. The force deflection curve from the numerical simulation and corresponding experimental values is shown in Figure 4.4. Figure 4.4a shows the comparison of the curves for benign tumor cell and Figure 4.4b shows the corresponding curves for malignant tumor cells. From the figures it is evident that the numerical simulation closely matches with the experimental force deflection curves. This validates the constitutive modeling approach adopted in this work. So, it could be concluded form these results that the change in material property of cancerous cell is primarily attributed to the difference in the actin cytoskeleton concentration, which has been verified in the confocal images of cancerous cells available in literature.

For the material property, whose force deflection curve matches closely with the experimental data, the strain and displacement characteristics are studied. The strain distribution of both the normal and malignant cells is shown in Figures 4.5 (a) and (b) respectively. From the figures it is evident that the maximum strain occurs on the actin cortical layer which is in direct contact with the indenter. The inner cytoplasm and the nucleus directly below the indentation also suffer considerable strain and the intensity decreases away from the center. The deflection profiles for the benign and malignant cancer cells are shown in Figures 4.6 (a) and (b).

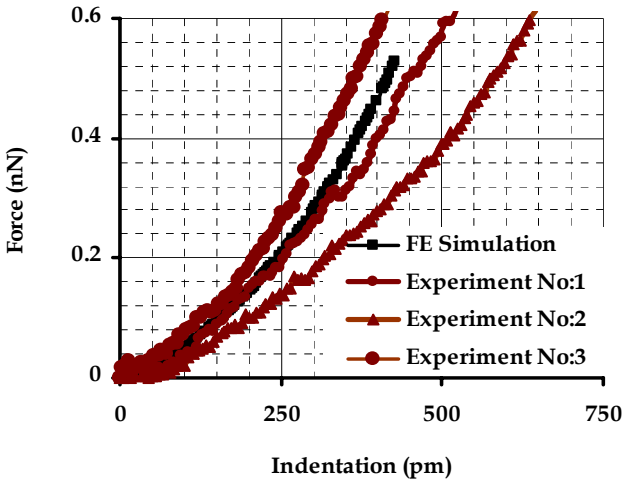

(a)

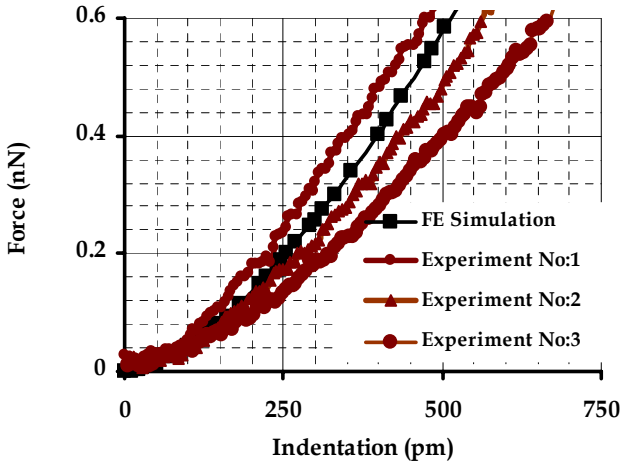

(b)

Figure 4.4. Force deflection curve for (a) benign and (b) malignant tumor cell.

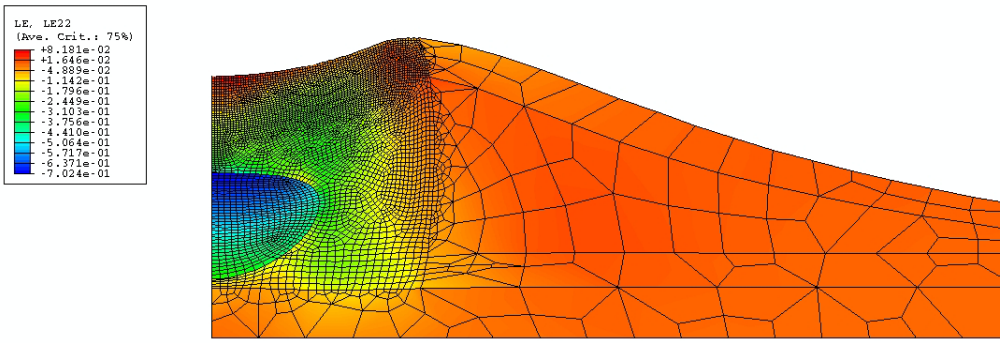

(a)

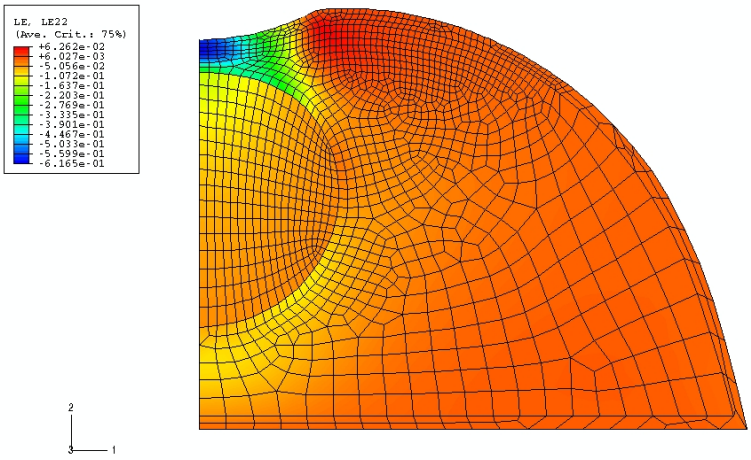

(b)

Figure 4.5. Strain distribution for AFM indentation simulation for (a) benign and (b) malignant tumor cell.

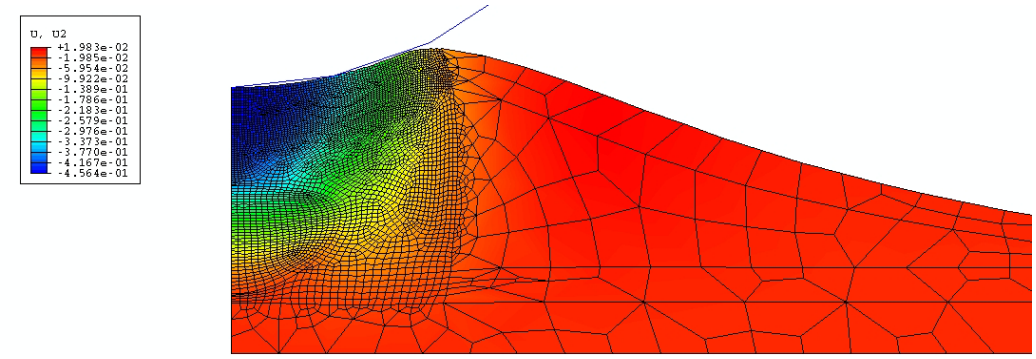

(a)

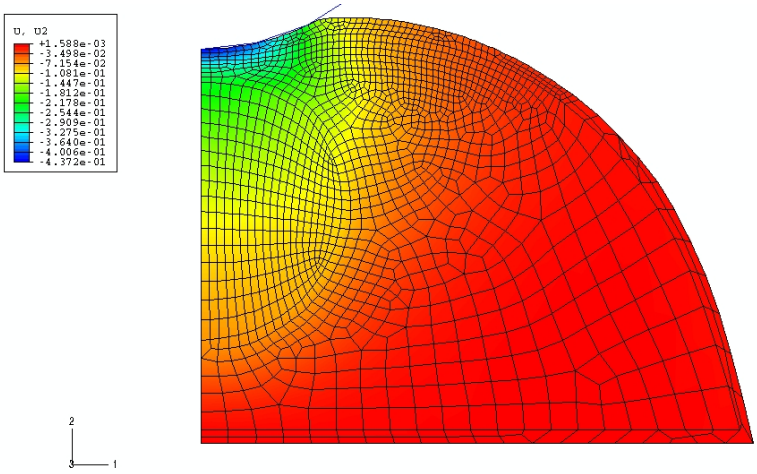

(b)

Figure 4.6. Displacement distribution for AFM indentation simulation for (a) benign and (b) malignant tumor cell.

C. Constitutive Modeling of Tumor Tissues

The tumor constitutive models are basically divided into discrete cell based and continuum based models. A good number of single cell based models accounting for cell characteristics like adhesion, motility and growth as well as excellent reviews on them are available in the literature (cellular automaton models, off lattice models [77]). In this chapter, the modeling of tumor tissues using continuum based approach is presented so that it can be considered in the computational modeling of tumor behavior using tools like FEA and computational fluid dynamics. Thus, the primary focus in this section is to provide an overview on the constitutive modeling of the tumor tissues in the study of general mechanical behavior of tissues as well as in the cancer growth.

In the macroscopic modeling of tumors, continuum assumption holds wherein representative volume element of the tumor contains sufficiently large number of cells and is continuous in space. The representative volume element (RVE) properties at any point in the tumor are considered as an average of properties over the local region centered at this point. The elastic stresses at any point in tumor is regarded as the average force per unit area between adjoining blocks of the tumor rather than as quantities determined by individual cell to cell interactions [78]. Based on the mechanics adopted in the modeling of tumor tissues, the constitutive models fall into two main categories: single phase models and multiphase models.

1. Single phase models

Single phase models, even though does not represent the exact physiology of the tumor tissues, are relatively easier to formulate compared to a multiphase material model. One of the simplest forms of liquid tumor model is the ideal fluid model given by

$$\boldsymbol{\sigma} = -p\mathbf{I} \tag{4.1}$$

where, σ is the stress and p is the pressure. An ideal fluid is isotropic. To capture the time dependent behavior of the tumor, various researchers have modeled tumor as viscous and incompressible material [79, 80]. An isotropic incompressible viscous fluid is represented as [53]

$$\boldsymbol{\sigma} = -p\mathbf{I} + 2\mu\mathbf{D} \tag{4.2}$$

where μ is the viscosity of the fluid, and D is the rate of deformation tensor.

Advantage of using liquid models over the solid models is that they work in an Eulerian framework, which will be helpful in considering the material before growth and deformation, and also to define the deformation with respect to a reference or a natural configuration. At the same time liquid models cannot consider the residual stresses which are significant in cases like tumor induced vascular collapse. To model this phenomenon, a solid material model would be more appropriate.

Solid tumor models ranges from simple linear elastic material to hyperelastic and viscoelastic models [78, 81-83]. A material is said to be hyperelastic if there exists a

free energy function $\psi = \psi(\mathbf{F})$ such that the following equation holds for compressible elastic material

$$\boldsymbol{\sigma}(\mathbf{F}) = \rho \frac{\partial \psi}{\partial \mathbf{F}} \mathbf{F}^{\mathrm{T}} \tag{4.3}$$

where, ρ is the material density, $\boldsymbol{\sigma}$ is the stress tensor, and $\mathbf{F}$ is the deformation gradient tensor. For an incompressible material, which does not show appreciable change in volume with deformation, the following relationship holds [84]

$$\boldsymbol{\sigma}(\mathbf{F}) = -p\mathbf{I} + \rho \frac{\partial \psi}{\partial \mathbf{F}} \mathbf{F}^{\mathrm{T}} \tag{4.4}$$

Different strain energies can be assigned to different materials, and are generally represented in terms of deformation gradient tensor F or left Cauchy-Green Tensor B.

A free energy function, assumed to be a linear function of the principal invariants of B, is represented as [53]

$$\psi = C_1 (I_B - 3) + C_2 (II_B - 3) \tag{4.5}$$

where C_1 and C_2 are constants, and I_B and II_B are the principal invariants of B. The stress tensor for the above strain energy function is given by

$$\boldsymbol{\sigma} = -p\mathbf{I} + \alpha\mathbf{B} + \beta\mathbf{B}^{-1} \tag{4.6}$$

where α and β are material parameters obtained from experiments. The above material representation is called Mooney-Rivlin material. Neo-Hookean materials have the constitutive equation defined by the equation

$$\boldsymbol{\sigma} = -p\mathbf{I} + 2\rho C_1 \mathbf{B} \tag{4.7}$$

Other hyperelastic models are also considered by authors in modeling tumor behavior [85].

It was proposed by Greenspan [85] that benign tumors could be modeled using neo-Hookean material or Mooney-Rivlin materials models while models for the malignant tumors should consider the invasive and metastatic characteristics and an Ogden model is appropriate. Liu et al. [86] also used a hyperelastic material based on Arruda-Boyce material model to capture the nonlinear behavior of pathological breast tissues. The parameters of the model were obtained by correlating force-deflection curves from indentation tests. Experimental works to obtain the mechanical property on the tumor breast tissues was also carried out in [87-89].

In Jones et al. [78], tumor is assumed to behave as a solid incompressible isotropic elastic material. By neglecting the body forces and assuming the forces acting on the tumor is in balance at all times, the following equation for isotropic growth strain is derived.

$$\frac{1}{2}\left(\nabla \mathbf{u} + \nabla \mathbf{u}^T\right) = \frac{1}{3} g\delta + \frac{1}{2E}\left(3\boldsymbol{\sigma} - \mathrm{Tr}\left(\boldsymbol{\sigma}\right)\delta\right) \tag{4.8}$$

where the left-hand side of the above equation is the strain tensor ε , the second term being the growth and third the stress response, g the growth factor, E the elastic modulus, and is applicable such that the change in g is sufficiently small and that the strain and stress tensors represent infinitesimal changes.

The growth factor with time is introduced using a total time derivative where the constitutive law to describe a linearly elastic tumor subjected to continuous volume growth is obtained as

$$\frac{1}{2}\left(\nabla \mathbf{v} + \nabla \mathbf{v}^T\right) = \frac{1}{3}\left(\nabla . \mathbf{v}\right)\delta + \frac{1}{2E}\left(\frac{D}{Dt}\left(3\boldsymbol{\sigma} - \mathrm{Tr}\left(\boldsymbol{\sigma}\right)\delta\right) + 3\left(\omega.\boldsymbol{\sigma}\text{-}\boldsymbol{\sigma}.\omega\right)\right) \tag{4.9}$$

where v and ω are the velocity vector and vorticity tensor, respectively.

The variation in mechanical property of tumor with time was captured in a time dependent strain energy formulation by Greenspan [85]. The benign and malignant tumors were modeled using different strain energy functions. The degree of malignancy/differentiation of the tumor was obtained through the variation of the strain energy function with time. The strain energy with time varying parameters is given as

$$W\left(\lambda, \mu_r, \alpha_r, t\right) = \sum_r \frac{\mu_r\left(t\right)}{\alpha_r\left(t\right)}\left\{\lambda_1^{\alpha_r(t)} + \lambda_2^{\alpha_r(t)} + \lambda_3^{\alpha_r(t)} - 3\right\} \tag{4.10}$$

As the tumor changes from a well differentiated tumor to a poorly differentiated tumor, the strain energy changes from $W(\lambda, \mu_r, \alpha_r)$ to $W^*(\lambda^*, \mu_r^*, \alpha_r^*)$. In this work, the strain energy function was further applied to model the cells causing different strain energy for normal cells and tumor cells.

Chaplain et al [81] developed a mathematical model for the growth of a solid tumor using membrane and thick shell theory. The material composition of the model was obtained through the strain-energy function and the analysis was carried out using nonlinear elasticity theory. In this work, the growing tumor is treated as an inflating

balloon, wherein the thin outer layer of cells is the membrane of the balloon characterized by a strain energy function. The internal pressure of the necrotic core is modeled as an inflationary pressure inside the balloon and the equilibrium equations from the membrane theory reproduces the pressure/surface tension balance on the boundary. Works on tumor modeling and analysis was also carried out in [73, 90-92].

A number of solid constitutive models have been implemented to capture the behavior of tumor tissues. The simplistic isotropic linear elastic representation is far from accurate in modeling biological materials which are inherently heterogeneous and nonlinear. Nonlinear material models like Mooney-Rivlin models, neo-Hookean models of tumor tissue have been implemented to capture the nonlinearity in the system. The material parameters of the hyperelastic models are generally obtained by fitting curves to experimental data [82]. Apart from the nonlinearity of the system, the heterogeneous nature of tumor tissues should also be considered in single phase modeling. Early stage tumors consist of an outer proliferating region of active cells, the inner necrotic core, and the intermediate region of active and dead cells. Derivation of material properties of the individual layers of tumor from mechanical testing is near impossible. The other option is to derive the mechanical property from mathematical models by incorporating the structural framework of the tumor regions, similar to the one carried out for cell modeling [84]. This requires a multiscale modeling procedure by first identifying the material properties of sub-cellular constituents, which change with the pathology, to obtain the property of the cell. With the identification of material property of the cell, the material properties of different regions of tumor can be developed.

2. Multiphase models

The theory of mixtures and poroelasticity are widely used multiphase models in the modeling of tumors. In a strict sense, poroelasticity could be considered as a subsidiary of the theory of mixtures model. The basic assumption of the modeling is that the tissue is considered as being an elastic medium having a localized flow and fluid injection and absorption points. The solid phase consists of the cells, collagen and proteoglycans of the extracellular matrix while the liquid phase consists of the free flowing fluid of the communicating pore space [93]. Through the derivation of governing equations, suitable material models are developed.

Please et al. [94] proposed one of the first multiphase liquid models of tumor in the study of tumor growth. In this work, the tumor was assumed to be composed of two phases of fluid: an inviscid tumor cell and the extracellular water. The force balance on the water is obtained by considering the extracellular water to flow between the cells of the tumor body, and the cell mass acting as the porous media. Breward et al. [95] used similar approach in modeling the tumor as a two-phase model, where the aqueous phase was inviscid and the cell was considered as a viscous material with the viscosity depended on the degree of differentiation of the cancerous cell. Using the constitutive relation derived through this method, the tumor growth was studied in a 1-D system.

The tumor growth in the vascular stage is characterized by the presence of vascular supply chains supporting the cancerous cells. These leaky blood vessels increase the fluid pressure inside the tumor tissue which affects the solid cells in tumor. This causes a strong solid-fluid coupling and attempts are made to model the tumor

using the multiphase continuum models. Ambrosi and Mollica [96] used a theory of mixtures model to develop the constitutive material model of tumor growth. The tumor is considered as a hyperelastic material that is capable of growing by assuming the characteristic time of rate dependent behavior is less than the characteristic time of growth. Specific constitutive assumption was used to model the tumor as a compressible nonlinearly elastic material from the generalized strain energy function. A general Blatz-Ko type strain energy function given as

$$W = \frac{vf}{2}\left[\left(\mathbf{I}-3\right)-\frac{2}{q}\left(\mathbf{III}^{q/2}-1\right)\right]+\frac{v\left(1-f\right)}{2}\left[\left(\frac{\mathbf{II}}{\mathbf{III}}-3\right)-\frac{2}{q}\left(\mathbf{III}^{q/2}-1\right)\right] \tag{4.11}$$

where, v q and f are material constants obtained from experiments with the following restrictions: $v>0, 0<f\le 1, q<0$ and $f=1$ is used, **I, II, III** are the first second and third invariants of deformation tensor.

Ambrosi and Preziosi [79] used a multiphase model for the multi-cell spheroids having two constituents: a liquid phase filling the extracellular space and a solid skeleton constituted by an ensemble of sticky cells each of which is considered as an elastic membrane filled by an organic fluid. To model the tumor growth, the ensemble of cell is assumed to be growing through the permeation of the organic fluid through the cell membrane. The porous material is assumed to be deformable and its constituents are capable of undergoing relative motion. The constitutive equation for the mixture, considering the cell interactions and no memory effects is given as

$$\mathbf{T}_m = -\left[P + \sum\left(\phi_T\right) - \lambda_T\left(\phi_T\right)\nabla.\mathbf{v}_T \right]\mathbf{I} + \mu_T\left(\phi_T\right)\left(\nabla\mathbf{v}_T + \left(\nabla\mathbf{v}_T\right)^{\mathrm{T}}\right) \tag{4.12}$$

where $\sum$ denotes the elastic cellular interactions, μ_T represents the shear resistance and ϕ_T is the density of cells. An extension along these lines was carried out by Byrne and Preziosi [97].Roose et al. [98], studied the stress generated by the tumor growth through a linear poroelastic model having a solid phase made up by the cells and the extracellular matrix by the fluid phase. The relation between the stress and strain on the cell/matrix phase of the tissue was given as

$$\sigma_{ij} = 2G_{ij} + \left(K - \frac{2}{3}G \right)\varepsilon_{kk}\delta_{ij} - p\delta_{ij} - K\eta\delta_{ij} \tag{4.13}$$

where $\varepsilon_{ij} = \frac{1}{2}\left(\frac{\partial u_i}{\partial x_j} + \frac{\partial u_j}{\partial x_i} \right)$ is the strain, *K* is the bulk modulus of the tissue, *G* the shear modulus and η is the volume of new tissue created per unit volume of tissue.

Byrne el at. [99] considered the tumor as a two-phase component where the cell and the water phases were treated as incompressible fluids. It is assumed that there are no voids or excluded volume in the tissue. The constitutive model is developed by treating the cell and water phases as incompressible fluids with the cell treated as a viscous fluid and the water as an inviscid fluid satisfying the following stress equations as

$$\boldsymbol{\sigma}_w = -p_w \mathbf{I} \tag{4.14}$$

$$\boldsymbol{\sigma}_c = -p_c \mathbf{I} + \mu_c \left(\nabla \mathrm{v}_c + \nabla \mathrm{v}_c^T \right) + \lambda_c \left(\nabla . \mathrm{v}_c \right) \mathbf{I} \tag{4.15}$$

where μ and λ are the shear and bulk viscosity coefficients of the cell phase. The model was used to study the tumor growth by treating it as a moving boundary problem.

Byrne et al [100] developed a two phase model of an avascular tumor consisting of a solid cellular phase and a liquid phase. Using the theory of mixtures, constitutive equations were incorporated with the governing equations of mass and momentum balances to calculate the stresses within the tumor. All the cells in this work were considered as solid skeleton assumed as a homogenous material, which is bathed in an organic liquid containing diffusible nutrients and growth factors. Through this model, the effect of proliferation of the cell due to the mechanical stresses was obtained in this work. Byrne and Preziosi [100] extended the previous work to the modeling of the solid tumor growth using the theory of mixtures in the modeling of avascular solid tumor.

Lubkin and Jackson [101] studied the capsule formation in tumors by considering a mechanical description of the tumor growth using a multiphase material model. A three-phase model was considered in this analysis, with the liquid extracellular phase and the fluid phase of normal cells and fibers and that of the tumor cells and fibers. Stokes fluid model is invoked for modeling the aqueous phase and the cell-fiber phase on the time scale of tumor growth. Sarntinoranont et al. [93] used a poroelastic model as formulated by Rice and Cleary [102] in the application of solid and rock mechanics. The growth strain model in a tumor tissue assumes the tissue to grow under zero stress condition. The growth model was based on isothermal, equilibrium of

pore fluid pressure, small incremental deformations, isotropic material properties and the constituents were assumed to be incompressible. The interstitial fluid pressure was modeled based on two mechanisms of equilibration: reversal of low from the interstitial space back into the blood vessels and exudation of fluid into surrounding normal tissue. Analysis was carried out for the growth of a spherical tumor with a moving boundary. Poroelastic models have been used to predict stress as well as interstitial pressure in tumor and surrounding host tissues [103-106]. A solid multiphase model of the growing with a linear elastic solid and an inviscid fluid assumption was developed by Araujo and McElwain [107]. Araujo and McElwain [83] also considered the extended version of the previous model to account the residual stress evolution in a growing multicell spheroid system.

D. Examples of Tumor Modeling

Computational models are being implemented for the diagnosis of tumor tissue in breast, spine and brain. Diagnosis and identification of most types of cancer occurs after the second stage of tumor growth, when a significant number of cancerous cells are formed within a healthy tissue. The tumor tissue, which has distinct material and structural property over a healthy tissue, makes it easy for real time diagnosis of tumor. Tools like finite element methods are integrated with techniques like MRI and elastography [108] to develop powerful diagnostic tools. The models are capable of predicting the behavior of tumor tissue when embedded in healthy tissue and to identify the size and location of tumor. Some of applications of finite element models

for tumor diagnosis along with the material model and salient results are provided in Table 4.1.

Table 4.1. Finite element modeling of breast, spine and brain tumor, with the material models and results.

Tumor	Material Model	Results
Finite element study on Breast tumor		
Kerdok et al [87]	Nonlinear hyperelastic (Arruda-Boyce)	Material parameters are obtained through the correlation of simulation with experimental results
Jordan et al [109]	Nonlinear visco-elastic (Combined hyperelastic 8-chain model and porous viscous model)	Solution of inverse problem for determination of material parameters
Azar et al [90]	Nonlinear material	Obtain the nonlinear behavior of the breast tissues to identify tumor location
Plewes et al [91]	Linear elastic	Identification of material modulus with experiment through an iterative procedure
Samani and Plewes [82]	Nonlinear hyperelastic	Correlation with experimental results to obtain the material properties of the breast tissues
Finite element study on Spine Tumor		
Whyne et al [110]	Poroelastic	Identifying relative risk of burst fracture initiation
Tschirhart et al [92]	Nonlinear hyperelastic	Effect of shape and location of tumor on burst fracture risk and displacement of spine
Finite element study on Brain Tumor		
Kyriacou et al [111]	Nonlinear hyperelastic	Studied the deformations on brain tissue due to tumor growth

Macroscopic level models are also handy in treatment plans like surgical removal, and chemotherapy. A simulation of tumor and surrounding tissue behavior during the surgery would make it easy for the surgery planning and removal of tumor tissue. Chemotherapy and medicinal treatment occurs through diffusion and convection processes. A macroscopic model of tumor showing the uptake of medicines and its concentration levels at different stages helps in the treatment of tumor.

E. Summary

Through a parametric study of the material properties of actin, cytoplasm and nucleus the elastic modulus of the different regions are determined from this study. For the first time a numerical study is able to correlate the concentration of actin filament with the material property, and ultimately to the experimentally determined force deflection curves from an AFM. The limitation of AFM in the diagnosis of cancer cells, imposed by the assumptions of Hertz model is overcome through this work. The close interaction of computational modeling process with the experimental procedure would be immensely helpful in the extensive application of AFM in the field of cancer diagnosis. A review of the mechanical models of tumor tissues is also provided in this chapter. From the review on tumor tissue models it could be concluded that the biphasic models are best suited for the analysis of tumor tissues for growth and in pharmaceutical applications.

CHAPTER V

MASS TRANSFER IN ARTERIES AND BIOREACTORS USING FLUID-BIPHASIC INTERFACE MODELS

A. Introduction

Studies on the transfer of solutes through the fluid and its uptake by tissues are critical in understanding physiological processes like initiation and development of artery diseases like atherosclerosis and in tissue engineering. Solute transfer is determined by the diffusion and convection processes and is mathematically represented by the mass transport equations. To simulate the uptake of solute in the tissue from the fluid, mass transport equations should be solved numerically in the tissue and fluid domain. Mathematically this is difficult as proper matching boundary conditions satisfying the continuity of mass, energy and momentum should be developed. Implementation of these boundary conditions in a numerical algorithm posses significant difficulties in modeling the interface region and in correlating the variables. These difficulties have lead to the development of computational models solving mass transport equations in the individual domains. The influence of other domains is inbuilt into the model through assumptions, which may not be always accurate.

In this chapter, the fluid-tissue finite element formulation described in Chapter III is extended to incorporate mass transfer phenomenon. Through the identification of suitable boundary conditions, solute transport in the blood-arterial wall transport and

in a bioreactor is simulated. The chapter is outlined as follows: A review of mathematical representation of mass transport phenomenon and its finite element implementation is presented in Section B. The application of the finite element model in the transfer of LDL from the blood to the arterial wall and the glucose transfer in a bioreactor is presented in Section C and Section D respectively, followed by a summary in Section E.

B. Finite Element Formulation

The mass transport within the biphasic material is given by the following convective-diffusion equation

$$\frac{\partial C}{\partial t} + \nabla.\left(\mathrm{v}_f C - D\nabla C\right) = q \qquad \text{in } \Omega \tag{5.1}$$

where, C is the concentration of the solute in the medium, $\mathbf{v}_f$ is the velocity of the fluid phase, q is the reaction rate that considers the generation, consumption or degradation of the solute mass, D is the diffusion coefficient. Diffusion coefficient is dependent on the molecular size, the solvent and temperature. As the molecular size increases the diffusion coefficient decreases which is a factor critical in the design of pharmaceuticals.

In convective transfer, the effect of molecular size is not prominent. So, convection plays a major role in the transfer of larger molecules through the system. In a biological system, the interstitial flows are quite small and the convection portion of the equation is neglected. However, the mass transfer occurring in an artery and in bioreactors is predominantly through convection transfer and cannot be neglected.

Finite element analysis of the governing differential equation (5.1) is carried out by assuming the approximation of the nutrient concentration over a typical element Ω_e as

$$C^e = \sum_{j=1}^{N} C_j^e \psi_j^e(x, y) \tag{5.2}$$

where, C_j^e is the concentration at the nodes of the finite element Ω_e and ψ_j^e are the Lagrange interpolation functions over the element. A weighted integral form of the diffusion-convection equation is obtained by multiplying equation (5.1) by the weight function δw over the element and is given as

$$\int_{\Omega} \delta w \left[\nabla . \left(\mathbf{v}_f C - D \nabla C \right) - q \right] d\Omega \,. \tag{5.3}$$

The weight function is selected as ψ_j^e and by trading the differentiation from C to δw using integration by parts, the weak form is derived. By the identification of primary and secondary boundary conditions the following finite element model for the convection-diffusion equation is derived [39, 40] as

$$\left[\mathbf{T^e} \right] \left\{ \mathbf{C^e} \right\} = \left\{ \mathbf{Q^e} \right\} \tag{5.4}$$

where

$$\begin{aligned} T_{ij}^e &= \int_{\Omega^e} \psi_i \left(v_f^x \frac{\partial \psi_i}{\partial x} + v_f^y \frac{\partial \psi_i}{\partial y} \right) dxdy + \int_{\Omega^e} D \left(\frac{\partial \psi_i}{\partial x} \frac{\partial \psi_j}{\partial x} + \frac{\partial \psi_i}{\partial y} \frac{\partial \psi_j}{\partial y} \right) dxdy \\ Q_{ij}^e &= \int_{\Omega^e} \psi_i q \, dxdy + \oint_{\Gamma^e} \psi_i q_n \, ds \end{aligned} \tag{5.5}$$

and v_f^x and v_f^y are the fluid velocities in the x and y directions, respectively.

The finite element model developed for mass transfer is then coupled with the biphasic finite element model presented in Chapter III. The fluid velocities are calculated from the biphasic model and incorporated into equation (5.5). The proposed formulation leads to five degrees of freedom per node, and the solute velocity is assumed to be the same as fluid velocity. To model fluid and biphasic interface for solute transfer, the interface between fluid and biphasic region falls along an interelement boundary. At the interface, continuity of mass is automatically satisfied as there is a continuity of fluid velocity and mass addition or deletion is not considered at the boundary interface.

C. Low Density Lipoprotein (LDL) Transfer in Artery Wall

1. Pathophysiology

Atherosclerosis is a pathogenic condition of the cardiovascular system affecting medium to large arteries [65]. Experimental and theoretical studies have conclusively proven that the transfer of atherogenic substances (like LDL) from the blood to the artery wall is a critical factor involved in the development of atherosclerosis. The arterial wall consists of primarily three layers: intima, media, and adventitia. The intima is the innermost region of the arterial wall, which comes in contact with the blood flow. It consists of a single layer of endothelial cells which acts as the primary barrier to mass influx from the blood.

Computational modeling of LDL uptake by the arterial wall requires mathematical models for the transfer of solutes in the blood, transfer of LDL from blood

into the wall through blood-wall interface, and diffusion of molecules in different regions of the arterial wall. Most of the previous works on LDL transport in an artery have concentrated on solute dynamics either in the fluid phase or in the tissue phase. Models implemented in the study of LDL transport through the artery have been generalized into four major categories: a) Fluid models in which the artery wall is substituted by appropriate boundary conditions, b) lumen-wall models, considering an interface of solid and fluid domains and c) arterial wall models, where the concentration at the lumen is considered using appropriate boundary conditions.

Lumen-wall interface regions are modeled using additional boundary conditions connecting the momentum of the fluid and tissue phase. Its implementation in a numerical simulation like finite element method has relied on the use of interface elements connecting fluid and tissue domains. This presented significant computational challenges and limited the usage of numerical methods in solving mass transfer from blood into the artery wall. In this work, a new computational model for the mass transfer in the blood and arterial wall is developed using the fluid-tissue biphasic interface model. The model assumes that the solid volume fraction in the tissue tends to zero near the interface. The mass transfer phenomenon is included in the mathematical model using the convection-diffusion equation.

2. Computational domain and boundary conditions

The transfer of solutes in the blood and its uptake by arterial systems involves parameters like diffusivity of molecules in the fluid, permeability of arterial wall,

concentration of the solutes, flow parameters, etc. The large number of variables, its proper identification and control to obtain valid data represents significant challenges in numerical analysis of solute transfer. To simplify the analysis, a simple geometric representation of blood flow through lumen is considered.

A straight tube artery with a multilayered arterial wall without the outer adventitia is modeled in this study. The lumen is assumed to be 0.0031 m in radius with the length assumed to be 0.083 m. The thin glycocalyx region of the artery is not modeled and the blood flowing through the lumen is in direct contact with the endothelial region. A fully developed flow is considered at the entrance with a mean velocity of 0.17 m/s. The domain is meshed using 4-node quadrilateral finite elements with the blood-wall interface lying along an interelement boundary region. Analysis is carried out to study the deposition of LDL in the artery wall and also the influence of various physiological factors in the LDL distribution. The permeability and porosity of the endothelial region are the two main factors that would be considered in this study. The domain is meshed using a 100×50 mesh of four-node quadrilateral finite elements with five degrees of freedom per node.

A fully developed velocity profile is provided at the inlet of the lumen with a mean velocity of 24 cm/s, and at the exit of the lumen a free flowing condition is prescribed. At the centre of the lumen symmetry boundary conditions are prescribed. At the inlet and exit of the artery wall zero axial velocity is provided. All the solid degrees of freedom are constrained in the fluid phase as well as the tissue domain. A constant LDL concentration at the inlet is prescribed, with zero transverse gradients at

the line of symmetry, with the continuity conditions at the interface automatically satisfied.

3. Results and discussion

The mass transfer in a blood-arterial wall for a straight arterial section is carried out using the developed biphasic tissue finite element model. The variation of the LDL concentrations in the lumen and in the arterial wall is shown in Figure 5.1. From the figure it is evident that the concentration remains the same in the lumen and there is a sharp decrease in the arterial wall. This shows that the convection effect on the LDL transport is prominent in the lumen. To show the decrease in the lumen, the concentration profile in the artery wall is magnified and is shown in Figure 5.2. The decrease in the artery wall LDL concentration is due to the endothelial resistance to LDL transport. At the intima and media the concentration remains constant, with a slight decrease occurring at the internal elastic lamina region. In the media consumption of LDL molecules occurs, which depletes the amount of molecule concentration. Figure 5.3 shows a nonlinear variation of the concentration in the lumen due to the uptake of molecules by the media.

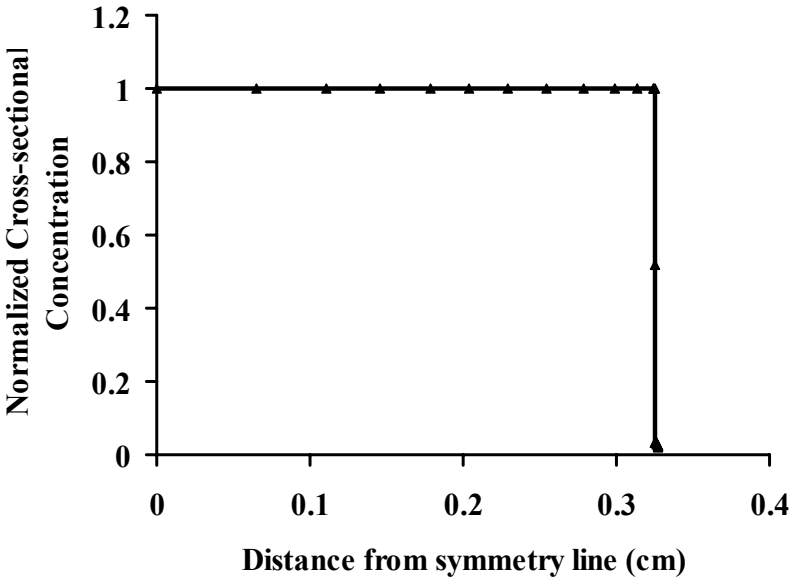

Figure 5.1. Concentration profile in lumen and artery wall.

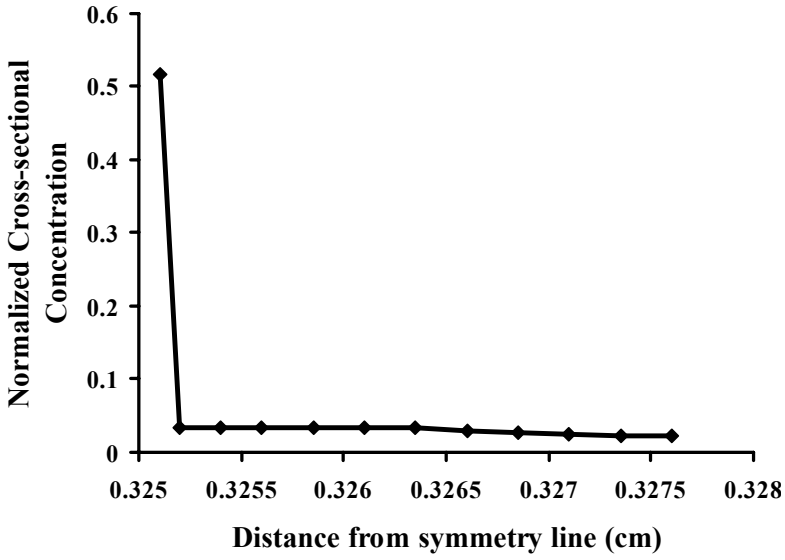

Figure 5.2. Concentration profile in artery wall.

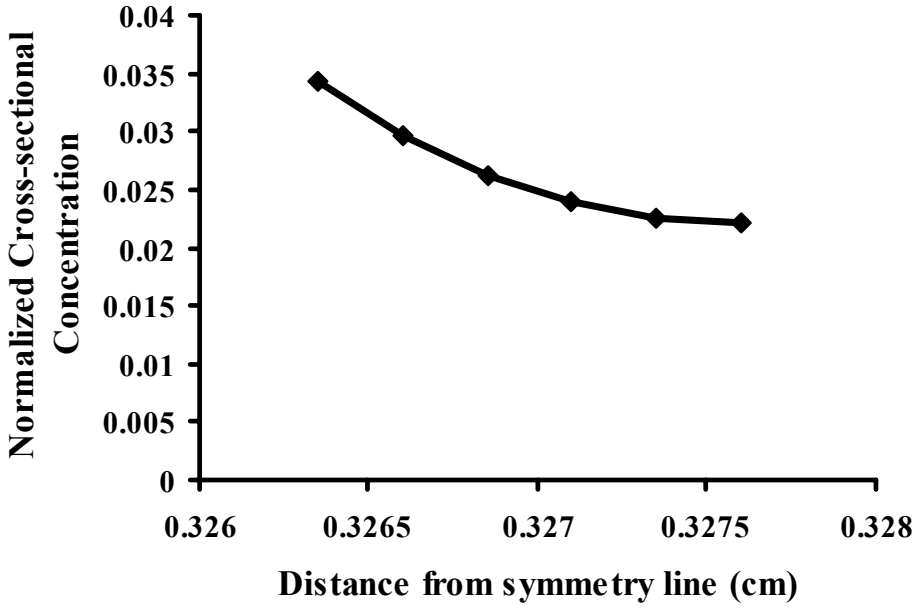

Figure 5.3. Concentration profile in media.

As indicated earlier, the endothelial layer forms the major barrier in restricting the entry of lipid molecules into the arterial wall. With a change in the material properties of the endothelial layer an increase in the uptake of LDL in the arterial walls has been reported by experimental analysis. The primary material parameters that determine the uptake of lipid molecules are the permeability and fluid phase volume fraction of the endothelial region.

The permeability of the endothelial layers is changed by factors of 10 and 100 times from the previous analysis to analyze its influence in LDL concentration in the artery. The variation of LDL concentration in the arterial wall which changes in the endothelial permeability is shown in Figure 5.4. It is evident from the figure that as the permeability increases the concentration of LDL in the artery wall also increases.

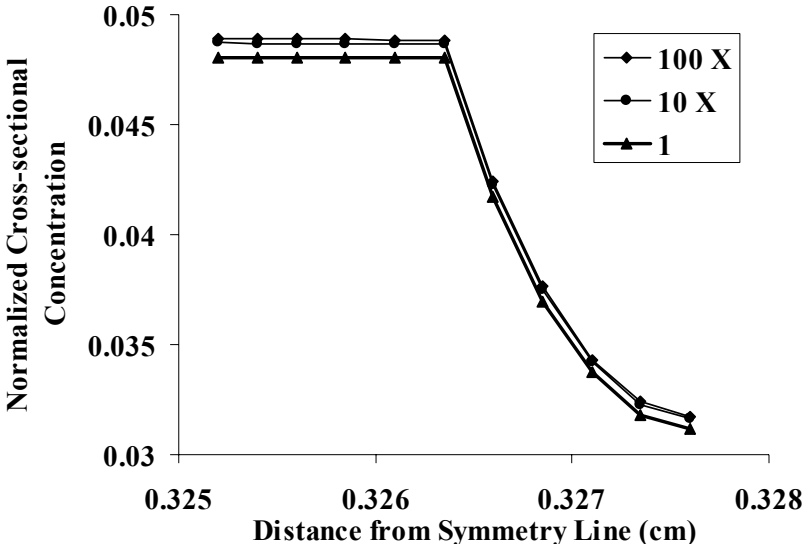

Figure 5.4. Concentration profile for different values of the endothelial permeability.

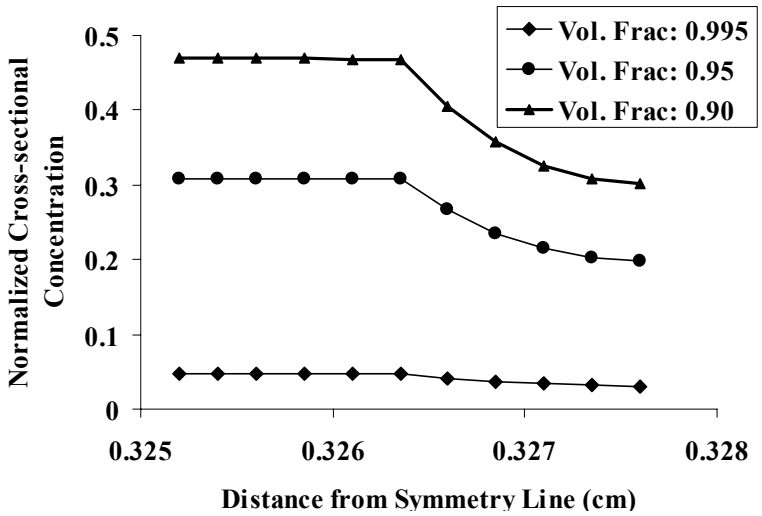

Figure 5.5. Concentration profile for varying solid phase volume fractions of endothelial layer.

The effect of volume fraction of the solid phase on LDL concentration for different values of volume fraction is studied next. Figure 5.5 shows that for a decrease in solid phase volume fraction of endothelial layer increases the arterial wall LDL concentration. For the range of values selected for the analysis, solid volume fraction of 0.9 shows maximum concentration in the artery wall. This shows that the transfer of LDL molecules in the arterial wall is primarily through the fluid convection process.

D. Nutrient Transport in Bioreactors

1. Tissue engineering

Damage and loss of tissue poses significant health hazard to humans. Substitution of tissues using artificial implants has limitations due to the risk of infections, rejection of the tissues, or limited time span. Of late, tissue engineered substitute is an emerging area utilized for the restoration of damaged tissues. Tissue engineering is defined as the application of principles and methods of engineering and life sciences for the development of biological substitutes, to restore maintain or improve tissue function [112]. *In-vitro* development of 3-D tissue substitutes are carried out by attaching the cells to a porous scaffold and encasing the tissue in a closed environment that is most suitable for growth. Tissue engineering of substitutes for cartilage, bones, liver and skin have been carried out by many researchers [113-115]. At present, grafts for skin and cartilage are the only lab grown tissues available for clinical purposes. The major parameters to be considered in the growth of tissues are the biological factors like type of cell, its functionality, mechanical conditioning and the

optimality of temperature and pressure. The major parameters in tissue growth are constantly controlled and monitored in an artificial environment called *bioreactor*.

Bioreactors are devices that provide tightly controlled environmental and operating conditions for the development of the tissue substitutes [27]. In tissue engineering, bioreactors can be applied either for the conditioning the cells for transplantation, or to grow 3-D tissues prior to human implantation or as organ supporting devices [116]. In this section, we analyze the effects of nutrient distributions required for the growth of tissues as a replacement for human tissues.

Tissues are formed from groups of cells by the action of external stimuli in the form of mechanical, electrical, or chemical impulses. In the absence of external stimuli tissue the cells become disorganized finally leading to cell death. Bioreactors apart from providing the environment for growth of the cells are also required to maintain shape and provide impulses in the form of mechanical conditioning or chemical signals for the generation of complex tissues from individual cells. The cells are initially attached onto a substrate through a process called '*seeding*'.

Scaffolds are biodegradable porous materials that provide mechanical support to the cells and shape to the final tissue substitute [117]. The mechanical properties of scaffolds like stiffness, porosity, permeability affect the tissue enhancement and the delivery of the final end product. Seeded scaffolds are then embedded in a growth medium inside the bioreactor culture chamber. Based on the design of culture chamber, bioreactors can be broadly classified into two types a) Rotating bioreactors, where the culture medium is constantly in rotation and b) Non-rotating bioreactors, where the

culture medium is stationary. The non-rotating bioreactors are generally advantageous for the development of complex shaped tissue substitutes.

Apart from providing ideal conditions for the growth of the cells into tissue, the bioreactors also provide growth factors like nutrients and also remove waste materials from the culture chamber. Nutrient rich fluid is passed through the culture medium through special passages called capillaries, and through a process of convection and diffusion, the nutrients reach the cells in the extra capillary space (ECS). Waste materials diffuse from the ECS into the capillaries and are removed from the culture chamber. A major limitation in the working of bioreactor is the transfer of the nutrients from the fluid flow to the extra cellular space. In *in-vivo* tissue blood supplies the nourishment and removes the waste materials. In a bioreactor the absence of blood supply system means that the nourishments supplied by the capillaries have to reach the cells through diffusion and convection from the boundaries of the scaffolds. At the cell surface the nutrients are absorbed by the cells, and as the consumption of nutrients becomes more than the supply, the surface concentration will fall. In such a situation, the cells beyond the scaffold boundaries have a non-homogenous distribution of nutrients. To avoid the nonhomogenous distribution of nutrients in the growth process, the size of artificial tissues is limited, which makes it clinically unusable. Thus, to make the scaffold of size suitable for clinical usage, the nonhomogenous distribution of nutrients is avoided by suitably designing the bioreactor parameters like porosity, stiffness and permeability of the scaffolds along with the flow speed and concentration of nutrients supplied.

Hollow fiber membrane bioreactor (HFMB) has been widely used for the tissue engineering of bones, cartilages because of their excellent nutrient transfer properties [118]. The HFMB consists of porous hollow fiber bundle enclosed in a culture reactor (see Figure 5.6). Fluid flowing through the capillaries supplies the nutrients into the culture chamber, which diffuses out of the lumen through the fiber membrane into the extra cellular space. The nutrients are transferred in the capillaries through the convective process, while diffusion dominates the transfer of nutrients in the scaffold. The diffusion of molecules from the lumen (fluid flowing region at the center) to the extra cellular space is dependent on the flow rate of the fluid, the porosity, and other mechanical properties of the fiber.

Of all the parameters involved in the design of bioreactors, the transfer of nutrient is the most critical. Experimental studies on the transfer properties of nutrients in a reactor are difficult due to the requirement of real time data, and also due to the difficulty in controlling different parameters. Numerical studies provide a perfect platform to carry out a large number of simulations to optimize the functioning of bioreactors. The presence of a fluid and a biphasic interface makes it very suitable for the application of fluid-biphasic interface finite element model developed in Chapter III and the mass transfer finite element model described in Section B of this chapter. The primary objective of this study is to predict the nutrient distribution in the scaffold for different material properties of the scaffold and fiber.

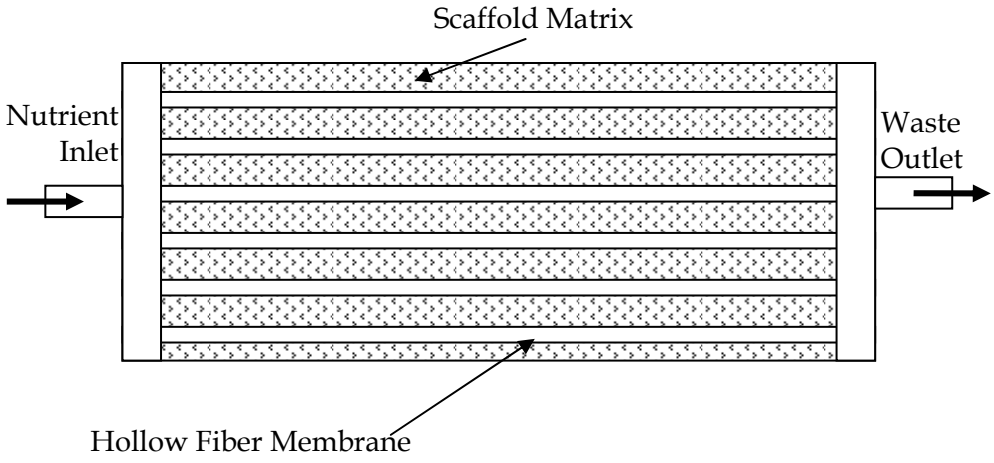

Figure 5.6. Schematic representation of Hollow Fiber Membrane Bioreactor (HFMB).

2. Computational domain

Hollow fiber membrane bioreactor consists of a number of fibers running parallel in the culture chamber. In this work, a single cylinder of the bioreactor is considered with the assumption that the flow through all the fibers is identical and transport behavior within each fiber is the same [118]. An axisymmetric half-section of the cylinder is considered for modeling. The cylinder is represented by a rectangular domain having a lumen radius of 0.01 cm, fiber thickness of 0.002 cm, and the external scaffold thickness of 0.02 cm. The total length of the fiber is taken as 0.3 cm. The material parameters for the fiber and scaffold namely the porosity, stiffness and permeability are taken from literature [118].

At the inlet of the lumen the fluid velocity of 0.007 m/s is prescribed and outlet flow region is assumed to be free. The top region of scaffold is considered as impermeable and all solid degrees of freedom are constrained. The concentration of

nutrient at the inlet is prescribed and the gradient on the top surface of the scaffold is taken as zero. The entire domain is represented by 1200 four-node quadrilateral elements and the interface between the fluid and fiber is made to lie across the interelement boundary region. The solid phase volume fraction is assumed to tend to zero near the interface as was the case for the blood artery wall interface. It is assumed that the cell density is uniform throughout the scaffold and the consumption of nutrients by the cells in scaffold is identical.

The permeability and porosity of the fiber was taken as 16.1×10^{-17} m^4/N.s, and 0.25, respectively, while for the scaffold a permeability of 6.62×10^{-14} m^4/N.s, and porosity of 0.85 was considered for the analysis. The diffusivity of glucose in the fluid is 5.4×10^{-10} m^2/s, in the fiber 5.4×10^{-11} m^2/s, and in the scaffold 1.1×10^{-10} m^2/s [118]. The glucose cell metabolic rate (V_k) is taken as 1.0×10^{-16} mol/cell/s. Using equation (5.6) the reaction rate for the consumption of nutrient by the cell is calculated for different seeding densities for a time period of 1.0 s.

The mass transport in the lumen and fiber is governed by equations as described previously. In the extra cellular space, the cells absorb the nutrients through metabolic activities. It is assumed that the reaction is governed by the simple zero-order reaction kinetics for the uniform cell seeded bioreactor. The reaction rate for the kth nutrient consumption is given by the following equation

$$R_k = V_k \times d \tag{5.6}$$

where, R_k is the consumption scalar quantity, V_k is the cell metabolic rate, d is the cell seeding density. For a specific nutrient the metabolic rate is taken from literature and is assumed to be constant throughout the simulation.

3. Results and discussion

Finite element analysis of a bioreactor for glucose distribution was carried out using the fluid-biphasic interface model for mass transfer. The analysis was carried out to understand the influence of material properties of fiber and scaffold on the glucose distribution in the bioreactor. For comparison of the concentration profile and normalized reaction rate is defined.

The normalized concentration unit is given as

$$c = \frac{C}{C_0} \tag{5.7}$$

where, C_0 is the inlet concentration (mol/cm^3), c is the normalized concentration. A normalized reaction rate is defined as

$$r_k = \frac{R_k}{C_0} \tag{5.8}$$

where, R is first order reaction rate value, mol/(cm^3.s) and defined in equation (5.6), k subscript defines the nutrient type.

The normalized axial and radial glucose distribution for different reaction rate (r) is shown in Figure 5.7. From the figure it is seen that the glucose distribution decreases in the scaffold region due to the lack of convection and also due to the uptake of glucose by the cell. As the reaction rates increases, i.e. as the number of cells in the scaffold increases the glucose concentration decreases considerably in the scaffold. At low values of glucose concentration the cells may die and the tissue scaffold becomes unusable.

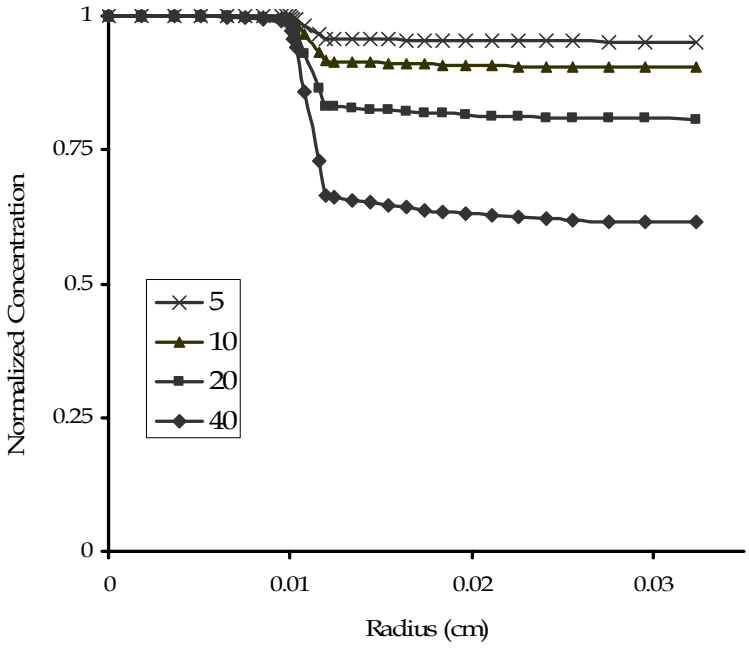

Figure 5.7 Distribution of glucose concentration in the bioreactor for different reaction rates.

The radial distribution of glucose at different axial lengths of the scaffold is shown in Figure 5.8 for a reaction rate of $10.0\times10^{-9}1/\mathrm{s}$. The maximum concentration of glucose is at the entrance of fluid with a decrease observed in the culture medium. A

marginal decrease in the radial concentration of glucose is also observed along the length of the bioreactor. To provide a uniform distribution of nutrients it is required to maintain a sufficient inlet flow velocity.

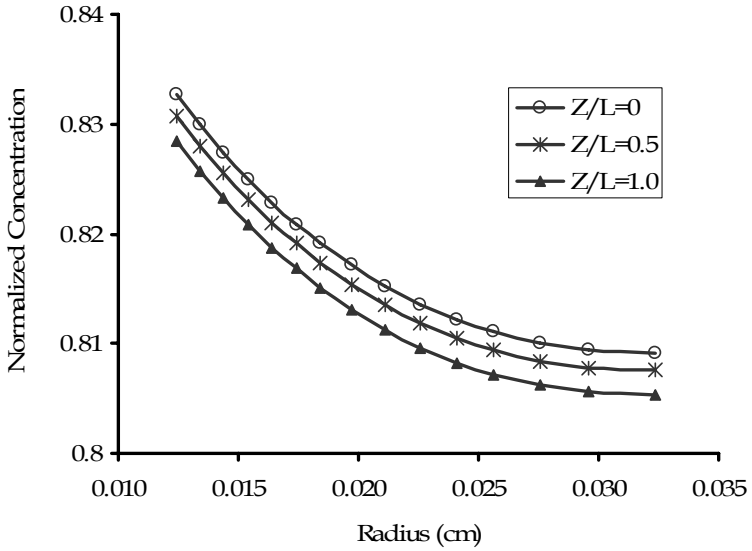

Figure 5.8. Radial variation of glucose along the axial length of the bioreactor.

The variation of glucose concentration with the solid phase volume fraction of the scaffold is shown in Figure 5.9. From the analysis it is observed that the concentration of nutrients increases with a decrease in the solid phase volume fraction. The primary aim of the inlet fluid is to provide a constant supply of the nutrients into the bioreactor. Thus design considerations require only little perfusion from the lumen into the scaffold as the scaffolds are already encased in a fluid medium. It can be achieved by the proper design of the fiber and scaffold permeability. The axial fluid velocity distribution in the bioreactor is shown in Figure 5.10. As can be observed from

the figure, the permeability of the fiber and the scaffold allows only little seepage through the fiber membrane into the scaffold, satisfying the design requirements.

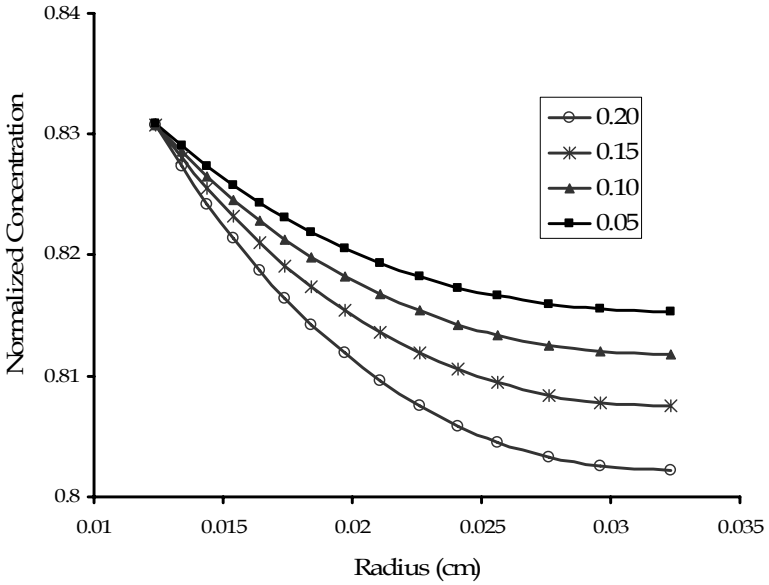

Figure 5.9. Radial variation of nutrient concentration with solid phase volume fraction of scaffold.

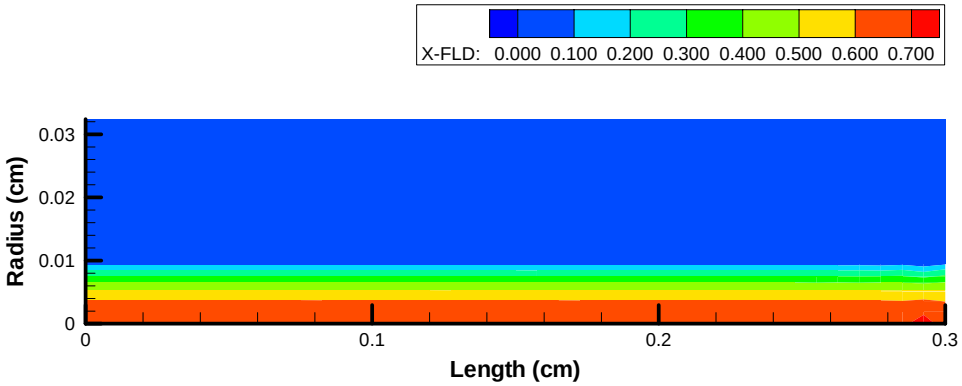

Figure 5.10. Axial fluid velocity distribution in the bioreactor.

E. Summary

Computational modeling of mass transfer across a fluid-tissue domain requires the treatment of physical phenomenon acting in the individual phases and also at the interface between the fluid and the tissue. Most of the previous works on mass transfer across the tissue-fluid domain focused either on the solid or the fluid phase and the interface were treated as a hard boundary. A new mathematical model for the mass transfer of solutes in the artery wall and in a bioreactor is presented. LDL transport from the blood stream to the arterial wall and nutrient transport in a bioreactor is analyzed using the new formulation in this chapter. The material properties of arterial wall influencing LDL deposition in the artery wall are studied along with the parameters affecting glucose distribution in a Hollow Fiber Membrane Bioreactor (HFMB). The biphasic finite element representation of the bioreactor provides a fluid-scaffold coupling, thus studying the fluid and scaffold domains simultaneously.

CHAPTER VI

CONCLUSIONS

A. Concluding Remarks and Summary

In this dissertation, mechanical modeling of cells and tissues that explicitly incorporate the structural components of biological materials are developed. In the constitutive modeling of cell, a homogenous continuum model of a *generalized* cell incorporating the stress fibers was developed. Through the model it was identified that the stress fibers are the primary reason behind the wide disparity of the experimentally derived modulus for even the same cell type. A finite element simulation of some of the widely used experiments in the determination of cell properties was carried out to verify the developed constitutive model. In atomic force microscopy (AFM) finite element simulations, it was observed that the force-deflection curves obtained matches well with the experimental results. Similarly, in magnetic twisting cytometry (MTC) simulation, the stress fibers influence on the angle of twisting due to a magnetic torque was determined. The guidelines for derivation of mechanical property from the experiments are also provided in this work.

As the embedding environment is also important for the response of cells *in-vivo*, a material modeling of soft tissue were carried out in Chapter III. The soft tissues constitutive models was developed using a biphasic approach, by incorporating the solid and fluid phases in a tissue. The biphasic material model is further extended to study the fluid-tissue interface, as seen in blood-arterial wall interface. The macroscopic

behavior of tissue and fluid flow is simultaneously studied using the proposed interface model. The interface model presented in this chapter reduces the computational overhead as the fluid and solid domain is analyzed concurrently.

Significant changes occur in a cell in the event of various pathologies like cancer. The cytoskeleton undergoes drastic changes to cater for the physiological requirements of the disease. Therefore, mechanical properties of the cells can form excellent diagnostic tools for the detection of cancer and malaria. With the developed constitutive model of cell incorporating the cytoskeletal filaments, the alterations in the mechanical property of cell for various stages of pathologies is studied in Chapter IV. Material models are developed for a cancerous cells and the finite element simulation of AFM indentation is carried out. The results are compared with experimental values provided by Mr. Qingsen and Dr. C.T. Lim of National University of Singapore, Singapore. The simulated results were found to be in close match with experimental results, thereby validating the constitutive material model.

Mass transport in tissues is critical to the various physiological processes like growth and development of diseases. In Chapter V, the transfer of low-density lipoprotein from the blood to the arterial wall was analyzed using an extension of the fluid-biphasic interface model. Suitable interface boundary conditions for the mass conservation are incorporated and the simultaneous analysis of the fluid and tissue domain was carried out. The main design challenge in a bioreactor is to provide sufficient nutrients for the cells to growth and development. Using the mass transport finite element model the analysis of bioreactor was carried out to obtain the distribution

of glucose. The effect of material parameters of the scaffold on the nutrient distribution is also presented in Chapter V.

B. Future Works

As an extension to the computational framework presented in this study, the following works could be carried out.

a. Incorporate viscoelastic models of cell to represent other experiments, like micropipette aspiration, to determine the material properties of cells
b. Study the cellular phenomenon like cell migration and cell adhesion
c. Analyze the fluid-structure interactions of the tissue in a larger domain
d. Study the influence of nutrients in growth and remodeling of tissues

REFERENCES

[1] Na, S., Sun, Z., Meininger, G. A., and Humphrey, J. D., 2004, "On atomic force microscopy and the constitutive behavior of cells," Biomech. Model. Mechanobiol., **3**, pp. 75-84.

[2] Karcher, H., Lammerding, J., Huang, H., Lee, R. T., Kamm, R. D., and Kaazempur-Mofrad, M. R., 2003, "A three-dimensional viscoelastic model for cell deformation with experimental verification," Biophysical Journal, **85**(5), pp. 3336–3349.

[3] Ohayon, J., and Tracqui, P., 2005, "Computation of adherent cell elasticity for critical cell-bead geometry in magnetic twisting experiments," Annals of Biomedical Engineering, **33**(2), pp. 131-141.

[4] Costa, K. D., Sim, A. J., and Yin, F. C. P., 2006, "Non-Hertzian approach to analyzing mechanical properties of endothelial cells probed by atomic force microscopy," *ASME* Journal of Biomechanical Engineering, **128**(2), pp. 176-184.

[5] Rotsch, C., and Radmacher, M., 2000, "Drug-Induced changes of cytoskeletal structure and mechanics in fibroblasts: An atomic force microscopy study " Biophysical Journal, **78**(1), pp. 520-535.

[6] Humphrey, J. D., 2002, "On mechanical modeling of dynamic changes in structure and properties in adherent cells," Math Mech. Solids, **7**, pp. 521-539.

[7] Wu, H. W., Kuhn, T., and Moy, V. T., 1998, "Mechanical properties of L929 cells measured by atomic force microscopy: Effects of anticytoskeletal drugs and membrane crosslinking," Scanning, **20**(5), pp. 389-397.

[8] Hu, S., Eberhard, L., Chen, J., and Love, J. C., 2004, "Mechanical anisotropy of adherent cells probed by a three-dimensional magnetic twisting device," Am. J. Physiol.: Cell Physiol., **287**, pp. C1184-C1191.

[9] Lekka, M., Laidler, P., Gil, D., Lekki, J., Stachura, Z., and Hrynkiewicz, A. Z., 1999, "Elasticity of normal and cancerous human bladder cells studied by scanning force microscopy," European Biophysics Journal, **28**(4), pp. 312-316.

[10] Rao, K. M., and Cohen, H. J., 1991, "Actin cytoskeletal network in aging and cancer," Mutation Research, **256**(2-6), pp. 139-148.

[11] Ingber, D. E., Heidemann, S. R., Lamoureux, P., and Buxbaum, R. E., 2000, "Opposing views on tensegrity as a structural framework for understanding cell mechanics," Journal of Applied Physiology, **89**, pp. 1663-1678.

[12] Secomb, T. W., and El-Kareh, A. W., 2001, "A theoretical model for the elastic properties of very soft tissues," Biorheology, **38**, pp. 305-317.

[13] Swan, C. C., Lakes, R. S., Brand, R. A., and Stewart, K. J., 2003, "Micromechanical based poroelastic modeling of fluid flow in haversion bone," *ASME* Journal of Biomechanical Engineering, **125**, pp. 25-37.

[14] Spilker, R. L., and Maxian, T. A., 1990, "A mixed-penalty finite element formulation of the linear biphasic theory for soft tissues," International Journal for Numerical Methods in Engineering, **30**(5), pp. 1063-1082.

[15] Grodzinsky, A. J., Levenston, M. E., Jin, M., and Frank, E. H., 2000, "Cartilage tissue remodeling in response to mechanical forces," Annu. Rev. Biomed. Eng, **2**, pp. 691-713.

[16] DiSilvestro, M. R., Zhu, Q., and Suh, J. F., 2001, "Biphasic poroviscoelastic simulation of the unconfined compression of articular cartilage: II—Effect of variable strain rates," *ASME* Journal of Biomechanical Engineering, **123**(2), pp. 198-200.

[17] Humphrey, J. D., and Yin, F. C. P., 1987, "A new constitutive formulation for characterizing the mechanical behaviour of soft tissues," Biophysical Journal, **52**, pp. 563-570.

[18] Bathe, M., and Kamm, R. D., 1999, "A fluid-structure interaction finite element analysis of pulsatile blood flow through a compliant stenotic artery," *ASME* Journal of Biomechanical Engineering, **21**, pp. 361–369.

[19] Tang, D., Yang, C., Kobayashi, S., and Ku, D. N., 2001, "Steady flow and wall compression in stenotic arteries: A three-dimensional thick-wall model with fluid–wall interactions," *ASME* Journal of Biomechanical Engineering, **123**(6), pp. 548-557.

[20] Hou, J. S., Holmes, M. H., Lai, W. M., and Mow, V. C., 1989, "Boundary conditions at the cartilage-synovial fluid interface for joint lubrication and theoretical verifications," *ASME* Journal of Biomechanical Engineering, **111**(1), pp. 78-87.

[21] Lee, K. W., and Xu, X. Y., 2002, "Modelling of flow and wall behaviour in a mildly stenosed tube," Medical Engineering & Physics, **24**, pp. 575-586.

[22] Chan, B., Donzelli, P. S., and Spilker, R. L., 2000, "A mixed-penalty biphasic finite element formulation incorporating viscous fluids and material interfaces," Annals of Biomedical Engineering, **28**(6), pp. 589-597.

[23] Hofer, M., Rappitsch, G., Perktold, K., Trubel, W., and Schima, H., 1996, "Numerical study of wall mechanics and fluid dynamics in end-to-side anastomoses and correlation to intimal hyperplasia," *ASME* Journal of Biomechanical Engineering, **29**(10), pp. 1297-1308.

[24] Lei, M., Archie, J. P., and Kleinstreuer, C., 1997, "Computational design of a bypass graft that minimizes wall shear stress gradients in the region of the distal anastomosis," Journal of Vascular Surgery, **25**(4), pp. 637-646.

[25] Alberts, B., Johnson, A., Lewis, J., Raff, M., Roberts, K., and Walter, P., 2002, *Molecular Biology of the Cell*, Garland, New York.

[26] Heidemann, S. R., and Wirtz, D., 2004, "Towards a regional approach to cell mechanics," Trends Cell Biol., **14**(4), pp. 160-166.

[27] Feneberg, W., Aepfelbacher, M., and Sackmann, E., 2004, "Microviscoelasticity of the apical cell surface of human umbilical vein endothelial cells (HUVEC) within confluent monolayers," Biophysical Journal, **87**, pp. 1338-1350.

[28] McGarry, J. G., and Prendergast, P. J., 2004, "A three-dimensional finite element model of an adherent eukaryotic cell," European Cells and Materials, **16**(7), pp. 27-33.

[29] Lim, C. T., Zhou, E. H., and Quek, S. T., 2006, "Mechanical models for living cells - A review," Journal of Biomechanics, **39**, pp. 195-216.

[30] Boal, D., 2002, *Mechanics of the Cell*, Cambridge University Press, Cambridge.

[31] Mathur, A. B., Truskey, G. A., and Reichert, W. M., 2000, "Atomic force and total internal reflection fluorescence microscopy for the study of force transmission in endothelial cells," Biophysical Journal, **78**(4), pp. 1725-1735.

[32] Ogden, R. W., 1984, *Nonlinear Elastic Deformations*, Dover, New York.

[33] Nasser, S. N., and Hori, M., 1999, *Micromechanics: Overall Properties of Heterogeneous Materials*, Elsevier Science, Amsterdam.

[34] Eshelby, J. D., 1957, "The determination of the elastic field of an ellipsoidal inclusion and related problems," Proceedings of the Royal Society of London. Series A, Mathematical and Physical Sciences, **241**(1226), pp. 376-396.

[35] MacKintosh, F. C., Kas, J., and Janmey, P. A., 1995, "Elasticity of semiflexible biopolymer networks," Physical Review Letters, **75**(24), pp. 4425-4428.

[36] Deguchi, S., Ohashi, T., and Sato, M., 2006, "Tensile properties of single stress fibers isolated from cultured vascular smooth muscle cells," Journal of Biomechanics, **39**(14), pp. 2603-2610.

[37] Tandon, G. P., and Weng, G. J., 1986, "Average stress in the matrix and effective moduli of randomly oriented composites," Composites Science and Technology, **27**, pp. 111-132.

[38] Costa, K. D., and Yin, F. C. P., 1999, "Analysis of indentation: Implications for measuring mechanical properties with atomic force microscopy," *ASME* Journal of Biomechanical Engineering, **121**(5), pp. 462-471.

[39] Reddy, J. N., 2006, *An Introduction to the Finite Element Method*, McGraw-Hill, New York.

[40] Reddy, J. N., 2004, *An Introduction to Nonlinear Finite Element Analysis*, Oxford University Press, Oxford.

[41] Hibbit, K., and Sorensen Inc, HKS, 2002, "ABAQUS Standard, Version 6.3-2," HKS, Providence, R.I.

[42] Mijailovich, S. M., Kojic, M., Zivkovic, M., Fabry, B., and Fredberg, J. J., 2002, "A finite element model of cell deformation during magnetic bead twisting," Journal of Applied Physiology, **93**, pp. 1429-1436.

[43] Ohayon, J., Tracqui, P., Fodil, R., Fereol, S., Laurent, V. M., Planus, E., and Isabey, D., 2004, "Analysis of nonlinear responses of adherent epithelial cells probed by magnetic bead twisting: A finite element model based on a homogenization approach," *ASME* Journal of Biomechanical Engineering, **126**, pp. 685-698.

[44] Karner, G., Perktold, K., and Zehentner, H. P., 2001, "Computational modeling of macromolecule transport in the arterial wall," Computer Methods in Biomechanics and Biomedical Engineering, **4**, pp. 491-504.

[45] Chakravarty, S., and Datta, A., 1992, "Pulsatile blood flow in a porous stenotic artery," Mathl. Comput. Modelling, **16**(2), pp. 35-54.

[46] Johnson, M., and Tarbell, J. M., 2001, "A biphasic, aniostropic model of the aortic wall," *ASME* Journal of Biomechanical Engineering, **123**(1), pp. 52-57.

[47] Almeida, E. S., and Spilker, R. L., 1998, "Mixed and penalty finite element models for the nonlinear behavior of biphasic soft tissues in finite deformation: Part II - Nonlinear examples," Computer Methods in Biomechanics and Biomedical Engineering, **1**(2), pp. 151-170.

[48] Alazmi, B., and Vafai, K., 2001, "Analysis of fluid and heat transfer interfacial conditions between a porous medium and a fluid layer," International Journal of Heat and Mass Transfer, **44**, pp. 1735-1749.

[49] Gartling, D. K., Hickox, C. E., and Givler, R. C., 1996, "Simulation of coupled viscous and porous flow problems," Computational Fluid Dynamics, **7**, pp. 23-48.

[50] Costa, V. A. F., Oliveira, L. A., Baliga, B. R., and Sousa, A. C. M., 2004, "Simulation of coupled flows in adjacent porous and open domains using a control volume finite element method," Numerical Heat Transfer, Part A, **45**, pp. 675-697.

[51] Cieszko, M., and Kubik, J., 1999, "Derivation of matching conditions at the contact surface between fluid-saturated porous solid and bulk fluid," Transport in Porous Medium, **34**, pp. 319-336.

[52] Massarotti, N., Nithiarasu, P., and Zienkiewicz, O. C., 2001, "Natural convection in porous medium-fluid interface problems," International Journal of Numerical Methods for Heat & Fluid Flow, **11**(5), pp. 473-490.

[53] Reddy, J. N., 2008, *An Introduction to Continuum Mechanics with Applications*, Cambridge University Press, NewYork.

[54] Suh, J. K., Spilker, R. L., and Holmes, M. H., 1991, "A penalty finite element analysis for nonlinear mechanics of biphasic hydrated soft tissue under large deformation," International Journal for Numerical Methods in Engineering, **32**(7), pp. 1411-1439.

[55] Ehlers, W., and Markert, B., 2001, "A linear viscoelastic biphasic model for soft tissues based on the theory of porous media," *ASME* Journal of Biomechanical Engineering, **123**(5), pp. 418-423.

[56] Vito, R. P., and Dixon, A. S., 2003, "Blood vessel constitutive models," Annual Review of Biomedical Engineering, **5**, pp. 413-439.

[57] Quarteroni, A., Tuveri, M., and Veneziani, A., 2000, "Computational vascular fluid dynamics: problems, models and methods," Comput. Visual Sci., **2**, pp. 163-197.

[58] Simon, B. R., Kaufman, M. V., Liu, J., and Baldwin, A. L., 1998, "Porohyperelastic-transport-swelling theory, material properties and finite element models for large arteries," International Journal of Solids and Structures, **35**, pp. 5021-5031.

[59] Huang, Z. J., and Tarbell, J. M., 1997, "Numerical simulation of mass transfer in porous media of blood vessel walls," American Journal of Physiology. Heart and Circulatory Physiology, **273**, pp. H464-H477.

[60] Kim, W. S., and Tarbell, J. M., 1994, "Macromolecular transport through the deformable porous media of an artery wall," *ASME* Journal of Biomechanical Engineering, **116**, pp. 156-163.

[61] Weinbaum, S., Tarbell, J. M., and Damiano, E. R., 2007, "The structure and function of the endothelial glycocalyx layer," Annual Review of Biomedical Engineering, **9**, pp. 121-167.

[62] Damiano, E. R., Duling, B. R., Ley, K., and Skalak, T. C., 1996, "Axisymmetric pressure driven flow of rigid pellets through a cylindrical tube lined with a deformable porous wall layer," J. Fluid Mech., **314**, pp. 163-189.

[63] Holzapfel, G. A., and Gasser, T. C., 2000, "A new constitutive framework for arterial wall mechanics and a comparative study of material models," Journal of Elasticity, **61**, pp. 1-48.

[64] Wei, H. H., Waters, S. L., Liu, S. Q., and Grotberg, J. B., 2003, "Flow in a wavy-walled channel lined with a poroelastic layer," J. Fluid Mech, **492**, pp. 23-45.

[65] Stangeby, D. K., and Ethier, C. R., 2002, "Computational analysis of coupled blood-wall arterial LDL transport," *ASME* Journal of Biomechanical Engineering, **124**(1), pp. 1-8.

[66] Yang, N., and Vafai, K., 2006, "Modeling of low-density lipoprotein (LDL) transport in the artery-effects of hypertension," International Journal of Heat and Mass Transfer, **49**, pp. 850-867.

[67] Prosi, M., Zunino, P., Perktold, K., and Quarteroni, A., 2005, "Mathematical and numerical models for transfer of low-density lipoproteins through the arterial walls: A new methodology for the model set up with applications to the study of disturbed lumenal flow," Journal of Biomechanics, **38**(4), pp. 903-917.

[68] Tang, D., Yang, J., Yang, C., and Ku, D. N., 1999, "A nonlinear axisymmetric model with fluid-wall interactions for steady viscous flow in stenotic elastic tubes," *ASME* Journal of Biomechanical Engineering, **121**, pp. 494-501.

[69] Theodorou, G., and Bellet, D., 1986, "Laminar flows of a non-newtonian fluid in mild stenosis," Computer Methods in Applied Mechanics and Engineering **54**(1), pp. 111-123.

[70] Liu, B., 2007, "The influences of stenosis on the downstream flow pattern in curved arteries," Medical Engineering & Physics, **29**(8), pp. 868-876.

[71] Pralhad, R. N., and Schultz, D. H., 2004, "Modeling of arterial stenosis and its application to blood diseases," Mathematical Biosciences, **190**, pp. 203-220.

[72] Varghese, S. S., and Frankel, S. H., 2003, "Numerical modeling of pulsatile turbulent flow in stenotic vessels," *ASME* Journal of Biomechanical Engineering, **125**, pp. 445-460.

[73] Wellman, P. S., Howe, R. D., Dalton, E., and Kern, A. K., 1999, "Breast tissue stiffness in compression is correlated to histological diagnosis," Technical Report, Harvard BioRobotics Laboratory.

[74] Guck, J., Schinkinger, S., and Lincoln, B., et al 2005, "Optical deformability as an inherent cell marker for testing malignant transformation and metastatic competence," Biophysical Journal, **88**, pp. 3689-3698.

[75] Yamaguchi, H., and Condeelis, J., 2007, "Regulation of the actin cytoskeleton in cancer cell migration and invasion," Biochimica et Biophysica Acta (BBA) - Molecular Cell Research, **1773**, pp. 642-652.

[76] Lambrechts, A., Troys, M. V., and Ampe, C., 2004, "The actin cytoskeleton in normal and pathological cell motility," International Journal of Biochemistry and Cell Biology, **36**, pp. 1890-1909.

[77] Drasdo, D., and Hohme, S., 2005, "A single cell based model of tumor growth in vitro: monolayers and spheroids," Physical Biology, **2**, pp. 133-147.

[78] Jones, A. F., Byrne, H. M., Gibson, J. S., and Dold, J. W., 2000, "A mathematical model of the stress induced during avascular tumour growth," Journal of Mathematical Biology, **40**(6), pp. 473-499.

[79] Ambrosi, D., and Preziosi, L., 2002, "On the closure of mass balance models for tumor growth," Mathematical Models and Methods in Applied Sciences, **12**(737-754).

[80] Breward, C. J., Byrne, H. M., and Lewis, C. E., 2002, "The role of cell-cell adhesions in a two-phase model for avascular tumour growth," J.Math.Biol, **45**, pp. 125-152.

[81] Chaplain, M. A. J., and Sleeman, B. D., 1993, "Modelling the growth of solid tumours and incorporating a method for their classification using nonlinear elasticity theory," Journal of Mathematical Biology, **31**(5), pp. 431-473.

[82] Samani, A., and Plewes, D., 2004, "A method to measure the hyperelastic parameters of ex vivo breast tissue samples," Physics in Medicine and Biology, **49** pp. 4395–4405.

[83] Araujo, R. P., and McElwain, D. L., 2005, "A mixture theory for the genesis of residual stresses in growing tissues II: Solutions to the biphasic equations for a multicell spheroid," SIAM Journal of Applied Mathematics, **66**(2), pp. 447-467.

[84] Unnikrishnan, G. U., Unnikrishnan, V. U., and Reddy, J. N., 2007, "Constitutive material modeling of cell: A micromechanics approach," *ASME* Journal of Biomechanical Engineering, **129**, pp. 315-323.

[85] Greenspan, H. P., 1976, "On the growth and stability of cell cultures and solid tumors," Journal of Theoretical Biology, **56**, pp. 229–242.

[86] Liu, Y., Kerdok, A. E., and Howe, R. D., 2004, "A nonlinear finite element model of soft tissue indentation," Second International Symposium on Medical Simulation, Springer Verlag, Cambridge, MA, pp. 67-76.

[87] Kerdok, A. E., Jordan, P., Wellman, P. S., Socrate, S., and Howe, R. D., 2005, "Identification of nonlinear constitutive law parameters of breast tissue," Summer BioEngineering Conference,Vail, Colarado.

[88] Skovoroda, A. R., Klishko, A. N., Gusakyan, D. A., Mayevskii, Y. I., and Yermilova, V. D., 1995, "Quantitative analysis of the mechanical characteristics of pathologically changed soft biological tissues.," Biophysics, **40**, pp. 1359-1364.

[89] Krouskop, T. A., Wheeler, T. M., Kallel, F., Garra, B. S., and Hall, T., 1998, "Elastic moduli of breast and prostate tissues under compression," Ultrasonic Imaging, **20**, pp. 260-274.

[90] Azar, F. S., Metaxas, D. N., and Schnall, M. D., 2000, "A finite element model of the breast for predicting mechanical deformations during biopsy Procedures," Proceedings of the IEEE Workshop on Mathematical Methods in Biomedical Image Analysis, pp. 38-45.

[91] Plewes, D. B., Bishop, J., Samani, A., and J, S., 2000, "Visualization and quantification of breast cancer biomechanical properties with magnetic resonance elastography," Physics in Medicine and Biology, **45**, pp. 1591-1610.

[92]Tschirhart, C. E., Nagpurkar, A., and Whyne, C. M., 2004, "Effects of tumor location, shape and surface serration on burst fracture risk in the metastatic spine," *ASME* Journal of Biomechanical Engineering, **37**(5), pp. 653-660.

[93] Sarntinoranont, M., Rooner, F., and Ferran, M., 2003, "Interstitial stress and fluid pressure within a growing tumor," Annals of Biomedical Engineering, **31**(3), pp. 327-335.

[94] Please, C. P., 1998, "A new approach to modeling the formation of necrotic regions in tumors," Appl. Math. Lett, **11**(3), pp. 89-94.

[95] Breward, C. J. W., Byrne, H., and Lewis, C. E., 2001, "Modelling the interactions between tumour cells and a blood vessel in a microenvironment within a vascular tumour," European Journal of Applied Mathematics, **12**, pp. 529-556.

[96] Ambrosi, D., and Mollica, F., 2002, "On the mechanics of a growing tumor," International Journal of Engineering Science, **40**, pp. 1297-1316.

[97] Byrne, H. M., King, J. R., McElwain, D. L. S., and Preziosi, L., 2003, "A two phase model of solid tumour growth," Appl. Math. Lett., **16**(4), pp. 567-573.

[98] Roose, T., Netti, P. A., Munn, L. L., Boucher, Y., and Jain, R. K., 2003, "Solid stress generated by spheroid growth estimated using a linear poroelasticity model," Microvascular Research, **66**, pp. 204-212.

[99] Chen, C. Y., Byrne, H. M., and King, J. R., 2001, "The influence of growth-induced stress from the surrounding medium on the development of multicell spheroids," Journal of Mathematical Biology, **43**(3), pp. 191-220.

[100] Byrne, H. M., and Preziosi, L., 2003, "Modelling solid tumours growth using the theory of mixtures," Mathematical Medicine and Biology **20**, pp. 341-366

[101] Lubkin, S. R., and Jackson, T., 2002, "Multiphase Mechanics of Capsule Formation in Tumors," *ASME* Journal of Biomechanical Engineering, **124**, pp. 237-243.

[102] Rice, J. R., and Cleary, M. P., 1976, "Some basic stress-diffusion solutions for fluid-saturated elastic porous media with compressible constituents," Reviews of Geophysics and Space Physics, **14**(2), pp. 227-241.

[103] Netti, P. A., Baxter, L. T., Boucher, Y., Skalak, R., and Jain, R. K., 1995, "A poroelastic model for interstitial pressure in tumors," Biorheology, **32**, p. 346.

[104] Rooney, F., Ferrari, M., and Imam, A., 1996, "On the pressure distribution within tumors," Math. Model. Sci. Comput., **6**, pp. 715–721.

[105] Sarntinoranont, M., Rooner, F., and Ferran, M., 1999, "A mechanical model of a growing solid tumor: Implications for vascular collapse and drug transport," Proceedings of The First Joint BMES/EMBS Conference Serving Humanity, Advancing Technology Atlanta, GA, USA.

[106] Netti, P. A., Baxter, L. T., Boucher, Y., Skalak, R., and Jain, R. K., 1995, "Time dependent behavior of interstitial fluid pressure in solid tumors: Implications for drug delivery," Cancer Research, **55**(22), pp. 5451-5458.

[107] Araujo, R. P., and McElwain, D. L., 2004, "A history of the study of solid tumour growth: the contribution of mathematical modelling," Bulletin of Mathematical Biology., **66**(5), pp. 1039-1091.

[108] Miga, M. I., 2003, "A new approach to elastography using mutual information and finite elements," Physics in Medicine and Biology, **48**, pp. 467-480.

[109] Jordan, P., Kerdok, A. E., Socrate, S., and Howe, R. D., 2005, "Breast tissue parameter identification for a nonlinear constitutive model," BMES Conference Baltimore, MD.

[110] Whyne, C. M., Hu, S. S., and Lotz, J. C., "Burst fracture in the metastatically involved spine: development, validation, and parametric analysis of a three-dimensional poroelastic finite-element model," Spine, **28**(7), pp. 652-660.

[111] Kyriacou, S. K., and Davatzikos, C., 1998, "A biomechanical model of soft tissue deformation, with applications to non-rigid registration of brain images with tumor pathology," Medical Image Computing and Computer-Assisted Intervention — MICCAI'98, pp. 531-538.

[112] Langer, R., and Vacanti, J. P., 1993, "Tissue engineering," Science, **260**, pp. 920-926.

[113] Pisu, M., Lai, N., Cincotti, A., Concas, A., and Cao, G., 2004, "Modeling of engineered cartilage growth in rotating bioreactors," Chemical Engineering Science, **59**, pp. 5035-5040.

[114] Lanza, R. P., Langer, R., and Vacanti, J. P., 2000, *Principles of Tissue Engineering*, Academic Press, San Diego.

[115] Thomas, A. C., Campbell, G. R., and Campbell, J. H., 2003, "Advances in vascular tissue engineering," Cardiovascular Pathology, **12**, pp. 271-276.

[116] Fischer, A. H., Young, K. A., and DeLellis, R. A., 2004, "Incorporating pathologists criteria of malignancy into the evolutionary model for cancer development," Journal of Cellular Biochemistry, **93**, pp. 28-36.

[117] Hollister, S. J., and Lin, C. Y., 2007, "Computational design of tissue engineering scaffolds," Computer Methods in Applied Mechanics and Engineering, **196**, pp. 2991-2998.

[118] Abdullah, N. S., and Das, D. B., 2007, "Modelling nutrient transport in hollow fibre membrane bioreactor for growing bone tissue with consideration of multi-component interactions," Chemical Engineering Science, **62**, pp. 5821-5839.

[119] Ellis, N., Jarman-Smitha, M., and Chaudhuri, J. B., 2005, "Bioreactor systems for tissue engineering: A four dimensional challenge," Bioreactors for Tissue Engineering, J. B. Chaudhari, and M. Al-Rubeai, eds., Springer Netherlands, Netherlands, pp. 1-18.

VITA

Ginu Unnithan Unnikrishnan received his Bachelor of Technology degree in mechanical engineering from the University of Kerala, India in 2000. He completed his Master of Science degree in 2003, from the Indian Institute of Technology Madras, India in civil engineering with a specialization in structural engineering and he worked on the shape optimization of the pneumatic tire using evolutionary optimization techniques in a distributed computing environment.

He joined the doctoral program at Texas A&M University in September 2003 and graduated in May 2008. His research interests include multiscale modeling of biological cells and tissues; growth mechanics of tumors and modeling of arterial pathological conditions like atherosclerosis and also mass transport analysis in the arteries and in bioreactors.

Mr. Ginu Unnikrishnan may be reached through Professor J. N. Reddy (jnreddy@tamu.edu) in the Department of Mechanical Engineering, Texas A&M University, 3123 TAMU, College Station TX 77843-3123.